

Estimates of Lightning NO_x Production based on High Resolution OMI NO₂ Retrievals over the Continental US

Response to Anonymous Referee #1

Xin Zhang, Yan Yin, Ronald van der A, Jeff L. Lapierre, Qian Chen,
Xiang Kuang, Shuqi Yan, Jinghua Chen, Chuan He and Rulin Shi

February 7, 2020

We thank the reviewer for his/her positive comments and very careful reading of the main article. The individual corrections suggested are addressed below. The reviewer's comments will be shown in **red**, our response in **blue**, and changes made to the paper are shown in **black** block quotes. Unless otherwise indicated, page and line numbers correspond to the original paper. Figures, tables, or equations referenced as "Rn" are numbered within this response; if these are used in the changes to the paper, they will be replaced with the proper number in the final paper.

General Comments

1) When revising the manuscript, the authors should emphasize why they believe their approach is less sensitive to the tropospheric background than other approaches and why it may be more suitable over polluted locations.

The Section 3.2 compares the different LNO_x productions based on different AMFs. The differences are partly caused by the different consideration of tropospheric background NO₂. To make it clearer, we add another section to discuss the improved background NO₂ consideration in our approach.

The patterns in Fig. 6 indicate the improvement of our approach is different in polluted and clean regions. To simplify the quantification, we select six grids with similar NO₂ profile (~ 100 pptv) above the cloud with CRF = 100%. These grid boxes contain the cities denoted by stars and triangles in Fig. 6a. Then, the differences between AMFs are dependent on fewer parameters:

$$AMF_{LNO_2} = \frac{\int_{p_{cloud}}^{p_{tp}} w_{cloudy}(p) NO_2(p) dp}{\int_{p_{surf}}^{p_{tp}} LNO_2(p) dp}$$

$$AMF_{NO_2Vis} = \frac{\int_{p_{cloud}}^{p_{tp}} w_{cloudy}(p) NO_2(p) dp}{\int_{p_{cld}}^{p_{tp}} NO_2(p) dp}$$

$$AMF_{LNO_2Clean} = \frac{\int_{p_{cloud}}^{p_{tp}} w_{cloudy}(p) LNO_2(p) dp}{\int_{p_{surf}}^{p_{tp}} LNO_2(p) dp}$$

Figure 7 (see Fig. R1) compares the mean profiles of NO₂, background NO₂ and background NO₂ ratio in polluted and clean grids. Generally, the profiles of background NO₂ ratio are C-shape because LNO₂ concentrations are higher than background NO₂ in the UT. However, the ratio profile in Fig. 7e has one peak between the cloud pressure and tropopause as background NO₂ increases and LNO₂ decreases. Besides, the percentage of UT background NO₂ in polluted regions is steady and higher than that in clean regions.

Table 4 (see Table R1) presents the relative changes among three methods in six cities. The difference between AMF_{LNO₂} (Eq. 7) and AMF_{LNO₂Clean} (Eq. 9) is the numerator: $\int_{p_{cloud}}^{p_{tp}} w_{cloudy}(p) NO_2(p) dp$ and $\int_{p_{cloud}}^{p_{tp}} w_{cloudy}(p) LNO_2(p) dp$. When the ratio of LNO₂ is higher or the region is cleaner, the relative difference is smaller (e.g. 5.0% – 12.0%, Fig. 7d – f). The largest relative difference (46.3%) occurs when the ratio of background NO₂ is continuously high in the UT (Fig. 7c). As a result, our approach is less sensitive to background NO₂ and more suitable for convections over polluted locations. In contrast, production estimated by our method is larger than that based on NO₂Vis due to the LNO₂ below the cloud. When the cloud is higher, especially the peak of LNO profile is lower than the cloud (Fig. 7b), the relative difference is larger (121.2%) because more LNO₂ can not be included into the NO₂Vis, which has been discussed in Sect. 3.2. The relative change between AMF_{LNO₂Clean} (Eq. 9) and AMF_{NO₂Vis} (Eq. 8) depends on $\int_{p_{cloud}}^{p_{tp}} w_{cloudy}(p) LNO_2(p) dp / \int_{p_{surf}}^{p_{tp}} w_{cloudy}(p) LNO_2(p) dp$, which is also affected by cloud not the background NO₂. The largest relative change is 153.8% among the six grids where the highest clouds occur.

2) They also need a more clear rationale for how they determined what detection efficiency to use for the ENTLN flashes.

Thanks. We have made it clearer (See No. 11 – 13, Sect. Specific comments).

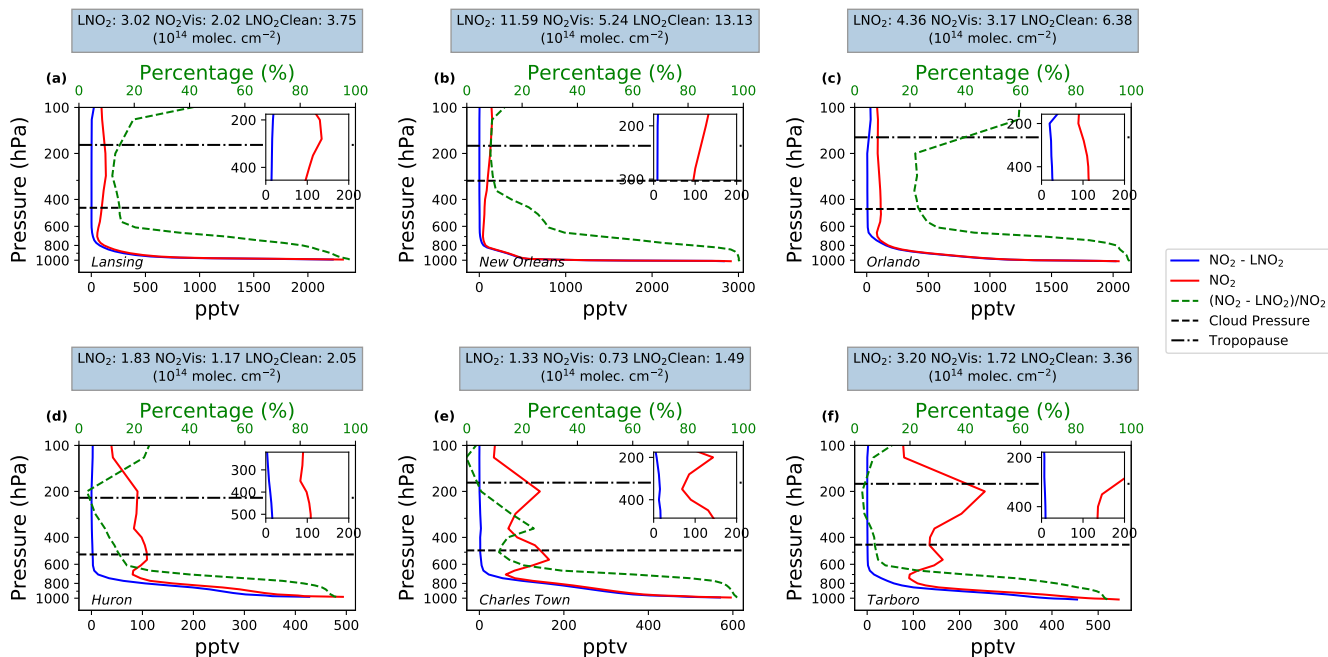


Figure R1 . Comparison of mean WRF-Chem NO_2 and background NO_2 profiles in six grids with $\text{CRF} \geq 100\%$ on specific days during MJJA 2014. The top row data are selected from polluted regions (stars in Fig. 6a) while the bottom row data are from clean regions (triangles in Fig. 6a). The green dashed lines are the mean ratio profiles of background NO_2 to NO_2 . The zoomed figures show the profiles from the cloud pressure to the tropopause. The titles present the mean productions based on three different methods mentioned in Sect. 2.4.

Table R1 . The percent change in the estimated production when using different methods based on the same a priori profiles.

	City ¹	$(\text{LNO}_2\text{Clean} - \text{LNO}_2)/\text{LNO}_2$	$(\text{LNO}_2 - \text{TropVis})/\text{TropVis}$	$(\text{LNO}_2\text{Clean} - \text{TropVis})/\text{TropVis}$
Polluted	Lansing	24.2%	49.5%	85.6%
	New Orleans	13.3%	121.2%	153.8%
	Orlando	46.3%	37.5%	101.3%
Clean	Huron	12.0%	56.4%	75.2%
	Charles Town	12.0%	82.2%	104.1%
	Tarboro	5.0%	86.0%	95.3%

¹Locations are denoted in Fig. 6a.

Specific Comments

1) L10: Put a positive spin on your method as opposed to a negative spin on others work, i.e. mention that your method reduces sensitivity to the background and includes much of the below-cloud NO_x .

Thank you. We have reformatted the sentence:

Focusing on the summer season during 2014, we find that the lightning NO_2 (LNO_2) PE is 44 ± 16 mol NO_2 flash $^{-1}$ and 8 ± 3 mol NO_2 stroke $^{-1}$ while LNO_x PE is 120 ± 52 mol NO_x flash $^{-1}$ and 22 ± 9 mol NO_x stroke $^{-1}$. **Results reveal that our method reduces sensitivity to the background NO_2 and includes much of the below-cloud LNO_2 .**

2) L30: Why does an increase in lightning lead to a net positive forcing but a decrease in lightning as no net effect?

Because the effect of CTH and IFLUX on radiative forcing from ozone and methane is different, the net effect should not be determined only by lightning. The detail of this is shown by Fig. 3 in Finney et al. (2018). To make this more clear, we have added the "radiative forcing" specifically.

Finney et al. (2018) found different impacts on atmospheric composition and radiative forcing between when simulating future lightning using a new upward cloud ice flux (IFLUX) method and when the commonly used cloud-top height (CTH) approach is used. While lightning is predicted to increase by 5 — 16% over the next century with the CTH approach (Clark et al., 2017; Banerjee et al., 2014; Krause et al., 2014), a 15% decrease in lightning was estimated with IFLUX in 2100 under a strong global warming scenario (Finney et al., 2018). **As a result of the different effects on radiative forcing from ozone and methane, a net positive radiative forcing was found with the CTH approach while there is little net radiative forcing with the IFLUX approach (Finney et al., 2018).**

3) L63: "Since they assumed NO_2 above the clouds are all NO_x ". I think this is misleading. Pickering et al. (2016) did not assume all NO_2 above the clouds was LNO_x . They assumed it included LNO_x and BL NO_x from pollution. They subtracted off a tropospheric background to account for the latter.

Although the tropospheric background NO_2 is subtracted as shown by Eq. 1 in Pickering et al. (2016), they didn't apply it to the rest of analysis. As explained by the fifth paragraph in Sect. 3.4 and the fifth paragraph in Sect. 4.4 (Pickering et al., 2016): "Given the difficulty in estimating the background, we focus on areas of active or very recently active convection where the lower tropospheric background is minimized." and "In our calculations of LNO_x in sections 4.1 through 4.3 we have assumed a zero tropospheric background due to uncertainty in how it should be determined." To make it more clear, we have rewritten the sentence:

To convert the S_{LNO_2} to the tropospheric vertical density (VCD) of LNO_x (V_{LNO_x}), an air mass factor (AMF) is calculated by dividing the a priori S_{LNO_2} by the a priori V_{LNO_x} . **Since they considered NO_2 above the cloud as LNO_2 in the algorithm due to the difficulty and uncertainty in determining of the background NO_2 , their AMF and derived VCD of LNO_x (LNO_2) is named as $\text{AMF}_{\text{LNO}_x\text{Clean}}$ ($\text{AMF}_{\text{LNO}_2\text{Clean}}$) and LNO_xClean (LNO_2Clean), respectively.**

4) L68: The 3 – 30% value is an estimate of $\text{LNO}_x/(\text{LNO}_x+\text{NO}_x$ from other sources). It is not an estimate of the uncertainty. Move the 3 – 30% parentheses to after "background NO_x ".

Moved.

Results for the Gulf of Mexico during 2007 – 2011 summer yield LNO_x production of 80 ± 45 mol NO_x per flash. **Among several substantial sources of uncertainty, significant uncertainty exists in characterizing background NO_x (3% ~ >30%) in this region (Pickering et al., 2016).**

5) L72: What do you mean by “weighted”?

"Weighted" means that box data are weighted according to the number of OMI pixels contributing to each. We have added the explanation of "weighted":

More recently Bucsele et al. (2019) obtained an average production efficiency (PE) of 180 ± 100 mol per flash over East Asia, Europe and North America based on the method used in Pickering et al. (2016). **The tropospheric NO_x background was removed by subtracting temporal average of NO_x at each box where the value was weighted by the number of OMI pixels which meet the optical cloud pressure and CRF criteria required to be considered deep convection but has 1 flash or less instead.**

6) L73: You need to specify whether the 15% adjustments were positive or negative also the “lofted pollution” was not corrected the “LNO_x production” was corrected.

They considered 15% of total NO_x is the transported pollution. Fixed.

The lofted pollution was considered as 15% of total NO_x according to the estimation from DeCaria et al. (2000, 2005) and the average chemical delay was adjusted by 15% following the 3-hour LNO_x lifetime in the nearby field of convection (Nault et al., 2017). However, there were negative LNO_x values caused by the overestimation of the tropospheric background at those locations.

7) L86: You may want to add that “Pickering et al. then subtracted off an estimate of the tropospheric background to obtain the LNO_x Production.

As mentioned before (*Response 3, Sect. Specific Comments*), they did not subtract off the background NO₂.

8) L93: The bias of AMF relative to what?

The bias of AMF is related to aircraft observations. Fixed.

Meanwhile, Laughner and Cohen (2017) showed that the OMI AMF is increased by ~35% for summertime when LNO₂ simulated by WRF-Chem is included in the a priori profiles to match aircraft observations. **The simulation agrees with observed NO₂ profiles and the bias of AMF related to these observations is reduced to < ±4% for OMI viewing geometries.**

9) L106: Verify whether you used v3.0 or v3.1 of the NASA standard product

Verified.

For the current study, we used the NASA standard product **V3.0** (Krotkov et al., 2017) as input to the LNO_x retrieval algorithm.

10) L110: The bias with respect to what is subtracted off?

The bias is caused by an instrument artifact. Corrected.

A corrected ("de-striped") SCD is obtained by subtracting **the cross-track bias caused by an instrument artifact** from the measured slant column;

11) L127: What region did Rudlosky analyze? Are Rudlosky's value for CG, IC, or combined flashes? Are you using ENTLN flashes or flashes from a combined ENTLN/NLDN data set? The DE values found by Rudlosky of 35% or so need to be reconciled with the 88%/45% values found by Lapierre.

Thanks for your comments on lightning data. We have changed the DE values to focus on CONUS and specified the kind of ENTLN data.

Rudlosky (2015) compared ENTLN **combined events (IC and CG) with LIS flashes** and found that the relative flash detection efficiency of ENTLN **over CONUS increases from 62.4% during 2011 to 79.7% during 2013.**

12) L121-131: Why is the NLDN DE of IC pulses relevant?

Because we only used ENTLN data instead of the combined ENTLN and the NLDN dataset, it is necessary to clarify that the NLDN DE of IC pulses is lower than ENTLN's and ENTLN DE of CG flashes or strokes is high enough to keep unchanged.

Lapierre et al. (2019) also compared combined ENTLN and the NLDN dataset with data from the LIS during 2014 and the detection efficiencies of IC flashes and strokes are 88% and 45%, respectively. **Since we only use the ENTLN data in 2014 as Lapierre et al. (2019) and NLDN detection efficiency of IC pulses should be lower than 33% which is calculated by the data in 2016 (Zhu et al., 2016), only the IC flashes and strokes are corrected by 88% and 45%, respectively, while CG flashes and strokes are unchanged because of the high detection efficiency.**

13) L121-131: You may want to include a plot showing the mean ENTLN flashes during MJJA of 2014.

Added (Fig. R2).

In addition, lightning flash rate based on the Price and Rind level of neutral buoyancy parameterization (Price and Rind, 1992) and LNO_x parameterizations are activated (200 mol NO flash⁻¹, the factor to adjust the predicted number of flashes is set to 1; hereinafter referred to as "1×200 mol NO flash⁻¹"). **Although the simulated total flash densities are higher in the Southeast US and lower in the North Central US (Fig. 2), the criteria in Sect. 3.1 could limit this effect on the estimation of LNO_x production and Sect. 3.4 will use another simulation to test this problem.**

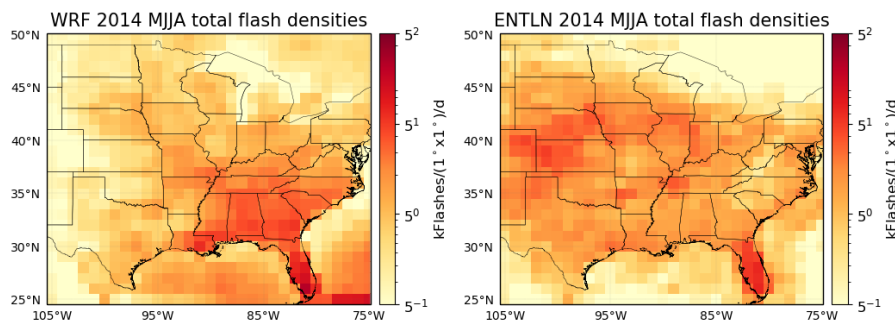


Figure R2 . Comparison between total flash densities from ENTLN and WRF-Chem during MJJA 2014.

14) L174: LNO_x is regridded. At this point in the manuscript it is unclear how you generated pixel level values of LNO_x that were regridded. Start paragraph by saying how you determined LNO_x and then mention regridding method. Is it as simple as multiplying VLNO_x by area?

Sorry for the misleading. This paragraph describes how to re-grid the V_{LNO_x} pixel values obtained in Section 2.4 to $0.05^\circ \times 0.05^\circ$ grids.

V_{LNO_x} is re-gridded to $0.05^\circ \times 0.05^\circ$ grids using the constant value method (Kuhlmann et al., 2014). Then, it is analyzed in $1^\circ \times 1^\circ$ grid boxes with a minimum of fifty valid $0.05^\circ \times 0.05^\circ$ grids which is equivalent to five satellite pixels in Pickering et al. (2016).

15) L181: Why does choosing the 350-400 hPa layer avoid biases in the simulation of high clouds?

If the model has biases in the 3D cloud fraction in the upper troposphere (higher than 350 hPa), our method is not sensitive to that bias since we don't consider the cloud fraction at levels above 350 hPa. This pressure layer was also used in Strode et al. (2017). We have added the reference for the method.

The CFs are defined as the maximum cloud fraction calculated by the Xu-Randall method between 350 and 400 hPa (Xu and Randall, 1996; Strode et al., 2017). This atmospheric layer (between 350 and 400 hPa) avoids any biases in the simulation of high clouds. We choose CFs $\geq 40\%$ suggested by Strode et al. (2017) to determine cloudy or clear for each simulation grid.

16) L193: I don't think "not polluted much" is appropriate for a 50% threshold. Simply state that more than half of the NO_x must have an LNO_x source.

Fixed.

The ratio $\geq 50\%$ indicates that more than half of the NO_x above the cloud **must have a LNO_x source**.

17) L216-220: Why do you think the production is relatively insensitive to the CRF threshold? Wouldn't you expect it to decrease as the CRF is increased due to less BL contamination?

Yes, it is true for the method of Pickering et al. (2016) and Lapierre et al. (2019). But, in our new method, the BL contamination is considered in the numerator of AMF_{LNO_x} (Eq. 2). As a result, when the CRF is increased from 70% to 90%, the LNO_x PE rises from 35.7 LNO_x/flash to 54.5 LNO_x/flash, which is opposite compared to the result of Pickering et al. (2016). On the other hand, the updraft would also affect the BL contamination detected by OMI. We have added these information to make the choice of CRF more reasonable:

The increment of LNO_x PE caused by the CRF increase from 70% to 90% is opposite to the result of Pickering et al. (2016). This is an effect of the consideration of NO₂ contamination transported from the boundary layer in our method. Although enhanced NO_x is often observed in regions with CRF > 70% (Pickering et al., 2016), the following analysis will be based on the criterion of CRF $\geq 90\%$ considering the contamination by low and mid-level NO₂ and comparisons with the results of Pickering et al. (2016) and Lapierre et al. (2019).

18) L228: 10-80% range is so wide as to be useless. In addition to this range include the mean and standard deviation.

Thank you for your remind. We have added the mean and standard deviation of the ratio of LNO_x below the cloud.

The simulation of GMI in Pickering et al. (2016) indicated that 25% – 30% of the LNO_x column lies below the CP, while the ratio in our WRF-Chem simulation is **56 ± 20%**.

19) L266: Are the differences between NO_2 Vis production and LNO_2 Vis production larger over polluted grid boxes?

Yes. We mentioned that in L265.

20) L271: Not sure what you mean by “trend”. Please re-write this sentence more clearly.

Clarified.

... the ratio of LNO_2 Vis to LNO_2 ranges from 10% – 80%. This may be caused by the height of the clouds and the profile of LNO_2 . If the CP is near 300 hPa, the ratio should be smaller because of the coverage of clouds. **The ratio would also be smaller** while peaks of the LNO_2 profile are below the CP.

21) L295-L300: State clearly why the difference is larger for LNO_x (25%) than for LNO_2 (11.5%)?

As suggested by Eric J. Bucsela in private, we have redone the linear regressions and stated the results instead of comparing the difference in LNO_2 PE and that in LNO_x PE.

For the linear regression method (Fig. 9), LNO_2 production is 29.8 ± 20.5 mol/flash which is 59.4% larger than the basic one (18.7 ± 18.1 mol/flash). Meanwhile, LNO_x production (increasing from 54.5 ± 48.1 mol/flash to 88.5 ± 61.1 mol/flash) **also depends on** the configuration of LNO production in WRF-Chem.

22) L300: I'd suggest deleting Figure 10. It is discussed in passing and the most important numbers from that Figure are already included in the text.

We agreed with you and have deleted that figure.

23) L334: Would the profile uncertainty be less than 13/26% for the LNO_2 Clean approach, although the latter (apparently) has more uncertainty due to the tropospheric background?

We have checked the profile uncertainty of retrieved LNO_2 and LNO_x productions for the LNO_2 Clean approach to be $\sim 0\%$ and 39% respectively. As a result, the LNO_2 Clean approach is suitable for clean regions and the effect of profile need to be considered carefully.

24) L335-338: Why don't uncertainties in the tropospheric background contribute to uncertainties in the production?

Yes, the tropospheric background NO_2 should affect the uncertainties in the estimation of production. We have added this to the section of uncertainty.

In addition, the estimation of LNO_x PE is also dependent on the tropospheric background NO_2 . In our method, main factors affecting this factor are the emissions inventory and the amount of transported NO_2 . For the emissions inventory, the sources of uncertainty are assumptions, methods, input data and calculation errors. As a result, the uncertainties for different species or pollutants related to NO_2 are different and EPA also doesn't publish the quantified uncertainty measures because the parties that submit emissions estimates to EPA are not asked to include quantitative uncertainty measurements or estimates (EPA, 2015). For the simulated convective transport, Li et al. (2018) compared the cloud-resolving simulations with

these based on convective parameterization and pointed out that the convective transport was weaker in the parameterization. But, we believe that the ratio condition ($LNO_2^{Vis}/NO_2^{Vis} \geq 50\%$) should reduce these two kinds of uncertainty and assume an uncertainty of 10%, which is less than 20% assigned in Allen et al. (2019) and Bucselá et al. (2019).

25) L335-338: How would biases in the modeled NO/NO₂ ratio contribute to uncertainties in the production of LNO_x?

We have added that kind of uncertainty according to Travis et al. (2016), Silvern et al. (2018) and Bucselá et al. (2019). The uncertainty in the production of LNO_x is 20%.

Recent works revealed that the modeled NO/NO₂ ratio departs from the data in the SEAC⁴RS aircraft campaign (Travis et al., 2016; Silvern et al., 2018). Silvern et al. (2018) attributed this to the positive interference on the NO₂ measurements or errors in the cold-temperature NO-NO₂-O₃ photochemical reaction rate. We assign an uncertainty of 20% to this error considering the possible positive NO₂ measurements interferences (Allen et al., 2019; Bucselá et al., 2019).

26) L392: Expand on why this approach can be used in polluted regions? Is this different than other approaches?

Added.

In this study, a new algorithm for retrieving LNO₂ (LNO_x) from OMI, including LNO₂ (LNO_x) below cloud, has been developed for application over active convection. **It works in both clean and polluted regions because of the consideration of tropospheric background pollution in the definition of AMFs.**

27) L391-409: Minimize the use to lesser known acronyms in the conclusion section. Many readers will only read the abstract and conclusions. For e.g., TL and ratio and LNO2Clean.

We reformatted the section, thanks.

Compared with former methods, our method has reduced the sensitive to background NO₂, while the method in Lapierre et al. (2019) underestimates LNO_x production efficiency because of the neglected below-cloud LNO₂ and LNO₂ production is overestimated using the method in Pickering et al. (2016) due to the over-cloud background NO₂ in polluted regions. Finally, implementing profiles generated with different model settings of lightning ($1 \times 200 \text{ mol NO flash}^{-1}$ and $2 \times 500 \text{ mol NO flash}^{-1}$), we find that the larger LNO production model setting leads to larger retrieval of LNO_x despite some regionally dependent effects caused by nonlinear calculation of AMF. Both the ratio of the tropospheric LNO₂ above the cloud to the total tropospheric LNO₂ and the ratio of LNO₂ to NO₂ cause different comprehensive effects due to the nonlinear calculation of AMF_{LNO_2} and AMF_{LNO_x} .

28) L401-402: The last sentence of the 2nd paragraph of the conclusion section is poorly written. Please re-write to make its meaning clear.

Rewritten as the response above.

29) Figure 1 caption. Please specify what is plotted here. Also, did you choose this domain or is this a standard domain used by EPA or others (e.g., US1 or US2 domain)? How many east-west and north-south grid points in domain?

We chose the simulation domain and the information has been added to the caption of Figure 1 (Fig. R3).

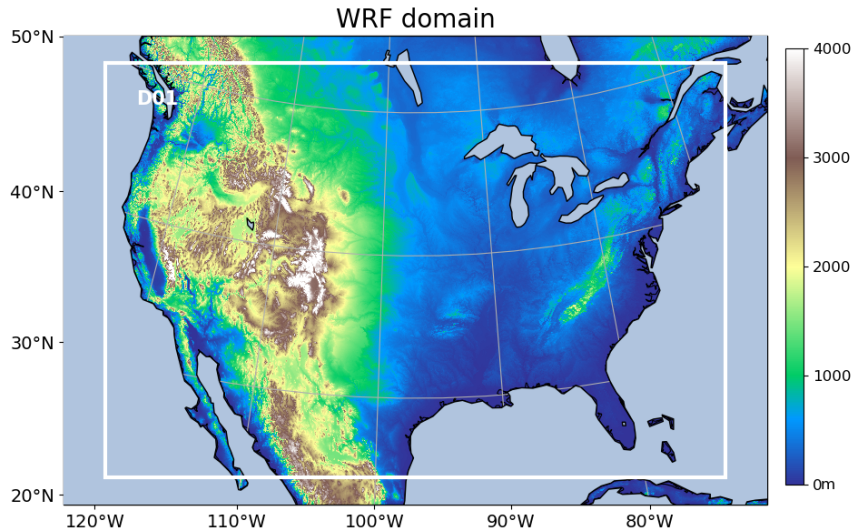


Figure R3 . Domain and terrain height (m) of the WRF-Chem simulation with 350 x 290 grid cells and a horizontal resolution of 12 km.

30) Table 1: Capitalize entln

Fixed (Table R2).

31) Table 2: under different conditions > for different thresholds

Fixed (Table R3).

32) Figure 3: May not be needed. Consider removing.

Figure 3 shows the time series of NO_2 Vis, LNO_2 Vis, LNO_2 and LNO_2 Clean production per day and compares those with the percent differences between NO_2 Vis and LNO_2 Vis and the percent differences between NO_2 Vis and LNO_2 Clean. Readers could distinguish the difference between different methods in one figure. For example, these peaks of LNO_2 Clean coincide with the NO_2 pollution above the cloud (the peaks of the percent differences between NO_2 Vis and LNO_2 Vis). As a result, we decide to keep this figure.

Table R2 . Definitions of the abbreviations for the criteria used in this study.

Abbreviations	Full form [source]
CRF	Cloud radiance fraction [OMI]
CP	Cloud optical pressure [OMI]
CF	Cloud fraction [WRF-Chem]
TL	Total lightning flashes [WRF-Chem]
ratio	modeled LNO ₂ Vis / modeled NO ₂ Vis [WRF-Chem]
CRF _α _ENTLN	CRF ≥ α + ENTLN flashes(strokes) ≥ 2400(8160) [ENTLN]
CRF _α _CF40_ENTLN	CRF ≥ α + ENTLN flashes(strokes) ≥ 2400(8160) + CF ≥ 40%
CRF _α _ENTLN_TL1000	CRF ≥ α + ENTLN flashes(strokes) ≥ 2400(8160) + TL ≥ 1000
CRF _α _CF40_ENTLN_TL1000	CRF ≥ α + ENTLN flashes(strokes) ≥ 2400(8160) + CF ≥ 40% + TL ≥ 1000
CRF _α _ENTLN_TL1000_ratio50	CRF ≥ α + ENTLN flashes(strokes) ≥ 2400(8160) + TL ≥ 1000 + ratio ≥ 50%
CRF _α _CF40_ENTLN_TL1000_ratio50	CRF ≥ α + ENTLN flashes(strokes) ≥ 2400(8160) + CF ≥ 40% + TL ≥ 1000 + ratio ≥ 50%

α has three options: 70%, 90% and 100%

Table R3 . LNO_x production for different thresholds of CRF with coincident ENTLN data, TL ≥ 1000 and ratio ≥ 50%.

CRF (%)	ENTLN data type ¹	LNO _x /flash or LNO _x /stroke	R value	Intercept (10 ⁵ mol)	Days ²
70	Flash	35.7 ± 36.8	0.21	4.91	85
90	Flash	54.5 ± 48.1	0.25	3.90	81
100	Flash	20.8 ± 37.4	0.13	5.67	71
70	Stroke	4.1 ± 3.9	0.21	5.16	96
90	Stroke	7.0 ± 4.8	0.29	4.16	93
100	Stroke	2.6 ± 4.0	0.14	5.41	82

¹The threshold of ENTLN data is 2400 flashes box⁻¹ and 8160 strokes box⁻¹ during the period of 2.4 h before OMI overpass time. ²The number of valid days with specific criteria in MJJA 2014.

Technical Corrections

1) L5: based on the program of new > that uses the

Fixed, thanks.

To apply satellite data in both clean and polluted regions, a new algorithm for calculating LNO_x has been developed **that uses the** Berkeley High Resolution (BEHR) v3.0B NO₂ product and the Weather Research and Forecasting-Chemistry (WRF-Chem) model.

2) L15: surface is > surface are

L16: originate largely > originates largely

Fixed.

Nitrogen oxides (NO_x) near the Earth's surface **are** mainly produced by soil, biomass burning and fossil fuel combustion, while NO_x in the middle and upper troposphere **originates** largely from lightning and aircraft emissions.

3) L27: method and the commonly used the widely used cloud-top > method versus the commonly used cloud-top

L27: As lightning > While lightning

L28: have reported 5 – 16% increases > is predicted to increase by 5 – 16%

Fixed.

Finney et al. (2018) found different impacts on atmospheric composition and radiative forcing when simulating future lightning using a new upward cloud ice flux (IFLUX) **method versus the commonly used** cloud-top height (CTH) approach. **While lightning is predicted to increase by 5 — 16%** over the next century with the CTH approach (Clark et al., 2017; Banerjee et al., 2014; Krause et al., 2014), a 15% decrease in lightning was estimated with IFLUX in 2100 under a strong global warming scenario (Finney et al., 2018).

4) L41: qualified > quantified

Fixed.

Recent studies have determined and **quantified** LNO_x using satellite observations.

5) L50: it is > this study

L50: without the contribution > and did not consider the contribution

Fixed.

However, **this study** assumed that all the enhanced NO₂ originated from lightning and **did not consider the contribution** of anthropogenic emissions.

6) L53: Replace sentence beginning with “The threshold of” > Their analysis was restricted to 30×60 km² satellite pixels where the flash rate exceeded 1 flash km⁻² hr⁻¹.

L54: But the results of LNO_x production are highly > But they found LNO_x production to be highly

Fixed.

Their analysis was restricted to $30 \times 60 \text{ km}^2$ satellite pixels where the flash rate exceeded $1 \text{ flash km}^{-2} \text{ hr}^{-1}$. But they found LNO_x production to be highly variable and correlations between flash rate densities and LNO_x production are low in some cases.

7) L72: removed by the weighted > removed by subtracting the weighted

L72: CRF criteria but has > CRF criteria required to be considered deep convection but has

Fixed.

The tropospheric NO_x background was removed by **subtracting** temporal average of NO_x at each box where the value was weighted by the number of OMI pixels which meet the optical cloud pressure and CRF criteria **required to be considered deep convection** but has 1 flash or less instead.

8) L76: at those locations > at some locations

Fixed.

However, there were negative LNO_x values caused by the overestimation of the tropospheric background at **some** locations.

9) L77: On another hand > On the other hand

L79: by strokes > using mean values of strokes

Fixed.

On the other hand, Lapierre et al. (2019) constrained LNO_2 to $1.1 \pm 0.6 \text{ mol NO}_2/\text{stroke}$ for intracloud (IC) strokes and $10.0 \pm 4.9 \text{ mol NO}_2/\text{stroke}$ for cloud-to-ground (CG) strokes over the continental US (CONUS). LNO_2 per stroke was scaled to $54.4 \text{ mol NO}_x/\text{flash}$ **using mean values of strokes** per flash and the ratio of NO to NO_2 in the UT.

10) L80: NO_2 can be "seen" > NO_2 that can be "seen"

Fixed.

They used the regrided Berkeley High-Resolution (BEHR) V3.0A $0.05^\circ \times 0.05^\circ$ "visible only" NO_2 VCD (V_{vis}) product which includes two parts of NO_2 **that** can be "seen" by the satellite.

11) L94: we focused on > we focus on

Fixed.

In this paper, we **focus** on the estimation of LNO_2 production per flash ($\text{LNO}_2/\text{flash}$) ...

12) L99: examines different sources of the uncertainty of > examines the effect of different sources of uncertainty on the

Fixed.

Section 4 examines **the effect of** different sources of the uncertainty **on** the results.

13) L128: and the detection > and found the detection

L128: are 88% > to be 88%

L130: corrected by 88% and 45% > divided by 0.88 and 0.45

Fixed.

Lapierre et al. (2019) also compared combined ENTLN and the NLDN dataset with data from the LIS during 2014 and **found** the detection efficiencies of IC flashes and strokes **to be** 88% and 45%, respectively. Since we only use the ENTLN data in 2014 as Lapierre et al. (2019) and NLDN detection efficiency of IC pulses should be lower than 33% which is calculated by the data in 2016 (Zhu et al., 2016), only the IC flashes and strokes are **divided by 0.88 and 0.45**, respectively, while CG flashes and strokes are unchanged because of the high detection efficiency.

14) L137: was used to generate > were used to generate

Fixed.

Outputs from the version 4 of Model for Ozone and Related chemical Tracers (MOZART-4; Emmons et al., 2010) **were** used to generate the initial and boundary conditions of chemical species.

15) L170: part of the NO₂ originated from lightning > part of the NO₂ within the cloud originating from lightning

Fixed.

The sensitivity study of Beirle et al. (2009) compared the chemical compositions from the cloud bottom to the cloud top and revealed that a significant fraction the NO₂ within the cloud **originating** from lightning can be detected by the satellite.

16) L180: convections > convection

Fixed.

Furthermore, another criterion of cloud fractions (CFs) is applied to the WRF-Chem results for the successful simulation of **convection**.

17) L184: properties of cloud > cloud properties

Fixed.

Besides **cloud properties**, the time period and sufficient flashes (or strokes) are required for fresh LNO_x detected by OMI.

18) L187: box⁻¹ are chosen > box⁻¹ per 2.4 hour time window are chosen

Fixed.

Meanwhile, 2400 flashes box⁻¹ and 8160 strokes box⁻¹ **per 2.4 hour time window** are chosen as sufficient for detecting LNO_x (Lapierre et al., 2019).

19) L191: sources except LNO₂ > sources in addition to LNO₂

Fixed.

In view of other NO₂ sources **in addition to** LNO₂, the ratio of modeled lightning NO₂ above cloud (LNO₂Vis) to modeled NO₂ above cloud (NO₂Vis) is defined to check whether enough LNO₂ can be detected by OMI.

20) L208: search of NO₂ > search of the NO₂

L206-210: When referring to combinations use the abbreviations given in Table 1.

Rewritten.

A daily search of **the** NO₂ product for coincident ENTLN flash (stroke) data results in 99 (102) valid days under the CRF90_ENTLN condition. Taking the flashes type ENTLN data as an example, the number of valid days decreases from 99 to 81 **under the CRF90_ENTLN_TL1000_ratio50 condition**, while LNO_x/flash increases from 86.0 ± 14.0 mol/flash to 114.8 ± 18.2 mol/flash. The result is almost the same as that under **the CRF90_ENTLN_TL1000 condition which is without the condition of ratio ≥ 50%**.

21) L225: productions are > production values are

Fixed.

LNO₂ **production values** are mostly in the range from 20 to 80 mol/flash.

22) L275: 0.8 to 0.2 while the cloud is higher (smaller pressure value) > 0.8 to 0.2 as the cloud pressure decreases from 600 to 300 hPa. Note: Please correct my pressure ranges if incorrect.

Fixed, thanks. The range of cloud pressure is right.

Since the ratio of LNO₂Vis to LNO₂ decreases from 0.8 to 0.2 **as the cloud pressure decreases from 600 to 300 hPa ...**

23) L279: we can not derive that higher LNO₂ production relates to higher clouds > we cannot derive the relationship between LNO₂ production and cloud pressure

Fixed.

Because of the limited amount of large LNO₂ production and lightning data, we cannot derive **the relationship between LNO₂ production and cloud pressure** or different lightning properties at this stage.

24) L284: larger than normal > larger in anomalous than normal

Fixed.

Because updrafts are stronger and flash rates are higher in anomalous storms, UT LNO_x concentrations is **larger in anomalous than normal** polarity storms.

25) L292: chose the same method > chose the same value

Fixed.

Zhao et al. (2009) set a NO_x production rate of 250 mol NO per flash in a regional-scale model, while Bela et al. (2016) chose the **same value** (330 mol NO per flash) that was used by Barth et al. (2012).

26) L313: relative distribution > relative distributions

L314: is similar > are similar

L315: the unrealistic > an unrealistic

Fixed.

Although the **relative distributions** of mean LNO and LNO₂ profiles **are** similar in both regions, the magnitude differs with a factor of 10. This phenomenon implies that the performance of lightning parameterization in WRF-Chem is region dependent and **an** unrealistic profile could appear in the UT.

27) L319: carefully in our research > carefully into consideration

Fixed.

However, the relative distribution of LNO₂ within the UT should be **taken carefully into consideration**.

28) L321: are involved > are important

Fixed.

When the condition of high LNO₂/NO₂ is not met, both relative distribution and ratio are **important**.

29) L401: find that the regionally > find a regionally

Rewritten.

Finally, implementing profiles generated with different model settings of lightning (1×200 mol NO flash⁻¹ and 2×500 mol NO flash⁻¹), we find that the larger LNO production in model leads to larger retrieval of LNO_x despite some regionally dependent effects.

30) L403: pollutions than > pollution than

Fixed.

Since other regions, like China and India, have much more NO₂ **pollution** than the CONUS, it is necessary to consider the background NO₂ in detail.

31) L409: level > scales

Fixed.

Applying current method in future studies may enhance the accuracy of LNO_x production at both local and global **scales**.

References

- Allen, D. J., Pickering, K. E., Bucsel, E. J., Krotkov, N., and Holzworth, R.: Lightning NO_x Production in the Tropics as Determined Using OMI NO₂ Retrievals and WWLLN Stroke Data, *Journal of Geophysical Research: Atmospheres*, <https://doi.org/10.1029/2018JD029824>, 2019.
- Banerjee, A., Archibald, A. T., Maycock, A. C., Telford, P., Abraham, N. L., Yang, X., Braesicke, P., and Pyle, J. A.: Lightning NO_x, a key chemistry–climate interaction: impacts of future climate change and consequences for tropospheric oxidising capacity, *Atmospheric Chemistry and Physics*, 14, 9871–9881, <https://doi.org/10.5194/acp-14-9871-2014>, 2014.
- Barth, M. C., Lee, J., Hodzic, A., Pfister, G., Skamarock, W. C., Worden, J., Wong, J., and Noone, D.: Thunderstorms and upper troposphere chemistry during the early stages of the 2006 North American Monsoon, *Atmospheric Chemistry and Physics*, 12, 11 003–11 026, <https://doi.org/10.5194/acp-12-11003-2012>, 2012.
- Beirle, S., Salzmann, M., Lawrence, M. G., and Wagner, T.: Sensitivity of satellite observations for freshly produced lightning NO_x, *Atmospheric Chemistry and Physics*, 9, 1077–1094, <https://doi.org/10.5194/acp-9-1077-2009>, 2009.
- Bela, M. M., Barth, M. C., Toon, O. B., Fried, A., Homeyer, C. R., Morrison, H., Cummings, K. A., Li, Y., Pickering, K. E., Allen, D. J., Yang, Q., Wennberg, P. O., Crouse, J. D., St. Clair, J. M., Teng, A. P., O’Sullivan, D., Huey, L. G., Chen, D., Liu, X., Blake, D. R., Blake, N. J., Apel, E. C., Hornbrook, R. S., Flocke, F., Campos, T., and Diskin, G.: Wet scavenging of soluble gases in DC3 deep convective storms using WRF-Chem simulations and aircraft observations, *Journal of Geophysical Research: Atmospheres*, 121, 4233–4257, <https://doi.org/10.1002/2015JD024623>, 2016.
- Bucsel, E. J., Pickering, K. E., Allen, D. J., Holzworth, R., and Krotkov, N. A.: Midlatitude lightning NO_x production efficiency inferred from OMI and WWLLN data, *Journal of Geophysical Research: Atmospheres*, <https://doi.org/10.1029/2019JD030561>, 2019.
- Clark, S. K., Ward, D. S., and Mahowald, N. M.: Parameterization-based uncertainty in future lightning flash density, *Geophysical Research Letters*, 44, 2893–2901, <https://doi.org/10.1002/2017GL073017>, 2017.
- DeCaria, A. J., Pickering, K. E., Stenchikov, G. L., Scala, J. R., Stith, J. L., Dye, J. E., Ridley, B. A., and Laroche, P.: A cloud-scale model study of lightning-generated NO_x in an individual thunderstorm during STERAO-A, *Journal of Geophysical Research*, 105, 11 601–11 616, <https://doi.org/10.1029/2000JD900033>, 2000.
- DeCaria, A. J., Pickering, K. E., Stenchikov, G. L., and Ott, L. E.: Lightning-generated NO_x and its impact on tropospheric ozone production: A three-dimensional modeling study of a Stratosphere-Troposphere Experiment: Radiation, Aerosols and Ozone (STERAO-A) thunderstorm, *Journal of Geophysical Research*, 110, n/a–n/a, <https://doi.org/10.1029/2004JD005556>, 2005.
- Emmons, L. K., Walters, S., Hess, P. G., Lamarque, J.-F., Pfister, G. G., Fillmore, D., Granier, C., Guenther, A., Kinnison, D., Laepple, T., Orlando, J., Tie, X., Tyndall, G., Wiedinmyer, C., Baughcum, S. L., and Kloster, S.: Description and evaluation of the Model for Ozone and Related chemical Tracers, version 4 (MOZART-4), *Geoscientific Model Development*, 3, 43–67, <https://doi.org/10.5194/gmd-3-43-2010>, 2010.
- EPA, U.: 2011 National Emissions Inventory, version 2—Technical support document, US Environmental Protection Agency, Office of Air Quality Planning and Standards. Accessed August 2017., 2015.
- Finney, D. L., Doherty, R. M., Wild, O., Stevenson, D. S., MacKenzie, I. A., and Blyth, A. M.: A projected decrease in lightning under climate change, *Nature Climate Change*, 8, 210–213, <https://doi.org/10.1038/s41558-018-0072-6>, 2018.
- Krause, A., Kloster, S., Wilkenskeld, S., and Paeth, H.: The sensitivity of global wildfires to simulated past, present, and future lightning frequency, *Journal of Geophysical Research: Biogeosciences*, 119, 312–322, <https://doi.org/10.1002/2013JG002502>, 2014.
- Krotkov, N. A., Lamsal, L. N., Celarier, E. A., Swartz, W. H., Marchenko, S. V., Bucsel, E. J., Chan, K. L., Wenig, M., and Zara, M.: The version 3 OMI NO₂ standard product, *Atmospheric Measurement Techniques*, 10, 3133–3149, <https://doi.org/10.5194/amt-10-3133-2017>, 2017.
- Kuhlmann, G., Hartl, A., Cheung, H. M., Lam, Y. F., and Wenig, M. O.: A novel gridding algorithm to create regional trace gas maps from satellite observations, *Atmospheric Measurement Techniques*, 7, 451–467, <https://doi.org/10.5194/amt-7-451-2014>, 2014.
- Lapierre, J. L., Laughner, J. L., Geddes, J. A., Koshack, W., Cohen, R. C., and Pusede, S. E.: Observing regional variability in lightning NO_x production rates, *Journal of Geophysical Research*, in review, 2019.
- Laughner, J. L. and Cohen, R. C.: Quantification of the effect of modeled lightning NO₂ on UV–visible air mass factors, *Atmospheric Measurement Techniques*, 10, 4403–4419, <https://doi.org/10.5194/amt-10-4403-2017>, 2017.
- Li, Y., Pickering, K. E., Barth, M. C., Bela, M. M., Cummings, K. A., and Allen, D. J.: Evaluation of Parameterized Convective Transport of Trace Gases in Simulation of Storms Observed During the DC3 Field Campaign, *Journal of Geophysical Research: Atmospheres*, 123, 11,238–11,261, <https://doi.org/10.1029/2018JD028779>, 2018.
- Nault, B. A., Laughner, J. L., Woodriddle, P. J., Crouse, J. D., Dibb, J., Diskin, G., Peischl, J., Podolske, J. R., Pollack, I. B., Ryerson, T. B., Scheuer, E., Wennberg, P. O., and Cohen, R. C.: Lightning NO_x Emissions: Reconciling Measured and Modeled Estimates With Updated NO_x Chemistry, *Geophysical Research Letters*, 44, 9479–9488, <https://doi.org/10.1002/2017GL074436>, 2017.

- Pickering, K. E., Bucsele, E., Allen, D., Ring, A., Holzworth, R., and Krotkov, N.: Estimates of lightning NO_x production based on OMI NO_2 observations over the Gulf of Mexico, *Journal of Geophysical Research: Atmospheres*, 121, 8668–8691, <https://doi.org/10.1002/2015JD024179>, 2016.
- Price, C. and Rind, D.: A simple lightning parameterization for calculating global lightning distributions, *Journal of Geophysical Research*, 97, 9919–9933, <https://doi.org/10.1029/92JD00719>, 1992.
- Rudlosky, S.: Evaluating ENTLN performance relative to TRMM/LIS, *Journal of Operational Meteorology*, 3, 11–20, <https://doi.org/10.15191/nwajom.2015.0302>, 2015.
- Silvern, R. F., Jacob, D. J., Travis, K. R., Sherwen, T., Evans, M. J., Cohen, R. C., Laughner, J. L., Hall, S. R., Ullmann, K., Crouse, J. D., Wennberg, P. O., Peischl, J., and Pollack, I. B.: Observed NO/NO_2 ratios in the upper troposphere imply errors in $\text{NO}-\text{NO}_2-\text{O}_3$ cycling kinetics or an unaccounted NO_x reservoir, *Geophysical Research Letters*, <https://doi.org/10.1029/2018GL077728>, 2018.
- Strode, S. A., Douglass, A. R., Ziemke, J. R., Manyin, M., Nielsen, J. E., and Oman, L. D.: A Model and Satellite-Based Analysis of the Tropospheric Ozone Distribution in Clear Versus Convectively Cloudy Conditions, *Journal of Geophysical Research: Atmospheres*, 122, 11,948–11,960, <https://doi.org/10.1002/2017JD027015>, 2017.
- Travis, K. R., Jacob, D. J., Fisher, J. A., Kim, P. S., Marais, E. A., Zhu, L., Yu, K., Miller, C. C., Yantosca, R. M., Sulprizio, M. P., Thompson, A. M., Wennberg, P. O., Crouse, J. D., St Clair, J. M., Cohen, R. C., Laughner, J. L., Dibb, J. E., Hall, S. R., Ullmann, K., Wolfe, G. M., Pollack, I. B., Peischl, J., Neuman, J. A., and Zhou, X.: Why do Models Overestimate Surface Ozone in the Southeastern United States?, *Atmospheric Chemistry and Physics*, 16, 13 561–13 577, <https://doi.org/10.5194/acp-16-13561-2016>, 2016.
- Xu, K.-M. and Randall, D. A.: A Semiempirical Cloudiness Parameterization for Use in Climate Models, *Journal of the Atmospheric Sciences*, 53, 3084–3102, [https://doi.org/10.1175/1520-0469\(1996\)053<3084:ASCPFU>2.0.CO;2](https://doi.org/10.1175/1520-0469(1996)053<3084:ASCPFU>2.0.CO;2), 1996.
- Zhao, C., Wang, Y., Choi, Y., and Zeng, T.: Summertime impact of convective transport and lightning NO_x production over North America: modeling dependence on meteorological simulations, *Atmospheric Chemistry and Physics*, 9, 4315–4327, <https://doi.org/10.5194/acp-9-4315-2009>, 2009.
- Zhu, Y., Rakov, V. A., Tran, M. D., and Nag, A.: A study of National Lightning Detection Network responses to natural lightning based on ground truth data acquired at LOG with emphasis on cloud discharge activity, *Journal of Geophysical Research: Atmospheres*, 121, 14,651–14,660, <https://doi.org/10.1002/2016JD025574>, 2016.

Estimates of Lightning NO_x Production based on High Resolution OMI NO₂ Retrievals over the Continental US

Response to Anonymous Referee #2

Xin Zhang, Yan Yin, Ronald van der A, Jeff L. Lapierre, Qian Chen,
Xiang Kuang, Shuqi Yan, Jinghua Chen, Chuan He and Rulin Shi

February 7, 2020

We thank the reviewer for his/her positive comments and very careful reading of the main article. The individual corrections suggested are addressed below. The reviewer's comments will be shown in **red**, our response in **blue**, and changes made to the paper are shown in **black** block quotes. Unless otherwise indicated, page and line numbers correspond to the original paper. Figures, tables, or equations referenced as "Rn" are numbered within this response; if these are used in the changes to the paper, they will be replaced with the proper number in the final paper.

Major Comments

The new methods that are discussed should provide better accounting for background NO_x; however, it is not made clear in the manuscript how this is achieved. This point needs to be addressed in a revision.

Thank you for your advice. This is the same comment mentioned by Reviewer#1 (See *No. 1, Sect. General Comments*). We have made it clearer in a new section (Sect. 3.3).

Minor Comments

1) Line 10: previous work does not neglect below-cloud LNO₂. Full LNO₂ and LNO_x profiles extending to the surface are used from the GMI model is such work as Pickering et al. (2016); Bucseba et al. (2019); Allen et al. (2019).

Thank you for your correction. Instead of the negative spin on others' work, we have reformatted the sentence to put a positive spin on our method, as mentioned in the Response to Reviewer#1 (See *No. 1, Sect. Specific Comments*). Because Lapierre et al. (2019) neglected the below-cloud LNO₂, it is still necessary to mention that in the summarization of our results.

Focusing on the summer season during 2014, we find that the lightning NO₂ (LNO₂) PE is 44 ± 16 mol NO₂ flash⁻¹ and 8 ± 3 mol NO₂ stroke⁻¹ while LNO_x PE is 120 ± 52 mol NO_x flash⁻¹ and 22 ± 9 mol NO_x stroke⁻¹. **Results reveal that our method reduces sensitivity to the background NO₂ and includes much of the below-cloud LNO₂.**

2) line 15:surface are...

line 16: originates

Corrected.

Nitrogen oxides (NO_x) near the Earth's surface **are** mainly produced by soil, biomass burning and fossil fuel combustion, while NO_x in the middle and upper troposphere **originates** largely from lightning and aircraft emissions.

3) lines 26-27: ...radiative forcing between when simulating future lightning using a new upward cloud ice flux (IFLUX) method and when the commonly used cloud-top height (CTH) approach is used.

Corrected.

Finney et al. (2018) found different impacts on atmospheric composition and radiative forcing when simulating future lightning using a new upward cloud ice flux (IFLUX) **method versus the commonly used** cloud-top height (CTH) approach.

4) line 28-29: 5 – 16% increases in what? 15% decrease in what?

These percentage is relative to the current lightning. Corrected.

While **lightning** is predicted to increase by 5 — 16% over the next century with the CTH approach (Clark et al., 2017; Banerjee et al., 2014; Krause et al., 2014), a 15% **decrease in lightning** was estimated with IFLUX in 2100 under a strong global warming scenario (Finney et al., 2018).

5) line 30:radiative forcing due to ozone was found.... line 31: also need to compare with results of Romps et al. (2014)

We have reformatted the sentence and added the discussion of Romps et al. (2014) and Romps (2019).

As a result of the different effects on radiative forcing **from ozone and methane**, a net positive radiative forcing was found with the CTH approach while there is little net radiative forcing with the IFLUX approach (Finney et al., 2018). **However, the convective available potential energy (CAPE) times the precipitation rate (P) proxy predicts a $12 \pm 5\%$ increase in the Continental US (CONUS) lightning strike rate per kelvin of global warming (Romps et al., 2014), while the IFLUX proxy predicts the**

lightning will only increase 3.4%/K over the CONUS. Recently, Romps (2019) compared the CAPE \times P proxy and IFLUX method in cloud-resolving models. They report that higher CAPE and updraft velocities caused by global warming could lead to the large increases in tropical lightning simulated by CAPE \times P proxy, while IFLUX proxy predicts little change in tropical lightning because of the small changes in water mass fluxes.

6) line 39: Satellite...

Corrected.

Satellite measurements of NO₂ are a powerful tool compared to conventional platforms, because of its global coverage, constant instrument features and temporal continuity.

7) line 48: convection.

Corrected.

As these methods focus on monthly or yearly mean NO₂ column densities, more recent studies applied specific approaches to investigate LNO_x directly over active **convection**.

8) line 71:based on a modification of the method.... Need to describe what is different.

Thank you for your advice. We have added more descriptions about the method of Bucsele et al. (2019).

More recently Bucsele et al. (2019) obtained an average production efficiency (PE) of 180 ± 100 mol per flash over East Asia, Europe and North America based on **a modification of** the method used in Pickering et al. (2016). **A power function between LNO_x and lightning flash rate was established, while the minimum flash-rate threshold was not applied.**

9) line 75: Are you sure that it is the background subtraction causing the negatives? Many of the negatives resulted from the removal of the stratospheric slant column NO₂ from the total NO₂ slant column.

Sorry for the incomplete consideration. We have added the effect of overestimated stratospheric slant column NO₂ to the sentence.

However, there were negative LNO_x values caused by the overestimation of the tropospheric background **and stratospheric NO₂** at some locations.

10) line 80: two parts of NO₂ that can be....

Fixed.

They used the regridded Berkeley High-Resolution (BEHR) V3.0A $0.05^\circ \times 0.05^\circ$ "visible only" NO₂ VCD (V_{vis}) product which includes two parts of NO₂ **that** can be "seen" by the satellite.

11) line 81:above clouds (pixels with CRF > 0.9) and....

Fixed.

The first part is the NO₂ above clouds (**pixels with CRF > 0.9**) and the second part is the NO₂ detected from cloud free areas.

12) line 88:contamination by anthropogenic....

Corrected.

To apply the approach used by Bucselá et al. (2010), Pickering et al. (2016), Bucselá et al. (2019) and Lapierre et al. (2019) without geographic restrictions, contamination **by** anthropogenic emissions must be taken into account in detail.

13) lines 129-130: not sure why this phrase about NLDN is here when you are using ENTLN and not NLDN. Remove?

Because we only used ENTLN data instead of the combined ENTLN and NLDN dataset, it is necessary to clarify that the NLDN DE of IC pulses is lower than ENTLN's and ENTLN DE of CG flashes or strokes is high enough to keep unchanged.

Lapierre et al. (2019) also compared combined ENTLN and the NLDN dataset with data from the LIS during 2014 and found the detection efficiencies of IC flashes and strokes to be 88% and 45%, respectively. **Since we only use the ENTLN data in 2014 as Lapierre et al. (2019) and NLDN detection efficiency of IC pulses should be lower than 33% which is calculated by the data in 2016 (Zhu et al., 2016), only the IC flashes and strokes are divided by 0.88 and 0.45, respectively**, while CG flashes and strokes are unchanged because of the high detection efficiency.

14) line 142: How is flash rate parameterized?

The flash rate is parameterized by the Price and Rind level of neutral buoyancy parameterization.

In addition, lightning flash rate **based on the level of neutral buoyancy parameterization (Price and Rind, 1992)** and LNO_x parameterizations are activated (200 mol NO flash⁻¹, the factor to adjust the predicted number of flashes is set to 1; hereinafter referred to as "1×200 mol NO flash⁻¹").

15) line 175: how is this comparison of pixels computed?

The area of one satellite pixel is about 312 km². The minimum count of 0.5×0.5 degree grids per box is set to 50 (~ 1300 km²) which is between 3 satellite pixels (~ 940 km²) used in Bucselá et al. (2019) and 5 satellite pixels (~ 1560 km²) set in Pickering et al. (2016). In other words, the number of 50 should be enough to minimize the noise. We have written the sentence to make it more clear.

Then, it is analyzed in 1° × 1° grid boxes with a minimum of fifty valid 0.05° × 0.05° grids **to minimize the noise. The minimum value is between five satellite pixels in Pickering et al. (2016) and three satellite pixels in Bucselá et al. (2019) or Allen et al. (2019).**

16) line 181: Does the Xu and Randall method consider subgrid convective clouds or only grid-scale cloud based on the microphysics parameterization that generates the gridscale clouds? If it is the latter, this method is not appropriate as a criterion to evaluate model convection.

We applied the Xu and Randall method based on the ice and cloud water fields from both Grell 3D cumulus parameterization and Lin microphysics scheme.

17) line 184: a time period.....LNO_x to be detected by

Corrected.

Besides cloud properties, a time period and sufficient flashes (or strokes) are required for fresh LNO_x to be detected by OMI.

18) lines 184-188: Using these criteria will result in a low bias in the PE results. Bucselá et al. (2019) found that PE is larger at small flash rates. These small flash rates are being discarded here.

Thank you for your remind about the smaller PE at high flash rates. We have added these information at the end of the paragraph.

These criteria will result in a low bias in the PE results, as Bucselá et al. (2019) found that the PE is larger at small flash rates which are discarded here.

19) line 203: daily summations Is this what is done in Pickering et al. (2016)?

Yes. But, we discussed with Eric J. Bucselá recently and he suggested us to redo the linear regressions based on the daily mean LNO_x and flashes. As a result, we have updated the plots of linear regression and analysis related to that.

(1) summation method: dividing the sum of LNO_x by the sum of flashes (or strokes) in each 1° × 1° box in MJJA 2014;

(2) linear regression method: applying the linear regression to daily **mean values** of LNO_x and flashes (or strokes).

20) line 218:....(Table 2), as the CRF criterion increases from 70% to 90% and to 100%.

Fixed.

Apart from the fewer valid days under higher CRF conditions (CRF ≥ 90% and CRF = 100%), LNO_x/flash increases from 109.0 ± 15.3 mol/flash to 114.8 ± 18.2 mol/flash and decreases again to 99.4 ± 15.3 mol/flash while LNO_x/stroke enhances from 16.7 ± 2.6 mol/stroke to 17.8 ± 2.9 mol/stroke and drops again to 15.6 ± 3.1 mol/stroke (Table 3), **as the CRF criterion increases from 70% to 90% and to 100%.**

21) line 223:....to derive production per flash (production efficiency, PE).

Fixed.

In order for our results to be comparable with those of Pickering et al. (2016) and Lapierre et al. (2019), we choose NO₂ instead of NO_x to derive production **per flash (production efficiency, PE)**.

22) line 228: cloud properties

line 229: PEs

Corrected.

The effect of **cloud properties** on LNO_x production will be discussed in more detail in section 3.3. Generally, the order of estimated daily **PEs** is LNO₂Clean > LNO₂ > NO₂Vis > LNO₂Vis.

23) line 259: ratio of CG to IC I don't think there was any particular assumption of this ratio in Pickering et al. (2016).

Yes, you are right. Because Lapiere et al. (2019) found evidence that CG strokes produce more NO_2 than IC strokes and Pickering et al. (1996) focused on the Gulf of Mexico, that ratio could lead to the different results. Since the geographic location has been mentioned in the sentence, we have deleted the ratio of CG to IC.

... possibly due to the differences in geographic location, lightning data and chemistry model considered by Pickering et al. (2016) and this study.

24) lines 263-264: this is not obvious from the Figure 5 plots

To make it clear, we have replotted that figure with annotation (Fig. R1).

The LNO_2 and LNO_x production are both higher in the Southeast U.S. (denoted by the red box in Fig. 5 panels, $75^\circ\text{W} - 95^\circ\text{W}$, $25^\circ\text{N} - 37^\circ\text{N}$), consistent with Lapiere et al. (2019) and Bucsela et al. (2019).

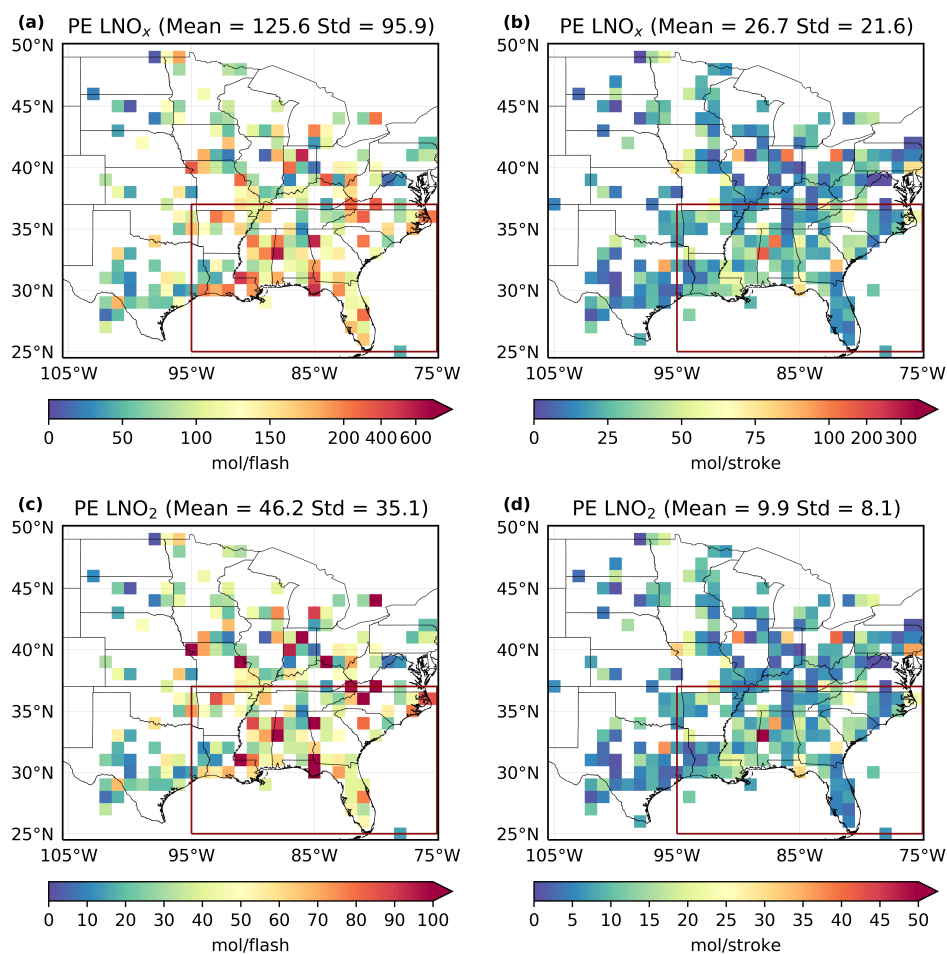


Figure R1 . (a) and (c) Maps of $1^\circ \times 1^\circ$ gridded values of mean LNO_x and LNO_2 production per flash with $\text{CRF} \geq 90\%$ for MJJA 2014. (b) and (d) Same as (a) and (c) except for strokes. The southeastern US is denoted by the red box in panels a – d.

25) line 271: peaks of the LNO₂ profile are...

Corrected.

The ratio would also be smaller while **peaks of the LNO₂ profile are** below the CP.

26) line 275: from 0.8 to 0.2 as the cloud height increases ...

Thanks. We have corrected that sentence with exact interval of the cloud pressure.

Since the ratio of LNO₂Vis to LNO₂ decreases from 0.8 to 0.2 as the cloud pressure **decreases from 600 to 300 hPa** ...

27) line 278: LNO₂ production (< 30 mol/stroke) occurs

Corrected.

However, smaller LNO₂ **production (< 30 mol/stroke) occurs** on all levels between 650 hPa and 200 hPa.

28) line 284: Is this necessarily true? LNO_x production per flash may be smaller in high flash rate storms.

Sorry for the misleading. It should be the LNO_x concentrations instead of LNO_x production per flash. Corrected.

Because updrafts are stronger and flash rates are higher in anomalous storms, **UT LNO_x concentrations** is larger in anomalous than normal polarity storms.

29) lines 287-288: ... (postconvection) in which LNO_x has already been redistributed.....uses LNO_x production profiles.....(Allen et al., 2012; Luo et al., 2017)

Corrected.

There are mainly two methods of distributing LNO_x in models: LNO_x profiles (postconvection) **in which LNO_x has already been redistributed** by convective transport, while the other one (preconvection) **uses LNO_x production profiles** made before the redistribution of convective transport (Allen et al., 2012; Luo et al., 2017).

30) line 296: $2 \times 500 \text{ mol NO flash}^{-1}$ This designation can be confusing. Some readers may think you mean 1000 mol/flash

We prefer that designation, because we actually changed the adjusting factor and the LNO production at the same time instead of only changing the LNO production per flash. The definition of $1 \times 200 \text{ mol NO flash}^{-1}$ has been used in the model description (Section 2.3). If readers think we use 1000 mol/flash, that should be fine because the effect of that on LNO_x estimation is the same.

31) line 308: different than that....

Corrected.

Note that the LNO₂ accounts for a fraction of NO₂ above the clouds, the magnitude of increasing denominator could be **different than that** of increasing numerator, resulting in a different effect on the AMF_{LNO₂} and AMF_{LNO_x}.

32) line 401-402: we find that the effect is regionally dependent. Both.....NO₂ cause different comprehensive effects due to nonlinear.....

Thanks. We have rewritten these sentences.

Finally, implementing profiles generated with different model settings of lightning ($1 \times 200 \text{ mol NO flash}^{-1}$ and $2 \times 500 \text{ mol NO flash}^{-1}$), we find that **the larger LNO production model setting leads to larger retrieval of LNO_x despite some regionally dependent effects**. Both the ratio of the tropospheric LNO₂ above the cloud to the total tropospheric LNO₂ and the ratio of LNO₂ to NO₂ **cause different comprehensive effects due to** the nonlinear calculation of AMF_{LNO₂} and AMF_{LNO_x}.

33) Table 2: How many grid boxes per day typically qualify under your criteria?

The mean number of valid grid boxes is 4.2 and 5.3 for flash and stroke data, respectively, as shown in the time series of valid grid boxes (Fig. R2).

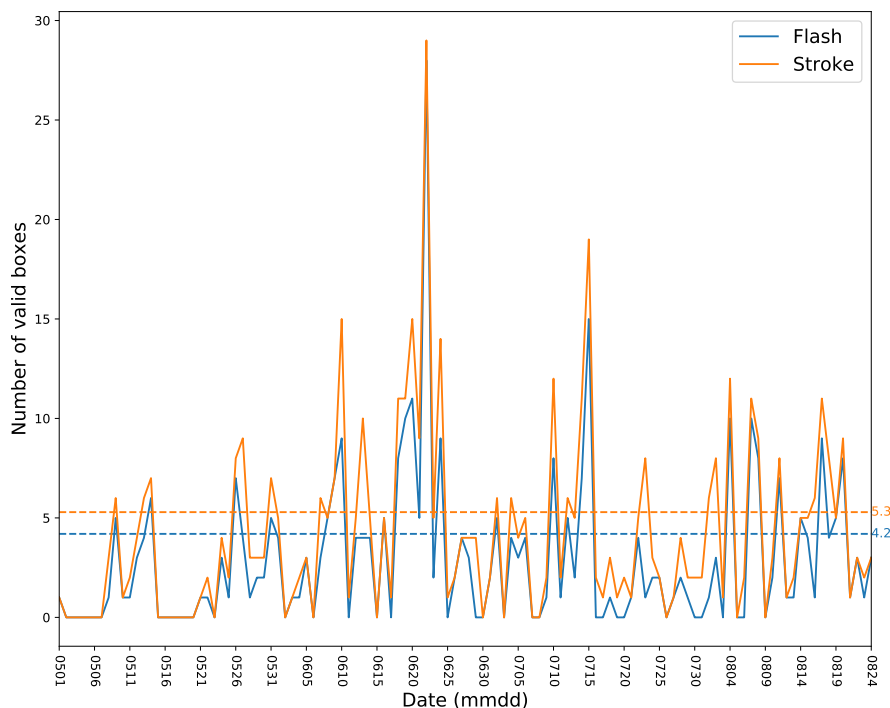


Figure R2 . Time series of valid grid boxes over the CONUS for MJJA 2014 with the criteria (CRF $\geq 90\%$, entln flashes(strokes) $\geq 2400(8160)$, TL ≥ 1000 and ratio $\geq 50\%$).

34) Table 3: Need to indicate how the percentage difference was calculated in the caption. Which one was in the denominator?

The percentage difference was calculated by raising and lowering the perturbed value, this will effectively calculate a mean percent difference. The equation is: $PE_{\text{uncertainty}} = (\text{Error}_{\text{raising perturbed value}} - \text{Error}_{\text{lowering perturbed value}})/2$ where $\text{Error}_{\text{perturbed value}} = (PE_{\text{perturbed value}} - PE_{\text{original value}})/PE_{\text{original value}}$. We have added these information to the caption of that table (Table R1).

Table R1 . Uncertainties for the estimation of LNO₂/flash, LNO_x/flash, LNO₂/stroke and LNO_x/stroke.

Type	Perturbation	LNO ₂ /flash ⁵	LNO _x /flash ⁵	LNO ₂ /stroke ⁵	LNO _x /stroke ⁵
BEHR tropopause pressure ¹	NASA product tropopause	6	4	6	4
Cloud radiance fraction ¹	± 5%	2	2	2	2
Cloud pressure ²	Constant AMF: 0.46	23	23	23	23
Surface pressure ¹	± 1.5%	0	0	0	0
Surface reflectivity ¹	± 17%	0	0	0	0
LNO ₂ profile ¹	2×500 mol NO flash ⁻¹	15	29	14	29
Profile location ¹	Quasi-Monte Carlo	0	1	0	1
Lightning detection efficiency ³	IC: ± 16%, CG: ± 5%	15	15	15	15
t _{window} ³	2 – 4 hours	10	10	8	8
LNO _x lifetime ³	2 – 12 hours	24	24	24	24
V _{strat} ⁴	-	10	10	10	10
Systematic errors in slant column ⁴	-	5	5	5	5
Tropospheric background ⁴	-	10	10	10	10
NO/NO ₂ ⁴	-	20	20	20	20
Net	-	48	54	47	54

$PE_{\text{uncertainty}} = (\text{Error}_{\text{raising perturbed value}} - \text{Error}_{\text{lowering perturbed value}})/2$ where $\text{Error}_{\text{perturbed value}} = (PE_{\text{perturbed value}} - PE_{\text{original value}})/PE_{\text{original value}}$.

¹Laughner et al. (2019) ²Beirle et al. (2009) ³Lapierre et al. (2019) ⁴Allen et al. (2019) and Bucsele et al. (2019) ⁵Uncertainty (%)

35) Figures 7 and 8: What do the various colors of shading indicate? What are the scales for the horizontal plot at the top and the vertical plot on the side?

The colors of shading correspond to the regions, which contain the respective normalized density estimated by kernel density estimation, using kdeplot in the Python package named seaborn (<https://seaborn.pydata.org/generated/seaborn.kdeplot.html>). Because the shading has shown the density, the marginal plots have been removed in case of any confusions (Fig. R3).

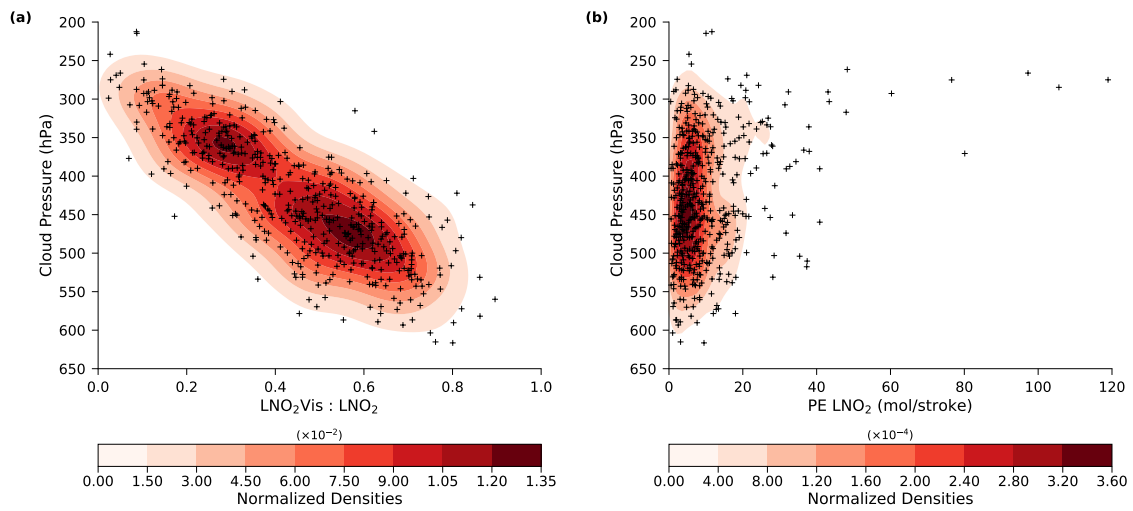


Figure R3 . Kernel density estimation of the (a) daily ratio of LNO_2Vis to LNO_2 and (b) daily LNO_2 production efficiency versus the daily cloud pressure measured by OMI with $\text{CRF} \geq 90\%$ for MJJA 2014.

References

- Allen, D. J., Pickering, K. E., Pinder, R. W., Henderson, B. H., Appel, K. W., and Prados, A.: Impact of lightning-NO on eastern United States photochemistry during the summer of 2006 as determined using the CMAQ model, *Atmospheric Chemistry and Physics*, 12, 1737–1758, <https://doi.org/10.5194/acp-12-1737-2012>, 2012.
- Allen, D. J., Pickering, K. E., Bucsel, E. J., Krotkov, N., and Holzworth, R.: Lightning NO_x Production in the Tropics as Determined Using OMI NO₂ Retrievals and WWLLN Stroke Data, *Journal of Geophysical Research: Atmospheres*, <https://doi.org/10.1029/2018JD029824>, 2019.
- Banerjee, A., Archibald, A. T., Maycock, A. C., Telford, P., Abraham, N. L., Yang, X., Braesicke, P., and Pyle, J. A.: Lightning NO_x, a key chemistry–climate interaction: impacts of future climate change and consequences for tropospheric oxidising capacity, *Atmospheric Chemistry and Physics*, 14, 9871–9881, <https://doi.org/10.5194/acp-14-9871-2014>, 2014.
- Beirle, S., Salzmann, M., Lawrence, M. G., and Wagner, T.: Sensitivity of satellite observations for freshly produced lightning NO_x, *Atmospheric Chemistry and Physics*, 9, 1077–1094, <https://doi.org/10.5194/acp-9-1077-2009>, 2009.
- Bucsel, E. J., Pickering, K. E., Huntemann, T. L., Cohen, R. C., Perring, A., Gleason, J. F., Blakeslee, R. J., Albrecht, R. I., Holzworth, R., Cipriani, J. P., Vargas-Navarro, D., Mora-Segura, I., Pacheco-Hernández, A., and Laporte-Molina, S.: Lightning-generated NO_x seen by the Ozone Monitoring Instrument during NASA's Tropical Composition, Cloud and Climate Coupling Experiment (TC⁴), *Journal of Geophysical Research*, 115, 793, <https://doi.org/10.1029/2009JD013118>, 2010.
- Bucsel, E. J., Pickering, K. E., Allen, D. J., Holzworth, R., and Krotkov, N. A.: Midlatitude lightning NO_x production efficiency inferred from OMI and WWLLN data, *Journal of Geophysical Research: Atmospheres*, <https://doi.org/10.1029/2019JD030561>, 2019.
- Clark, S. K., Ward, D. S., and Mahowald, N. M.: Parameterization-based uncertainty in future lightning flash density, *Geophysical Research Letters*, 44, 2893–2901, <https://doi.org/10.1002/2017GL073017>, 2017.
- Finney, D. L., Doherty, R. M., Wild, O., Stevenson, D. S., MacKenzie, I. A., and Blyth, A. M.: A projected decrease in lightning under climate change, *Nature Climate Change*, 8, 210–213, <https://doi.org/10.1038/s41558-018-0072-6>, 2018.
- Krause, A., Kloster, S., Wilkenskeld, S., and Paeth, H.: The sensitivity of global wildfires to simulated past, present, and future lightning frequency, *Journal of Geophysical Research: Biogeosciences*, 119, 312–322, <https://doi.org/10.1002/2013JG002502>, 2014.
- Lapierre, J. L., Laughner, J. L., Geddes, J. A., Koshack, W., Cohen, R. C., and Pusede, S. E.: Observing regional variability in lightning NO_x production rates, *Journal of Geophysical Research*, in review, 2019.
- Laughner, J. L., Zhu, Q., and Cohen, R. C.: Evaluation of version 3.0B of the BEHR OMI NO₂ product, *Atmospheric Measurement Techniques*, 12, 129–146, <https://doi.org/10.5194/amt-12-129-2019>, 2019.
- Luo, C., Wang, Y., and Koshak, W. J.: Development of a self-consistent lightning NO_x simulation in large-scale 3-D models, *Journal of Geophysical Research: Atmospheres*, 122, 3141–3154, <https://doi.org/10.1002/2016JD026225>, 2017.
- Pickering, K. E., Thompson, A. M., Wang, Y., Tao, W.-K., McNamara, D. P., Kirchhoff, V. W. J. H., Heikes, B. G., Sachse, G. W., Bradshaw, J. D., Gregory, G. L., and Blake, D. R.: Convective transport of biomass burning emissions over Brazil during TRACE A, *Journal of Geophysical Research*, 101, 23 993–24 012, <https://doi.org/10.1029/96JD00346>, 1996.
- Pickering, K. E., Bucsel, E., Allen, D., Ring, A., Holzworth, R., and Krotkov, N.: Estimates of lightning NO_x production based on OMI NO₂ observations over the Gulf of Mexico, *Journal of Geophysical Research: Atmospheres*, 121, 8668–8691, <https://doi.org/10.1002/2015JD024179>, 2016.
- Price, C. and Rind, D.: A simple lightning parameterization for calculating global lightning distributions, *Journal of Geophysical Research*, 97, 9919–9933, <https://doi.org/10.1029/92JD00719>, 1992.
- Romps, D. M.: Evaluating the future of lightning in cloud-resolving models, *Geophysical Research Letters*, <https://doi.org/10.1029/2019GL085748>, 2019.
- Romps, D. M., Seeley, J. T., Vollaro, and Molinari, J.: Projected increase in lightning strikes in the United States due to global warming, *Atmospheric Chemistry and Physics*, 14, 851–854, <https://doi.org/10.1126/science.1259100>, 2014.
- Zhu, Y., Rakov, V. A., Tran, M. D., and Nag, A.: A study of National Lightning Detection Network responses to natural lightning based on ground truth data acquired at LOG with emphasis on cloud discharge activity, *Journal of Geophysical Research: Atmospheres*, 121, 14,651–14,660, <https://doi.org/10.1002/2016JD025574>, 2016.

Estimates of Lightning NO_x Production based on High Resolution OMI NO₂ Retrievals over the Continental US

Response to Anonymous Referee #3

Xin Zhang, Yan Yin, Ronald van der A, Jeff L. Lapierre, Qian Chen,
Xiang Kuang, Shuqi Yan, Jinghua Chen, Chuan He and Rulin Shi

February 7, 2020

We thank the reviewer for his/her positive comments and very careful reading of the main article. The individual corrections suggested are addressed below. The reviewer's comments will be shown in **red**, our response in **blue**, and changes made to the paper are shown in **black** block quotes. Unless otherwise indicated, page and line numbers correspond to the original paper. Figures, tables, or equations referenced as "Rn" are numbered within this response; if these are used in the changes to the paper, they will be replaced with the proper number in the final paper.

Major Comments

1) The authors derive equations for LNO_x by treating clouds as reflecting surfaces. This simplification is required for many radiative transfer models which can not handle multiple scattering in 3d clouds. Thus, several previous studies follow this approach. However, the authors should still be aware of this simplification and state this clearly in the manuscript. Formulations like "NO₂ above/below the cloud" are misleading, as for thick thunderstorm clouds, most of the LNO_x is WITHIN the cloud, with a high sensitivity from OMI at the cloud top, gradually decreasing towards the cloud bottom. In this context, the authors should discuss what the "cloud top" derived from OMI O₂-O₂ measurements actually means for a thunderstorm cloud.

We appreciate the reviewer's suggestion on the "cloud top" and have added the discussion of this concept in Sect. 2.4.

The concept of AMF_{LNO_x} was also used in Beirle et al. (2009) to investigate the sensitivity of satellite instruments for freshly produced lightning NO_x.

....

Please note that the CP is a reflectance-weighted pressure retrieved by the collision-induced O₂-O₂ absorption band near 477 nm (Acarreta et al., 2004; Snee et al., 2008; Stammes et al., 2008). For a deep convective cloud with lightning, the CP lies below the geometrical cloud top which is much closer to that detected by thermal infrared sensors, such as the CloudSat and the Aqua MODerate-resolution Imaging Spectrometer (MODIS) (Vasilkov et al., 2008; Joiner et al., 2012). Hence, the tropospheric NO₂ measured by OMI lies inside the cloud rather than above the cloud top. In the following, "above cloud" or "below cloud" is relative to the cloud pressure detected by OMI. The sensitivity study of Beirle et al. (2009) compared the chemical compositions from the cloud bottom to the cloud top and revealed that a significant fraction the NO₂ within the cloud originating from lightning can be detected by the satellite. This valuable cloud pressure concept has been applied not only in the LNO_x research but also in the cloud slicing method of deriving the UT O₃ and NO_x (Ziemke et al., 2009; Choi et al., 2014; Strode et al., 2017; Ziemke et al., 2017; Marais et al., 2018). As discussed in Pickering et al. (2016), the ratio of V_{LNO_2} seen by OMI to V_{LNO_x} is partly influenced by p_{cloud} . The effects of LNO_2 below the cloud will be discussed in Sect. 3.4.

2) There is one crucial omission which might require major revisions: The derived $AMFLNO_x$ will strongly depend on p_{cloud} (e.g. eq. 2). But this key input parameter is missing in the error budget in table 3. This has to be revised and the uncertainties caused by p_{cloud} have to be discussed accordingly.

We have added the uncertainty caused by p_{cloud} (Table R1), Thanks.

We determine the uncertainty due to BEHR tropopause pressure, cloud radiance fraction, **cloud pressure**, surface pressure, surface reflectivity, profile shape, profile location, V_{strat} , the detection efficiency of lightning, t_{window} and LNO_2 lifetime numerically by perturbing each parameter in turn and re-retrieval of the LNO_2 and LNO_x with the perturbed values (Table 3). The GEOS-5 monthly tropopause pressure, which is consistent with the NASA Standard Product, is applied instead of the variable WRF tropopause height to evaluate the uncertainty (6% for LNO_2 and 4% for LNO_x) caused by the BEHR tropopause pressure. **Beirle et al. (2009) obtained a mean total sensitivity of 0.46 ($\sigma = 0.09$) for LNO_x in the sensitivity study, implying an uncertainty of 23% due to cloud pressure in our study.**

Table R1 . Uncertainties for the estimation of LNO₂/flash, LNO_x/flash, LNO₂/stroke and LNO_x/stroke.

Type	Perturbation	LNO ₂ /flash ⁵	LNO _x /flash ⁵	LNO ₂ /stroke ⁵	LNO _x /stroke ⁵
BEHR tropopause pressure ¹	NASA product tropopause	6	4	6	4
Cloud radiance fraction ¹	± 5%	2	2	2	2
Cloud pressure ²	Constant AMF: 0.46	23	23	23	23
Surface pressure ¹	± 1.5%	0	0	0	0
Surface reflectivity ¹	± 17%	0	0	0	0
LNO ₂ profile ¹	2×500 mol NO flash ⁻¹	15	29	14	29
Profile location ¹	Quasi-Monte Carlo	0	1	0	1
Lightning detection efficiency ³	IC: ± 16%, CG: ± 5%	15	15	15	15
t _{window} ³	2 – 4 hours	10	10	8	8
LNO _x lifetime ³	2 – 12 hours	24	24	24	24
V _{strat} ⁴	-	10	10	10	10
Systematic errors in slant column ⁴	-	5	5	5	5
Tropospheric background ⁴	-	10	10	10	10
NO/NO ₂ ⁴	-	20	20	20	20
Net	-	48	54	47	54

PE_{uncertainty} = (Error_{rising perturbed value} - Error_{lowering perturbed value})/2 where Error_{perturbed value} = (PE_{perturbed value} - PE_{original value})/PE_{original value}.

¹Laughner et al. (2019) ²Beirle et al. (2009) ³Lapierre et al. (2019) ⁴Allen et al. (2019) and Bucselo et al. (2019) ⁵Uncertainty (%)

Minor Comments

1) 5: Skip "program of".

Fixed.

To apply satellite data in both clean and polluted regions, a new algorithm for calculating LNO_x has been developed that uses **the Berkeley High Resolution (BEHR) v3.0B NO₂ product** and the Weather Research and Forecasting-Chemistry (WRF-Chem) model.

2) 130: must be square km.

Fixed.

The present study uses WRF-Chem version 3.5.1 (Grell et al., 2005) with a horizontal grid size of 12 × 12 km² and 29 vertical levels.

3) 146: The concept of defining an "AMF" for converting SNO₂ into LNO_x was also used in Beirle et al., AMT 9, 1077-1094, 2009, (see eq. 9 therein).

Thank you for your remind of that paper we did not read before. It actually could help us explain our methods and results a lot. We have added that concept before discussing the "Cloud Top" (See *No. 1, Sect. Major comments*).

4) 268: I recommend to extend "Production" to "Production estimates"

Extended.

The negative differences are caused by background NO₂ carried by the updraft while parts of the below-cloud LNO₂ results in more LNO₂ production **estimates** than NO₂Vis production **estimates**.

5) 395: "we find that the regionally dependent effect" - unclear, please revise.

Revised.

Finally, implementing profiles generated with different model settings of lightning (1×200 mol NO flash⁻¹ and 2×500 mol NO flash⁻¹), **we find that the larger LNO production model setting leads to larger retrieval of LNO_x despite some regionally dependent effects caused by nonlinear calculation of AMF.**

6) Fig. 1: Please make the legends clearer and remove cryptic labels ("crf90_entin_tl")

After we discussed with Eric J. Bucsela privately, we have redone the linear regressions based on the daily mean LNO_x and flashes, as mentioned in the Response to Reviewer#2 (See *No. 19*). Because the different colors and dots could mislead readers, we have decided to summarize the linear regression results in Table 2 (Table R2).

7) Figs. 2 and 9: Please use less, but larger labels on x-axis.

Table R2 . LNO_x production for different combinations of criteria defined in Table 1.

Condition ¹	ENTLN data type ²	LNO _x /flash or LNO _x /stroke	R value	Intercept (10 ⁶ mol)	Days ³
CRF90_ENTLN	Flash	52.1 ± 51.1	0.20	0.21	99
CRF90_CF40_ENTLN	Flash	84.2 ± 31.5	0.54	-0.04	70
CRF90_ENTLN_TL1000	Flash	61.9 ± 49.1	0.27	0.33	83
CRF90_CF40_ENTLN_TL1000	Flash	63.4 ± 52.9	0.38	0.26	38
CRF90_ENTLN_TL1000_ratio50	Flash	54.5 ± 48.1	0.25	0.39	81
CRF90_CF40_ENTLN_TL1000_ratio50	Flash	90.0 ± 65.0	0.46	0.15	32
CRF90_ENTLN	Stroke	6.7 ± 4.1	0.31	0.23	102
CRF90_CF40_ENTLN	Stroke	10.3 ± 3.6	0.55	0.08	79
CRF90_ENTLN_TL1000	Stroke	7.5 ± 5.1	0.29	0.38	94
CRF90_CF40_ENTLN_TL1000	Stroke	8.6 ± 6.2	0.39	0.27	46
CRF90_ENTLN_TL1000_ratio50	Stroke	7.0 ± 4.8	0.29	0.42	93
CRF90_CF40_ENTLN_TL1000_ratio50	Stroke	8.9 ± 7.0	0.39	0.31	40

¹These conditions are defined in Table 1. ²The threshold of ENTLN data is 2400 flashes box⁻¹ and 8160 strokes box⁻¹ during the period of 2.4 h before OMI overpass time. ³The number of valid days with specific criteria in MJJA 2014.

We have modified the former figure (Fig. 3/ Fig. R1) and deleted the later one as mentioned in the Response to Reviewer#1 (See No. 22, Sect. Specific Comments).

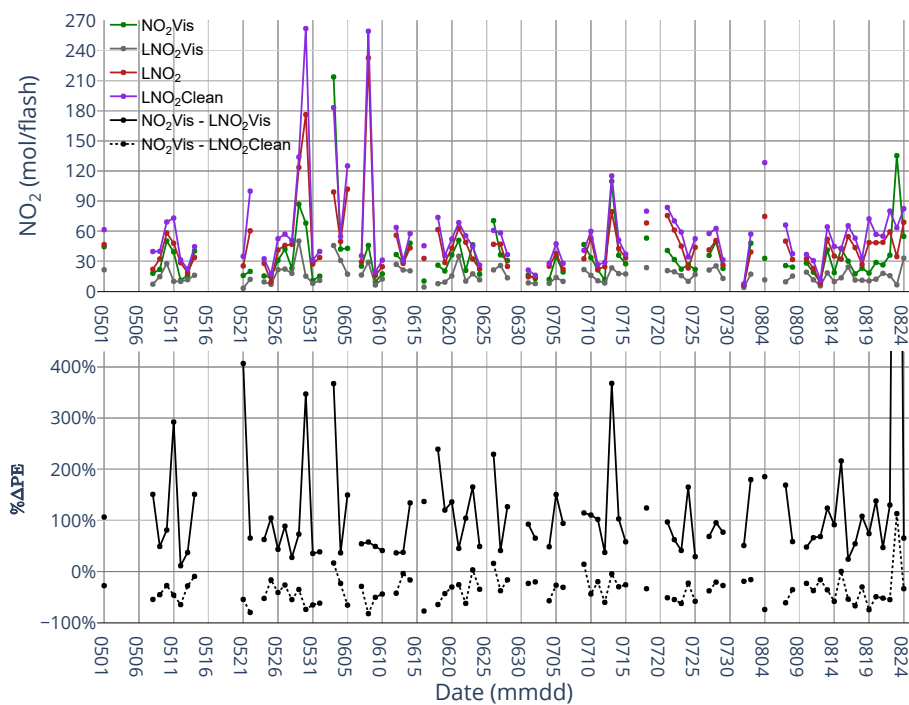


Figure R1 . (top) Time series of NO₂ Vis, LNO₂ Vis, LNO₂ and LNO₂Clean production per day over the CONUS for MJJA 2014 with CRF $\geq 90\%$ and a flash threshold of 2400 flashes per 2.4 h. (bottom) Time series of the percent differences between NO₂ Vis and LNO₂ Vis and the percent differences between NO₂ Vis and LNO₂Clean with CRF $\geq 90\%$. The value of black dot on August 23 (not shown) is 1958%.

References

- Acarreta, J. R., de Haan, J. F., and Stammes, P.: Cloud pressure retrieval using the O₂-O₂ absorption band at 477 nm, *Journal of Geophysical Research*, 109, 2165, <https://doi.org/10.1029/2003JD003915>, 2004.
- Allen, D. J., Pickering, K. E., Bucselá, E. J., Krotkov, N., and Holzworth, R.: Lightning NO_x Production in the Tropics as Determined Using OMI NO₂ Retrievals and WWLLN Stroke Data, *Journal of Geophysical Research: Atmospheres*, <https://doi.org/10.1029/2018JD029824>, 2019.
- Beirle, S., Salzmann, M., Lawrence, M. G., and Wagner, T.: Sensitivity of satellite observations for freshly produced lightning NO_x, *Atmospheric Chemistry and Physics*, 9, 1077–1094, <https://doi.org/10.5194/acp-9-1077-2009>, 2009.
- Bucselá, E. J., Pickering, K. E., Allen, D. J., Holzworth, R., and Krotkov, N. A.: Midlatitude lightning NO_x production efficiency inferred from OMI and WWLLN data, *Journal of Geophysical Research: Atmospheres*, <https://doi.org/10.1029/2019JD030561>, 2019.
- Choi, S., Joiner, J., Choi, Y., Duncan, B. N., Vasilkov, A., Krotkov, N., and Bucselá, E.: First estimates of global free-tropospheric NO₂ abundances derived using a cloud-slicing technique applied to satellite observations from the Aura Ozone Monitoring Instrument (OMI), *Atmospheric Chemistry and Physics*, 14, 10565–10588, <https://doi.org/10.5194/acp-14-10565-2014>, 2014.
- Grell, G. A., Peckham, S. E., Schmitz, R., McKeen, S. A., Frost, G., Skamarock, W. C., and Eder, B.: Fully coupled “online” chemistry within the WRF model, *Atmospheric Environment*, 39, 6957–6975, <https://doi.org/10.1016/j.atmosenv.2005.04.027>, 2005.
- Joiner, J., Vasilkov, A. P., Gupta, P., Bhartia, P. K., Veefkind, P., Sneep, M., de Haan, J., Polonsky, I., and Spurr, R.: Fast simulators for satellite cloud optical centroid pressure retrievals; evaluation of OMI cloud retrievals, *Atmospheric Measurement Techniques*, 5, 529–545, <https://doi.org/10.5194/amt-5-529-2012>, 2012.
- Lapierre, J. L., Laughner, J. L., Geddes, J. A., Koshack, W., Cohen, R. C., and Pusede, S. E.: Observing regional variability in lightning NO_x production rates, *Journal of Geophysical Research*, in review, 2019.
- Laughner, J. L., Zhu, Q., and Cohen, R. C.: Evaluation of version 3.0B of the BEHR OMI NO₂ product, *Atmospheric Measurement Techniques*, 12, 129–146, <https://doi.org/10.5194/amt-12-129-2019>, 2019.
- Marais, E. A., Jacob, D. J., Choi, S., Joiner, J., Belmonte-Rivas, M., Cohen, R. C., Beirle, S., Murray, L. T., Schiferl, L., Shah, V., and Jaeglé, L.: Nitrogen oxides in the global upper troposphere: interpreting cloud-sliced NO_x observations from the OMI satellite instrument, *Atmospheric Chemistry and Physics Discussions*, pp. 1–14, <https://doi.org/10.5194/acp-2018-556>, 2018.
- Pickering, K. E., Bucselá, E., Allen, D., Ring, A., Holzworth, R., and Krotkov, N.: Estimates of lightning NO_x production based on OMI NO₂ observations over the Gulf of Mexico, *Journal of Geophysical Research: Atmospheres*, 121, 8668–8691, <https://doi.org/10.1002/2015JD024179>, 2016.
- Sneep, M., de Haan, J. F., Stammes, P., Wang, P., Vanbauce, C., Joiner, J., Vasilkov, A. P., and Levelt, P. F.: Three-way comparison between OMI and PARASOL cloud pressure products, *Journal of Geophysical Research*, 113, D05 204, <https://doi.org/10.1029/2007JD008694>, 2008.
- Stammes, P., Sneep, M., de Haan, J. F., Veefkind, J. P., Wang, P., and Levelt, P. F.: Effective cloud fractions from the Ozone Monitoring Instrument: Theoretical framework and validation, *Journal of Geophysical Research*, 113, D05 204, <https://doi.org/10.1029/2007JD008820>, 2008.
- Strode, S. A., Douglass, A. R., Ziemke, J. R., Manyin, M., Nielsen, J. E., and Oman, L. D.: A Model and Satellite-Based Analysis of the Tropospheric Ozone Distribution in Clear Versus Convectively Cloudy Conditions, *Journal of Geophysical Research: Atmospheres*, 122, 11,948–11,960, <https://doi.org/10.1002/2017JD027015>, 2017.
- Vasilkov, A., Joiner, J., Spurr, R., Bhartia, P. K., Levelt, P., and Stephens, G.: Evaluation of the OMI cloud pressures derived from rotational Raman scattering by comparisons with other satellite data and radiative transfer simulations, *Journal of Geophysical Research*, 113, D05 204, <https://doi.org/10.1029/2007JD008689>, 2008.
- Ziemke, J. R., Joiner, J., Chandra, S., Bhartia, P. K., Vasilkov, A., Haffner, D. P., Yang, K., Schoeberl, M. R., Froidevaux, L., and Levelt, P. F.: Ozone mixing ratios inside tropical deep convective clouds from OMI satellite measurements, *Atmospheric Chemistry and Physics*, 9, 573–583, <https://doi.org/10.5194/acp-9-573-2009>, 2009.
- Ziemke, J. R., Strode, S. A., Douglass, A. R., Joiner, J., Vasilkov, A., Oman, L. D., Liu, J., Strahan, S. E., Bhartia, P. K., and Haffner, D. P.: A cloud-ozone data product from Aura OMI and MLS satellite measurements, *Atmospheric Measurement Techniques*, 10, 4067–4078, <https://doi.org/10.5194/amt-10-4067-2017>, 2017.

Estimates of Lightning NO_x Production based on High Resolution OMI NO₂ Retrievals over the Continental US

Xin Zhang^{1,2}, Yan Yin^{1,2}, Ronald van der A^{2,3}, Jeff L. Lapierre⁴, Qian Chen^{1,2}, Xiang Kuang^{1,2},
Shuqi Yan², Jinghua Chen^{1,2}, Chuan He^{1,2}, and Rulin Shi^{1,2}

¹ Collaborative Innovation Center on Forecast and Evaluation of Meteorological Disasters/Key Laboratory for Aerosol-Cloud-Precipitation of China Meteorological Administration, Nanjing University of Information Science and Technology (NUIST), Nanjing 210044, China

² Department of Atmospheric Physics, Nanjing University of Information Science and Technology (NUIST), Nanjing 210044, China

³ Royal Netherlands Meteorological Institute (KNMI), Department of Satellite Observations, De Bilt, the Netherlands

⁴ Earth Networks, Germantown, Maryland, USA

Correspondence: Yan Yin (yinyan@nuist.edu.cn)

Abstract. Lightning serves as the dominant source of nitrogen oxides (NO_x = NO + NO₂) in the upper troposphere (UT), with strong impact on ozone chemistry and the hydroxyl radical production. However, the production efficiency (PE) of lightning nitrogen oxides (LNO_x) is still quite uncertain (32 – 1100 mol NO per flash). ~~Satellites~~ Satellite measurements are a powerful tool to estimate LNO_x directly as compared to conventional platforms. To apply satellite data in both clean and polluted regions, a new algorithm for calculating LNO_x has been developed ~~based on the program of new~~ that uses the Berkeley High Resolution (BEHR) v3.0B NO₂ product and the Weather Research and Forecasting-Chemistry (WRF-Chem) model. LNO_x PE over the continental US is estimated using the NO₂ product of the Ozone Monitoring Instrument (OMI) satellite and the Earth Networks Total Lightning Network (ENTLN) data. Focusing on the summer season during 2014, we find that the lightning NO₂ (LNO₂) PE is ~~44-32~~ ± 16-15 mol NO₂ flash⁻¹ and ~~8-6~~ ± 3 mol NO₂ stroke⁻¹ while LNO_x PE is ~~120-90~~ ± 52-49 mol NO_x flash⁻¹ and ~~22-17~~ ± 9 mol NO_x stroke⁻¹. Results reveal that ~~former methods are more sensitive to our method reduces sensitivity to~~ the background NO₂ and ~~neglect~~ includes much of the below-cloud LNO₂. As the LNO_x parameterization varies in studies, the sensitivity of our calculations to the setting of the amount of lightning NO (LNO) is evaluated. Careful consideration of the ratio of LNO₂ to NO₂ is also needed, given its large influence on the estimation of LNO₂ PE.

1 Introduction

Nitrogen oxides (NO_x) near the Earth's surface ~~is-are~~ mainly produced by soil, biomass burning and fossil fuel combustion, while NO_x in the middle and upper troposphere ~~originate~~ originates largely from lightning and aircraft emissions. NO_x plays an important role in the production of ozone (O₃) and the hydroxyl radical (OH). While the anthropogenic sources of NO_x are largely known, lightning nitrogen oxides (LNO_x) are still the source with the greatest uncertainty, though they are estimated to range between 2 and 8 Tg N yr⁻¹ (Schumann and Huntrieser, 2007). LNO_x is produced in the upper troposphere (UT) by O₂ and N₂ dissociation in the hot lightning channel as described by the Zel'dovich mechanism (Zel'dovich and Raizer, 1967).

With the recent updates of UT NO_x chemistry, the day time lifetime of UT NO_x is evaluated to be ~ 3 h near thunderstorms and ~ 0.5 – 1.5 days away from thunderstorms (Nault et al., 2016, 2017). This results in enhanced O₃ production in the cloud outflow of active convection (Pickering et al., 1996; Hauglustaine et al., 2001; DeCaria et al., 2005; Ott et al., 2007; Dobber et al., 2008; Allen et al., 2010; Finney et al., 2016). As O₃ is known as a greenhouse gas, strong oxidant and absorber of ultraviolet radiation (Myhre et al., 2013), the contributions of LNO_x to O₃ production also have an effect on climate forcing. Finney et al. (2018) found different impacts on atmospheric composition and radiative forcing when simulating future lightning using a new upward cloud ice flux (IFLUX) method ~~and versus~~ the commonly used ~~the widely used~~ cloud-top height (CTH) approach. ~~As lightning with the CTH approach have reported~~ While lightning is predicted to increase by 5 — 16% increases over the next century with the CTH approach (Clark et al., 2017; Banerjee et al., 2014; Krause et al., 2014), a 15% decrease in lightning was estimated with IFLUX in 2100 under a strong global warming scenario (Finney et al., 2018). As a result of the different effects on ~~compositions~~ radiative forcing from ozone and methane, a net positive radiative forcing was found with the CTH approach while there is little net radiative forcing with the IFLUX approach ~~-(Finney et al., 2018)~~. However, the convective available potential energy (CAPE) times the precipitation rate (P) proxy predicts a 12 ± 5% increase in the Continental US (CONUS) lightning strike rate per kelvin of global warming (Romps et al., 2014), while the IFLUX proxy predicts the lightning will only increase 3.4%/K over the CONUS. Recently, Romps (2019) compared the CAPE × P proxy and IFLUX method in cloud-resolving models. They report that higher CAPE and updraft velocities caused by global warming could lead to the large increases in tropical lightning simulated by CAPE × P proxy, while IFLUX proxy predicts little change in tropical lightning because of the small changes in water mass fluxes.

In the view of the region dependent lifetime of NO_x and the difficulty of measuring LNO_x directly, a better understanding of the LNO_x production is required, especially in the tropical and mid-latitude regions in summer. Using its distinct spectral absorption lines in the near-ultraviolet (UV) and visible (VIS) range (Platt and Perner, 1983), NO₂ can be measured by satellite instruments like the Global Ozone Monitoring Experiment (GOME; Burrows et al., 1999; Richter et al., 2005), Scanning Imaging Absorption Spectrometer for Atmospheric Chartography (SCIAMACHY; Bovensmann et al., 1999), the Second Global Ozone Monitoring Experiment (GOME-2; Callies et al., 2000) and the Ozone Monitoring Instrument (OMI; Levelt et al., 2006). OMI has the highest spatial resolution, least instrument degradation and longest record among these satellites (Krotkov et al., 2017). ~~Satellites~~ Satellite measurements of NO₂ are a powerful tool compared to conventional platforms, because of its global coverage, constant instrument features and temporal continuity.

Recent studies have determined and ~~qualified~~ quantified LNO_x using satellite observations. Beirle et al. (2004) constrained the LNO_x production to 2.8 (0.8 – 14) Tg N yr⁻¹ by combining GOME NO₂ data and flash counts from the Lightning Imaging Sensor (LIS) aboard the Tropical Rainfall Measurement Mission (TRMM) over Australia. Boersma et al. (2005) estimated the global LNO_x production of 1.1 – 6.4 Tg N yr⁻¹ by comparing GOME NO₂ with distributions of LNO₂ modeled by Tracer Model 3 (TM3). Martin et al. (2007) analyzed SCIAMACHY NO₂ columns with Goddard Earth Observing System chemistry model (GEOS-Chem) simulations to identify LNO_x production amounting to 6 ± 2 Tg N yr⁻¹.

As these methods focus on monthly or yearly mean NO₂ column densities, more recent studies applied specific approaches to investigate LNO_x directly over active ~~convections~~ convection. Beirle et al. (2006) estimated LNO_x as 1.7 (0.6 – 4.7) Tg N yr⁻¹

based on a convective system over the Gulf of Mexico, using National Lightning Detection Network (NLDN) observations and GOME NO₂ column densities. However, ~~it is this study~~ assumed that all the enhanced NO₂ originated from lightning ~~without and did not consider~~ the contribution of anthropogenic emissions. Beirle et al. (2010) analyzed LNO_x production systematically using the global dataset of SCIAMACHY NO₂ observations combined with flash data from the World Wide Lightning Location Network (WWLLN). ~~The threshold of high flash rates is that the summation of the corrected flashes within the satellite pixel (Their analysis was restricted to 30×60 km²) in the last one hour must be greater than satellite pixels where the flash rate exceeded 1 flashes/km²/h. But the results of flash km² hr⁻¹. But they found~~ LNO_x production ~~are to be~~ highly variable and correlations between flash rate densities and LNO_x production are low in some cases. Bucselá et al. (2010) estimate LNO_x production as ~ 100 – 250 mol NO_x/flash for four cases, using the DC-8 and OMI data during NASA's Tropical Composition, Cloud and Climate Coupling Experiment (TC⁴).

Based on the approach used by Bucselá et al. (2010), a special algorithm was developed by Pickering et al. (2016) to retrieve LNO_x from OMI and the WWLLN. The algorithm takes the OMI tropospheric slant column density (SCD) of NO₂ (S_{NO₂}) as the tropospheric slant column density of LNO₂ (S_{LNO₂}) by using cloud radiance fraction (CRF) greater than 0.9 to minimize or screen the lower tropospheric background. To convert the S_{LNO₂} to the tropospheric vertical density (VCD) of LNO_x (V_{LNO_x}), an air mass factor (AMF) is calculated by dividing the a priori S_{LNO₂} by the a priori V_{LNO_x}. Since they ~~assumed-considered~~ NO₂ above the cloud ~~are all as~~ LNO₂ ~~in the algorithm due to the difficulty and uncertainty in determining the background NO₂~~, their AMF and derived VCD of LNO_x (LNO₂) is named as AMF_{LNO_xClean} (AMF_{LNO₂Clean}) and LNO_xClean (LNO₂Clean), respectively. Unless otherwise specified, abbreviations S and V are respectively defined as the tropospheric SCD and VCD in this paper. The a priori S_{LNO₂} is calculated using a radiative transfer model and a profile of LNO₂ simulated by the NASA Global Modeling Initiative (GMI) chemical transport model. The a priori V_{LNO_x} is also obtained from the GMI model. Results for the Gulf of Mexico during 2007 – 2011 summer yield LNO_x production of 80 ± 45 mol NO_x per flash. Among several substantial sources of uncertainty, significant uncertainty ~~exists in characterizing background NO_x~~ (3% ~ >30%) ~~exists in characterizing background NO_x~~ in this region (Pickering et al., 2016).

More recently Bucselá et al. (2019) obtained an average production efficiency (PE) of 180 ± 100 mol per flash over East Asia, Europe and North America based on ~~a modification of~~ the method used in Pickering et al. (2016). ~~A power function between LNO_x and lightning flash rate was established, while the minimum flash-rate threshold was not applied.~~ The tropospheric NO_x background was removed by ~~the weighted subtracting~~ temporal average of NO_x at each box ~~which meets where the value was weighted by the number of OMI pixels which meet~~ the optical cloud pressure and CRF criteria ~~but has 0 — required to be considered deep convection but has 1 flashes-flash or less~~ instead. The lofted pollution was ~~corrected-by-considered as~~ 15% of ~~total NO_x~~ according to the estimation from DeCaria et al. (2000, 2005) and the average chemical delay was adjusted by 15% following the 3-hour LNO_x lifetime in the nearby field of convection (Nault et al., 2017). However, there were negative LNO_x values caused by the overestimation of the tropospheric background ~~at those and stratospheric NO₂ at some~~ locations.

On ~~another-the other~~ hand, Lapierre et al. (2019) constrained LNO₂ to 1.1 ± 0.6 mol NO₂/stroke for intracloud (IC) strokes and 10.0 ± 4.9 mol NO₂/stroke for cloud-to-ground (CG) strokes over the ~~continental-US (CONUS)~~ CONUS. LNO₂ per stroke was scaled to 54.4 mol NO_x/flash ~~by using mean values of~~ strokes per flash and the ratio of NO to NO₂ in the UT. They used the

regridded Berkeley High-Resolution (BEHR) V3.0A $0.05^\circ \times 0.05^\circ$ "visible only" NO_2 VCD (V_{vis}) product which includes two parts of NO_2 that can be "seen" by the satellite. The first part is the NO_2 above clouds ([pixels with CRF > 0.9](#)) and the second part is the NO_2 detected from cloud free areas. A threshold of 3×10^{15} molecules cm^{-2} , the typical urban NO_2 concentration, was applied to mask the contaminated grid cells (Beirle et al., 2010; Laughner and Cohen, 2017). The main difference between
95 Lapierre et al. (2019) and Pickering et al. (2016) is the air mass factor for lightning ($\text{AMF}_{\text{LNO}_x}$) implemented in the basic algorithm. In Lapierre et al. (2019), the air mass factor was used to convert S_{NO_2} to V_{vis} , while in Pickering et al. (2016) it was used to convert S_{LNO_2} to V_{LNO_x} , assuming that all S_{NO_2} is generated by lightning.

To apply the approach used by Bucselo et al. (2010), Pickering et al. (2016), Bucselo et al. (2019) and Lapierre et al. (2019) without geographic restrictions, contamination ~~of~~ [by](#) anthropogenic emissions must be taken into account in detail.
100 The Weather Research and Forecasting (WRF) model coupled with chemistry (WRF-Chem) has been employed to evaluate the convective transport and chemistry in many studies (Barth et al., 2012; Wong et al., 2013; Fried et al., 2016; Li et al., 2017). Meanwhile, Laughner and Cohen (2017) showed that the OMI AMF is increased by $\sim 35\%$ for summertime when LNO_2 simulated by WRF-Chem is included in the a priori profiles to match aircraft observations. The simulation agrees with observed NO_2 profiles and the bias of AMF [related to these observations](#) is reduced to $< \pm 4\%$ for OMI viewing geometries.

105 In this paper, we ~~focused~~ [focus](#) on the estimation of LNO_2 production per flash ($\text{LNO}_2/\text{flash}$), LNO_x production per flash ($\text{LNO}_x/\text{flash}$), LNO_2 production per stroke ($\text{LNO}_2/\text{stroke}$) and LNO_x production per stroke ($\text{LNO}_x/\text{stroke}$) in May–August (MJJA) 2014 by developing an algorithm similar to Pickering et al. (2016) based on the BEHR NO_2 retrieval algorithm (Laughner et al., 2018a, b), but it performs better over background NO_2 sources. Section 2 describes the satellite, lightning data, model settings and the algorithm in detail. Section 3 explores the suitable data criteria, compares different methods and evaluates the
110 effect of cloud and LNO_x parameterization on LNO_x production estimation. Section 4 examines [the effect of](#) different sources of the uncertainty ~~of~~ [on](#) the results. Conclusions are summarized in Section 5.

2 Data and Methods

2.1 Ozone Monitoring Instrument (OMI)

OMI is carried on the Aura satellite (launched in 2004), a member of A-train satellite group (Levelt et al., 2006, 2018). OMI
115 passes over the equator at $\sim 13:45$ LT (ascending node) and has a swath width of 2600 km, with a nadir field-of-view resolution of 13×24 km^2 . Since the beginning of 2007, some of the measurements have become useless as a result of anomalous radiances called the "row anomaly" (~~Dobber et al., 2008~~) ([Dobber et al., 2008](#); [KNMI, 2012](#)). For the current study, we used the NASA standard product ~~v3-V3.0~~ ([Krotkov et al., 2017](#)) as input to the LNO_x retrieval algorithm.

The main steps of calculating the NO_2 tropospheric VCD (V_{NO_2}) in the NASA product include:

- 120 1. SCDs are determined by the OMI-optimized differential optical absorption spectroscopy (DOAS) spectral fit;
2. A corrected ("de-stripped") SCD is obtained by subtracting the [bias-cross-track bias caused by an instrument artifact](#) from the measured slant column;

3. The AMF for stratospheric (AMF_{strat}) or tropospheric column (AMF_{trop}) is calculated from the NO_2 profile integrated vertically using weighted scattering weights with the a priori profiles. These profiles are obtained from GMI monthly mean profiles using four years (2004 – 2007) simulation;

4. The stratospheric NO_2 VCD (V_{strat}) is calculated from the subtraction of a priori contribution from tropospheric NO_2 and a three-step (interpolation, filtering, and smoothing) algorithm (Bucsela et al., 2013);

5. V_{strat} is converted to the slant column using AMF_{strat} and subtracted from the measured SCDs to yield S_{NO_2} , leading to $V_{NO_2} = S_{NO_2}/AMF_{trop}$.

130 Based on this method, we developed a new AMF_{LNO_x} to obtain the desired V_{LNO_x} ($V_{LNO_x} = S_{NO_2}/AMF_{LNO_x}$) to replace the original step 5. Details of this algorithm are discussed in section 2.4.

2.2 The Earth Networks Total Lightning Detection Network (ENTLN)

The Earth Networks Total Lightning Network (ENTLN) operates a system of over 1500 ground-based stations around the world with more than 900 sensors installed in the CONUS (Zhu et al., 2017). Both IC and CG lightning flashes are located by the sensors with detection frequency ranging from 1 Hz to 12 MHz based on the electric field pulse polarity and wave shapes. Groups of pulses are classified as a flash if they are within 700 ms and 10 km. In the preprocessed data obtained from the ENTLN, both strokes and lightning flashes composed of one or more strokes are included.

Rudlosky (2015) compared ENTLN ~~with LIS combined events (IC and CG) with LIS flashes~~ and found that the relative flash detection efficiency of ENTLN ~~increases from 21.6 over CONUS increases from 62.4%~~ during 2011 to ~~31.4~~79.7% during 2013. Lapierre et al. (2019) also compared combined ENTLN and the NLDN dataset with data from the LIS ~~and during 2014 and found~~ the detection efficiencies of IC flashes and strokes ~~are to be~~ 88% and 45%, respectively. Since we ~~only~~ use the ENTLN data in 2014 as Lapierre et al. (2019) and NLDN detection efficiency of IC pulses should be lower than 33% which is calculated by the data in 2016 (Zhu et al., 2016), only the IC flashes and strokes are ~~corrected by 88% and 45%~~divided by 0.88 and 0.45, respectively, while CG flashes and strokes are unchanged because of the high detection efficiency.

145 2.3 Model Description

The present study uses WRF-Chem version 3.5.1 (Grell et al., 2005) with a horizontal grid size of $12 \times 12 \text{ km}^2$ and 29 vertical levels (Fig. 1). The initial and boundary conditions of meteorological parameters are provided by the North American Regional Reanalysis (NARR) dataset with a 3 hourly time resolution. Based on Laughner et al. (2018b), 3D wind fields, temperature and water vapor are nudged towards the NARR data. Outputs from the version 4 of Model for Ozone and Related chemical Tracers (MOZART-4; Emmons et al., 2010) ~~was were~~ used to generate the initial and boundary conditions of chemical species. Anthropogenic emissions are driven by the 2011 National Emissions Inventory (NEI), scaled to model years by the Environmental Protection Agency annual total emissions (EPA and OAR, 2015). The Model of Emissions of Gases and Aerosol from Nature (MEGAN; Guenther et al., 2006) is used for biogenic emissions. The chemical mechanism is the version 2 of Regional Atmospheric Chemistry Mechanism (RACM2; Goliff et al., 2013) with updates from Browne et al. (2014) and Schwantes et al. (2015). In addition, lightning flash rate based on the level of neutral buoyancy parameterization (Price and Rind, 1992) and

LNO_x parameterizations are activated (200 mol NO flash⁻¹, the factor to adjust the predicted number of flashes is set to 1; hereinafter referred to as "1×200 mol NO flash⁻¹"). [Although the simulated total flash densities are higher in the Southeast US and lower in the North Central US \(Fig. 2\), the criteria in Sect. 3.1 could limit this effect on the estimation of LNO_x production and Sect. 3.4 will use another simulation to test this problem.](#) The bimodal profile modified from the standard Ott et al. (2010) profile (Laughner and Cohen, 2017) is employed as the vertical distribution of lightning NO (LNO) in WRF-Chem, while LNO and LNO₂ profiles are defined as the difference of vertical profiles between simulations with and without lightning.

2.4 Method for Deriving AMF

The V_{LNO_x} near convection is calculated according:

$$V_{LNO_x} = \frac{S_{NO_2}}{AMF_{LNO_x}} \quad (1)$$

where S_{NO_2} is the OMI-measured tropospheric slant column NO₂ and AMF_{LNO_x} is a customized lightning air mass factor. [The concept of \$AMF_{LNO_x}\$ is defined was also used in Beirle et al. \(2009\) to investigate the sensitivity of satellite instruments for freshly produced lightning NO_x. In order to estimate LNO_x, we define the \$AMF_{LNO_x}\$ as the ratio of the "visible" modeled NO₂ slant column to the total modeled tropospheric LNO_x vertical column \(derived from the a priori NO and NO₂ profiles, scattering weights, and radiance cloud fraction\):](#)

$$AMF_{LNO_x} = \frac{(1 - f_r) \int_{p_{surf}}^{p_{tp}} w_{clear}(p) NO_2(p) dp + f_r \int_{p_{cloud}}^{p_{tp}} w_{cloudy}(p) NO_2(p) dp}{\int_{p_{surf}}^{p_{tp}} LNO_x(p) dp} \quad (2)$$

where f_r is the radiance cloud fraction, p_{surf} is the surface pressure, p_{tp} is the tropopause pressure, p_{cloud} is the cloud optical pressure (CP), w_{clear} and w_{cloudy} are respectively the pressure dependent scattering weights from the TOMRAD lookup table (Bucsela et al., 2013) for clear and cloudy parts, and $NO_2(p)$ is the modeled NO₂ vertical profile. Details of these standard parameters and calculation methods are given in Laughner et al. (2018a). $LNO_x(p)$ is the LNO_x vertical profile calculated by the difference of vertical profiles between WRF-Chem simulations with and without lightning.

[Please note that the CP is a reflectance-weighted pressure retrieved by the collision-induced O₂-O₂ absorption band near 477 nm \(Acarreta et al., 2004; Sneep et al., 2008; Stammes et al., 2008\). For a deep convective cloud with lightning, the CP lies below the geometrical cloud top which is much closer to that detected by thermal infrared sensors, such as the CloudSat and the Aqua MODerate-resolution Imaging Spectrometer \(MODIS\) \(Vasilkov et al., 2008; Joiner et al., 2012\). Hence, the tropospheric NO₂ measured by OMI lies inside the cloud rather than above the cloud top. In the following, "above cloud" or "below cloud" is relative to the cloud pressure detected by OMI. The sensitivity study of Beirle et al. \(2009\) compared the chemical compositions from the cloud bottom to the cloud top and revealed that a significant fraction the NO₂ within the cloud originating from lightning can be detected by the satellite. This valuable cloud pressure concept has been applied not only in the LNO_x research but also in the cloud slicing method of deriving the UT O₃ and NO_x \(Ziemke et al., 2009; Choi et al., 2014; Strode et al., 2016\). As discussed in Pickering et al. \(2016\), the ratio of \$V_{LNO_2}\$ seen by OMI to \$V_{LNO_x}\$ is partly influenced by \$p_{cloud}\$. The effects of LNO₂ below the cloud will be discussed in Sect. 3.4.](#)

To compare our results with those of Pickering et al. (2016) and Lapierre et al. (2019), we calculate their $AMF_{LNO_x \text{Clean}}$ and $AMF_{NO_2 \text{Vis}}$ respectively:

$$AMF_{LNO_x \text{Clean}} = \frac{(1 - f_r) \int_{p_{\text{surf}}}^{p_{\text{tp}}} w_{\text{clear}}(p) LNO_2(p) dp + f_r \int_{p_{\text{cloud}}}^{p_{\text{tp}}} w_{\text{cloudy}}(p) LNO_2(p) dp}{\int_{p_{\text{surf}}}^{p_{\text{tp}}} LNO_x(p) dp} \quad (3)$$

190

$$AMF_{NO_2 \text{Vis}} = \frac{(1 - f_r) \int_{p_{\text{surf}}}^{p_{\text{tp}}} w_{\text{clear}}(p) NO_2(p) dp + f_r \int_{p_{\text{cloud}}}^{p_{\text{tp}}} w_{\text{cloudy}}(p) NO_2(p) dp}{(1 - f_g) \int_{p_{\text{surf}}}^{p_{\text{tp}}} NO_2(p) dp + f_g \int_{p_{\text{cloud}}}^{p_{\text{tp}}} NO_2(p) dp} \quad (4)$$

where f_g is the geometric cloud fraction and $LNO_2(p)$ is the modeled LNO_2 vertical profile. Besides these AMFs, another AMF called $AMF_{LNO_2 \text{Vis}}$ is developed for comparison later.

$$AMF_{LNO_2 \text{Vis}} = \frac{(1 - f_r) \int_{p_{\text{surf}}}^{p_{\text{tp}}} w_{\text{clear}}(p) NO_2(p) dp + f_r \int_{p_{\text{cloud}}}^{p_{\text{tp}}} w_{\text{cloudy}}(p) NO_2(p) dp}{(1 - f_g) \int_{p_{\text{surf}}}^{p_{\text{tp}}} LNO_2(p) dp + f_g \int_{p_{\text{cloud}}}^{p_{\text{tp}}} LNO_2(p) dp} \quad (5)$$

195 A full list of definitions of the used AMFs is shown in Appendix A.

$$AMF_{LNO_2 \text{Vis}} = \frac{(1 - f_r) \int_{p_{\text{surf}}}^{p_{\text{tp}}} w_{\text{clear}}(p) NO_2(p) dp + f_r \int_{p_{\text{cloud}}}^{p_{\text{tp}}} w_{\text{cloudy}}(p) NO_2(p) dp}{(1 - f_g) \int_{p_{\text{surf}}}^{p_{\text{tp}}} LNO_2(p) dp + f_g \int_{p_{\text{cloud}}}^{p_{\text{tp}}} LNO_2(p) dp}$$

200

~~Additionally, Vasilkov et al. (2008) found that p_{cloud} , retrieved by the OMI O_2-O_2 algorithm (Bucsela et al., 2013), is often significantly larger than the IR-derived cloud top. This means that the back-scattered UV-VIS light observed by OMI penetrates deeper into the cloud. As a result, part of the NO_2 originated from lightning can be detected by the OMI satellite. As discussed in Pickering et al. (2016), the ratio of V_{LNO_2} seen by OMI to V_{LNO_x} is partly influenced by p_{cloud} . The effects of LNO_2 below the cloud will be discussed in section 3.4.~~

2.5 Procedures for Deriving LNO_x

~~LNO_x - V_{LNO_x} is re-gridded to $0.05^\circ \times 0.05^\circ$ pixels like the BEHR product and grids using the constant value method (Kuhlmann et al., 2014). Then, it is analyzed in $1^\circ \times 1^\circ$ grid boxes with a minimum of fifty valid pixels which is equivalent to $0.05^\circ \times 0.05^\circ$ grids to minimize the noise. The minimum value is between five satellite pixels in Pickering et al. (2016) and three satellite pixels in Bucsela et al. (2019) or Allen et al. (2019).~~ The main procedures used to derive LNO_x are as follows:

210 CRFs (CRFs $\geq 70\%$, CRFs $\geq 90\%$ and CRFs = 100%) and CP ≤ 650 hPa are various criteria of deep convective clouds for OMI pixels (Ziemke et al., 2009; Choi et al., 2014; Pickering et al., 2016). The effect of different CRFs on the retrieved LNO_x is explored in section 3.2. Furthermore, another criterion of cloud fractions (CFs) is applied to the WRF-Chem results for the successful simulation of ~~convections~~ convection. The CFs are defined as the maximum cloud fraction calculated by the Xu-Randall method between 350 and 400 hPa (Xu and Randall, 1996)(Xu and Randall, 1996; Strode et al., 2017). This atmospheric layer (between 350 and 400 hPa) avoids any biases in the simulation of high clouds. We choose CFs $\geq 40\%$ suggested by Strode et al. (2017) to determine cloudy or clear for each simulation grid.

Besides ~~properties of cloud~~, the cloud properties, a time period and sufficient flashes (or strokes) are required for fresh LNO_x to be detected by OMI. The time window (t_{window}) is the hours prior to the OMI overpass time. t_{window} is limited to 2.4 h by the mean wind speed at pressure levels 500 – 100 hPa during OMI overpass time and the square root of the $1^\circ \times 1^\circ$ box over the CONUS (Lapierre et al., 2019). Meanwhile, 2400 flashes box^{-1} and 8160 strokes box^{-1} per 2.4 hour time window are chosen as sufficient for detecting LNO_x (Lapierre et al., 2019). These criteria will result in a low bias in the PE results, as Bucsel et al. (2019) found that the PE is larger at small flash rates which are discarded here.

To ensure that lightning flashes are simulated successfully by WRF-Chem, the threshold of simulated total lightning flashes (TL) per box is set to 1000, which is fewer than that used by the ENTLN lightning observation, considering the uncertainty of lightning parameterization. In view of other NO₂ sources except in addition to LNO₂, the ratio of modeled lightning NO₂ above cloud (LNO₂Vis) to modeled NO₂ above cloud (NO₂Vis) is defined to check whether enough LNO₂ can be detected by OMI. The ratio $\geq 50\%$ indicates that LNO₂ is not polluted much more than half of the NO_x above the cloud must have a LNO_x source.

Finally, the NO₂ lifetime against oxidation should be taken into account. As estimated by Nault et al. (2016), the lifetime (τ) of NO₂ in the near field of convections is ~ 3 h. The initial value of NO₂ is solved by Eq. 6 as

$$NO_2(0) = NO_2(OMI) \times e^{0.5t/\tau} \quad (6)$$

where $NO_2(0)$ is the moles of NO₂ emitted at time $t = 0$, $NO_2(OMI)$ is the moles of NO₂ measured at the OMI overpass time and $0.5t$ is the half cross grid time which is 1.2 h, assuming that lightning occurred at the center of each $1^\circ \times 1^\circ$ box. For each grid box, the mean LNO_x vertical column is obtained by averaging V_{LNO_x} values from all regridded $0.05^\circ \times 0.05^\circ$ pixels in the box. This mean value is converted to moles LNO_x using the dimensions of the grid box. Two methods are applied to estimate the seasonal mean LNO₂/flash, LNO_x/flash, LNO₂/stroke and LNO_x/stroke:

- (1) summation method: dividing the sum of LNO_x by the sum of flashes (or strokes) in each $1^\circ \times 1^\circ$ box in MJJA 2014;
- (2) linear regression method: applying the linear regression to daily summations mean values of LNO_x and flashes (or strokes).

3 Results

3.1 Criteria Determination

To determine the suitable criteria from conditions defined in section 2.5, six different combinations are defined (Table 1) and applied to the original data with a linear regression method (Fig-2Table 2).

A daily search of the NO₂ product for coincident ENTLN flash (stroke) data results in 99 (102) valid days under the condition of CRF $\geq 90\%$ CRF90_ENTLN condition. Taking the flashes type ENTLN data as an example, the number of valid days decreases from 99 to 81 under the basic condition coupled with TL ≥ 1000 and ratio $\geq 50\%$ CRF90_ENTLN_TL1000_ratio50 condition, while LNO_x/flash increases from 86.0-52.1 \pm 14.0-51.1 mol/flash to 114.8-54.5 \pm 18.2-48.1 mol/flash. The result is almost the same as the one without that under the CRF90_ENTLN_TL1000 condition which is without the condition of ratio

≥ 50%. Although this indicates the criterion of TL works well, it is better to include the ratio in case of some exceptions in the different AMF methods. Since $CF \geq 40\%$ leads to a sharp loss of valid numbers and production, therefore, it is not a suitable criterion. Instead the CRF criteria are used. Finally, coincident ENTLN data, $TL \geq 1000$ and $ratio \geq 50\%$ are chosen as the thresholds to explore the effects of three different CRF conditions ($CRF \geq 70\%$, $CRF \geq 90\%$ and $CRF = 100\%$) on LNO_x production (Table 3).

Apart from the fewer valid days under higher CRF conditions ($CRF \geq 90\%$ and $CRF = 100\%$), LNO_x/flash increases from $109.0 \pm 35.7 \pm 15.3 \pm 36.8$ mol/flash to $114.8 \pm 54.5 \pm 18.2 \pm 48.1$ mol/flash and decreases again to $99.4 \pm 20.8 \pm 15.3 \pm 37.4$ mol/flash while LNO_x/stroke enhances from $16.7 \pm 4.1 \pm 2.6 \pm 3.9$ mol/stroke to $17.8 \pm 7.0 \pm 2.9 \pm 4.8$ mol/stroke and drops again to $15.6 \pm 2.6 \pm 3.1 \pm 4.0$ mol/stroke (Table 3), as the CRF criterion increases from 70% to 90% and to 100%. The increment of LNO_x PE caused by the CRF increase from 70% to 90% is opposite to the result of Pickering et al. (2016). This is an effect of the consideration of NO₂ contamination transported from the boundary layer in our method. Although enhanced NO_x is often observed in regions with $CRF > 70\%$ (Pickering et al., 2016), the following analysis will be based on the criterion of $CRF \geq 90\%$ considering the contamination by low and mid-level NO₂ and comparisons with former studies the results of Pickering et al. (2016) and Lapierre et al. (2019).

~~Linear regression of daily total LNO_x summed over boxes with lightning 2.4 h prior to OMI overpass for MJJA 2014. (a) The comparison of LNO_x production by six different combinations for $CRF \geq 90\%$ with flash threshold of 2400 flashes. (b) Same as (a) except with a stroke threshold of 8160 strokes.~~

3.2 Comparison of LNO_x Production based on Different AMFs

Lapierre et al. (2019) derived LNO₂ production based on the BEHR NO₂ product. In order for our results to be comparable with those of Pickering et al. (2016) and Lapierre et al. (2019), we choose NO₂ instead of NO_x to derive productions production per flash (production efficiency, PE). In Fig. 3, time series of NO₂Vis, LNO₂Vis, LNO₂ and LNO₂Clean production per day over CONUS are plotted for MJJA 2014 with the criterion of $CRF \geq 90\%$ and a flash threshold of 2400 flashes per 2.4 h. LNO₂ productions production values are mostly in the range from 20 to 80 mol/flash. LNO₂Vis productions are smaller than LNO₂ productions which contain LNO₂ below clouds. The simulation of GMI in Pickering et al. (2016) indicated that 25% – 30% of the LNO_x column lies below the CP, while the ratio in our WRF-Chem simulation is ~~10%–80%~~ $56 \pm 20\%$. The effect of clouds cloud properties on LNO_x production will be discussed in more detail in section 3.4. Generally, the order of estimated daily production efficiencies (PEs) PEs is LNO₂Clean > LNO₂ > NO₂Vis > LNO₂Vis. The percent difference in the estimated PE (ΔPE) between NO₂Vis and LNO₂Vis indicates a certain amount of background NO₂ exists above clouds. Overall, the tendency of that ΔPE is consistent with another ΔPE between NO₂Vis and LNO₂Clean. When the region is highly polluted (ΔPE between NO₂Vis and LNO₂ is larger than 200%), PEs based on NO₂Vis and LNO₂Clean are significantly overestimated. In other words, NO₂Vis and LNO₂Clean are more sensitive to background NO₂. The extent of the overestimation of NO₂Vis is larger than that of LNO₂Clean in highly polluted regions, while it is usually opposite in most regions.

Figure 4 shows the linear regression for ENTLN data versus NO₂Vis, LNO₂Vis, LNO₂ and LNO₂Clean with the same criteria as shown in Fig. 3. LNO₂Clean production (the largest slope) is $49.1 \pm 25.2 \pm 8.4 \pm 22.3$ mol NO₂/flash with a correlation

280 of ~~0.79 and 7.5~~ 0.25 and 2.3 \pm ~~1.3-2.1~~ mol NO₂/stroke with a correlation of ~~0.77~~ 0.22. As shown in Fig. 3, the number of positive percent differences between NO₂Vis and LNO₂Clean production is much fewer than that of negative differences. As a result, NO₂Vis production (~~19.3-17.1~~ \pm ~~2.7-17.2~~ mol NO₂/flash and ~~3.6-0.4~~ \pm ~~0.5-1.0~~ mol NO₂/stroke) is smaller than LNO₂Clean production using the linear regression method.

285 If the CP \leq 650 hPa, TL \geq 1000 and ratio \geq 50% are removed from criteria, our result based on daily summed NO₂Vis values (3.8 ± 0.5 mol/stroke) is still larger than the value of 1.6 ± 0.1 mol/stroke mentioned in Lapierre et al. (2019). This may be caused by the different version of BEHR algorithm, as Lapierre et al. (2019) used BEHR V3.0A and our algorithm is based on BEHR V3.0B (Laughner et al., 2019). The input of S_{NO_2} in both versions is from the NASA standard product V3 and the major improvements of BEHR V3.0B are listed below:

1. The profile (V3.0B) closest to the OMI overpass time was selected instead of the last profile (V3.0A) before the OMI
290 overpass.
2. The AMF uses a variable tropopause height as opposed to the fixed 200 hPa tropopause.
3. The surface pressure is now calculated according to Zhou et al. (2009).

The detailed log of changes is available at <https://github.com/CohenBerkeleyLab/BEHR-core> (last access: February 7, 2020). Note that Lapierre et al. (2019) used the monthly NO₂ profile, while the daily profile is used in our study and the interval of our
295 outputs from WRF-Chem is 30 min which is more frequent than 1 h in the BEHR daily product, the AMF could be affected by different NO₂ profiles. In view of these factors, we compare different methods based on our data to minimize these effects.

Meanwhile, LNO₂ production (~~41.6-18.7~~ \pm ~~6.9-18.1~~ mol/flash and ~~6.3-2.1~~ \pm ~~1.1-1.8~~ mol/stroke) is between LNO₂Clean production and NO₂Vis production, which coincides with the daily results in Fig. 3. Furthermore, the calculated LNO_x production based on daily summed values (not shown) is 114.8 ± 18.2 mol/flash (or 17.8 ± 2.9 mol/stroke) which is larger than
300 91 mol/flash from the linear regression result of Pickering et al. (2016), possibly due to the differences in geographic location, lightning data, ~~chemistry model and the ratio of CG to IC~~ and chemistry model considered by Pickering et al. (2016) and this study.

The mean and standard deviation of LNO₂ production under CRF \geq 90% using the summation method is 46.2 ± 35.1 mol/flash and 9.9 ± 8.1 mol/stroke, while LNO_x production is 125.6 ± 95.9 mol/flash and 26.7 ± 21.6 mol/stroke (Fig. 5). The
305 LNO₂ and LNO_x production are both higher in the ~~South-Central-Southeast~~ U.S. (~~88°~~ denoted by the red box in Fig. 5 panels, ~~75°W - 103~~ 95°W, 28.5°N - 39°N) and Southeast U.S. (~~79°W - 85°W, 25°N - 35~~ 37°N), consistent with Lapierre et al. (2019) and Bucsela et al. (2019). Compared with Fig. 3, ~~Fig. 6(a) and (b)~~ Figure 6a and b present some large differences between NO₂Vis production and LNO₂Vis production, which are consistent with what we expect for polluted regions. Meanwhile, the differences between LNO₂ production and NO₂Vis production depend on background NO₂, the strength of updraft and the
310 profile. The negative differences are caused by background NO₂ carried by the updraft while parts of the below-cloud LNO₂ results in more LNO₂ production estimates than NO₂Vis production estimates (Fig. 6c). Figure 6(~~d~~) d shows that the ratio of LNO₂Vis to LNO₂ ranges from 10% – 80%. This may be caused by the height of the clouds and the profile of LNO₂. If the CP is near 300 hPa, the ratio should be smaller because of the coverage of clouds. The ratio would present the same trend while

the peaks of also be smaller while peaks of the LNO₂ profile is are below the CP. Therefore, a better understanding of LNO₂ profile and LNO_x below clouds is required.

3.3 Effects of Tropospheric Background on LNO_x Production

The patterns in Fig. 6 indicate the improvement of our approach is different in polluted and clean regions. To simplify the quantification, we select six grids with similar NO₂ profile (~ 100 pptv) above the cloud with CRF = 100%. These grid boxes contain the cities denoted by stars and triangles in Fig. 6a. Then, the differences between AMFs are dependent on fewer parameters:

$$AMF_{LNO_2} = \frac{\int_{p_{cloud}}^{p_{tp}} w_{cloudy}(p) NO_2(p) dp}{\int_{p_{surf}}^{p_{tp}} LNO_2(p) dp} \quad (7)$$

$$AMF_{NO_2Vis} = \frac{\int_{p_{cloud}}^{p_{tp}} w_{cloudy}(p) NO_2(p) dp}{\int_{p_{cld}}^{p_{tp}} NO_2(p) dp} \quad (8)$$

$$AMF_{LNO_2Clean} = \frac{\int_{p_{cloud}}^{p_{tp}} w_{cloudy}(p) LNO_2(p) dp}{\int_{p_{surf}}^{p_{tp}} LNO_2(p) dp} \quad (9)$$

Figure 7 compares the mean profiles of NO₂, background NO₂ and background NO₂ ratio in polluted and clean grids. Generally, the profiles of background NO₂ ratio are C-shape because LNO₂ concentrations are higher than background NO₂ in the UT. However, the ratio profile in Fig. 7e has one peak between the cloud pressure and tropopause as background NO₂ increases and LNO₂ decreases. Besides, the percentage of UT background NO₂ in polluted regions is steady and higher than that in clean regions.

Table 4 presents the relative changes among three methods in six cities. The difference between AMF_{LNO₂} (Eq. 7) and AMF_{LNO₂Clean} (Eq. 9) is the numerator: $\int_{p_{cloud}}^{p_{tp}} w_{cloudy}(p) NO_2(p) dp$ and $\int_{p_{cloud}}^{p_{tp}} w_{cloudy}(p) LNO_2(p) dp$. When the ratio of LNO₂ is higher or the region is cleaner, the relative difference is smaller (e.g. 5.0% – 12.0%, Fig. 7d – f). The largest relative difference (46.3%) occurs when the ratio of background NO₂ is continuously high in the UT (Fig. 7c). As a result, our approach is less sensitive to background NO₂ and more suitable for convections over polluted locations. In contrast, production estimated by our method is larger than that based on NO₂Vis due to the LNO₂ below the cloud. When the cloud is higher, especially the peak of LNO profile is lower than the cloud (Fig. 7b), the relative difference is larger (121.2%) because more LNO₂ can not be included into the NO₂Vis, which has been discussed in Sect. 3.2. The relative change between AMF_{LNO₂Clean} (Eq. 9) and AMF_{NO₂Vis} (Eq. 8) depends on $\int_{p_{cloud}}^{p_{tp}} w_{cloudy}(p) LNO_2(p) dp / \int_{p_{surf}}^{p_{tp}} w_{cloudy}(p) LNO_2(p) dp$, which is also affected by cloud not the background NO₂. The largest relative change is 153.8% among the six grids where the highest clouds occur.

3.4 Effects of Cloud and LNO_x Parameterization on LNO_x Production

340 Figure 7-8a presents the daily distribution of CP and the ratio of LNO₂Vis to LNO₂ during MJJA 2014 with the criteria defined in section 3.1 under CRF \geq 90%. Since the ratio of LNO₂Vis to LNO₂ decreases from 0.8 to 0.2 ~~while the cloud is higher (smaller pressure value) as the cloud pressure decreases from 600 to 300 hPa~~, NO₂Vis production is smaller than LNO₂ in relatively clean areas as shown in Fig. 4. Apart from LNO₂Vis, the LNO₂ production is also affected by CP. For LNO₂ production larger than 30 mol/stroke, the CPs are all smaller than 550 hPa (Fig. 88b). However, smaller LNO₂ ~~productions~~ ~~production~~ ($<$ 30 mol/stroke) ~~occur~~ ~~occurs~~ on all levels between 650 hPa and 200 hPa. Because of the limited amount of large LNO₂ production and lightning data, we ~~can not derive that higher~~ ~~cannot derive the relationship between~~ LNO₂ production ~~relates to higher clouds and cloud pressure~~ or different lightning properties at this stage. Because CP only represents the development of clouds, the vertical structure of flashes can not be derived from the CP values only. As discussed in several previous studies, flash channel length varies and depends on the environmental conditions (Carey et al., 2016; Mecikalski and Carey, 2017; Fuchs and Rutledge, 2018). Davis et al. (2019) compared two kinds of flashes: normal flashes and anomalous flashes. Because updrafts are stronger and flash rates are ~~larger~~ ~~higher~~ in anomalous storms, UT LNO_x ~~production is larger~~ ~~concentrations is larger in anomalous~~ than normal polarity storms. In general, normal flashes are coupled with an upper-level positive charge region and a mid-level negative charge region, while anomalous flashes are opposite (Williams, 1989). It is not straightforward to estimate the error resulting from the vertical distribution of LNO_x. There are mainly two methods of distributing LNO_x in models: LNO_x profiles (postconvection) ~~are simulated after in which~~ LNO_x ~~is~~ ~~has already been~~ redistributed by convective transport, while the other one (preconvection) uses LNO_x ~~production~~ profiles made before the redistribution of convective transport (~~Luo et al., 2017~~) (~~Allen et al., 2012; Luo et al., 2017~~). However, given the similarity of results compared to other LNO_x studies, we believe that our $1^\circ \times 1^\circ$ results based on postconvective LNO_x profile are sufficient for estimating average LNO_x production.

360 ~~Scatter plots of the daily LNO₂ production efficiency versus the daily cloud pressure measured by OMI with CRF \geq 90% for MJJA 2014.~~

The LNO production settings in WRF-Chem varied in different studies. Zhao et al. (2009) set a NO_x production rate of 250 mol NO per flash in a regional-scale model, while Bela et al. (2016) chose the same ~~method~~ ~~value~~ (330 mol NO per flash) that was used by Barth et al. (2012). Wang et al. (2015) assumed approximately 500 mol NO per flash which was derived by a cloud-scale chemical transport model and in-cloud aircraft observations (Ott et al., 2010). To illustrate the impact of LNO_x parameterization on LNO_x estimation, we apply another WRF-Chem NO₂ profile setting ($2 \times$ base flashrate, 500 mol NO flash⁻¹; hereinafter referred to as " 2×500 mol NO flash⁻¹") to a priori profiles and evaluate the changes in AMF_{LNO₂}, AMF_{LNO_x}, LNO₂ and LNO_x productions. For the linear regression method (Fig. 9), LNO₂ production is ~~46.4~~ ~~29.8~~ \pm ~~7.8~~ ~~20.5~~ mol/flash which is ~~11.5~~ ~~59.4~~% larger than the basic one (~~41.6~~ ~~18.7~~ \pm ~~6.9~~ ~~18.1~~ mol/flash). ~~However~~ ~~Meanwhile~~, LNO_x production (increasing from ~~114.8~~ ~~54.5~~ \pm ~~18.2~~ ~~48.1~~ mol/flash to ~~143.4~~ ~~88.5~~ \pm ~~24.0~~ ~~61.1~~ mol/flash) ~~depends to a large extent~~ ~~also depends~~ on the configuration of LNO production in WRF-Chem (~~Fig. 10~~). It remains unclear as to whether the NO-NO₂-

O₃ cycle or other LNO_x reservoirs accounts for the increment of LNO_x production. This would need detailed source analysis in WRF-Chem and is beyond the scope of this study.

Figure 10 shows the average percentage changes in AMF_{LNO₂}, AMF_{LNO_x}, LNO₂ and LNO_x between retrievals using profiles based on 1×200 mol NO flash⁻¹ and 2×500 mol NO flash⁻¹. These results were obtained by averaging data over MJJA 2014 based on the method described in Sect. 2.5 with the criterion of CRF ≥ 90%. The effects on LNO₂ and LNO_x retrieval from increasing LNO profile values show mostly the same tendency: smaller AMF_{LNO₂} and AMF_{LNO_x} leads to larger LNO₂ and LNO_x, but the changes are region-regionally dependent. This is caused by the nonlinear calculation of AMF_{LNO₂} and AMF_{LNO_x}. As the contribution of LNO₂ increases, both the numerator and denominator of Eq. (2) increase. Note that the LNO₂ accounts for a fraction of NO₂ above the clouds, the magnitude of increasing denominator could be different in-than that of increasing numerator, resulting in a different effect on the AMF_{LNO₂} and AMF_{LNO_x}. As mentioned in Zhu et al. (2019), the lightning densities in the Southeast U.S. might be overestimated using the 2×500 mol NO flash⁻¹ setting and the same lightning parameterization as ours. Fortunately, the AMFs and estimated LNO₂ change little in that region.

Figure 11 shows the comparison of the mean LNO and LNO₂ profiles in two specific regions where the 2×500 mol NO flash⁻¹ setting leads to both lower and higher LNO₂ production. The first one (Fig. 11a) is the region (36°N – 37°N, 89°W – 90°W) containing the minimal negative percent change in LNO₂ (Fig. 10c). The second one (31°N – 32°N, 97°W – 98°W), Figure 11b, has the largest positive percent change in LNO₂ (Fig. 10c). Although the relative distribution-distributions of mean LNO and LNO₂ profiles is-are similar in both regions, the magnitude differs with a factor of 10. This phenomenon implies that the performance of lightning parameterization in WRF-Chem is region dependent and the-an unrealistic profile could appear in the UT. Although this sensitivity analysis is false in some regions, it allows the calculation of an upper limit on the NO₂ due to LNO and LNO₂ profiles. As discussed in Laughner and Cohen (2017), the scattering weights are uniform under cloudy conditions and the sensitivity of NO₂ is nearly constant with different pressure levels because of the high albedo. However, the relative distribution of LNO₂ within the UT should be taken carefully in-our-research-into-consideration. If the LNO₂/NO₂ above the cloud is large enough (Fig. 11a), the AMF_{LNO₂} is largely determined by the ratio of LNO₂Vis to LNO₂ which is related to the relative distribution. When the condition of high LNO₂/NO₂ is not met, both relative distribution and ratio are involved-important (Fig. 11b).

To clarify this, we applied the same sensitivity test of different simulating LNO amounts for all four methods mentioned in Sect. 2.4: LNO₂, LNO₂Vis, LNO₂Clean and NO₂Vis (Fig. 12). Note that the threshold for CRF is set to 100% to simplify Eq. (2) to ÷

$$AMF_{LNO_x} = \frac{\int_{p_{cloud}}^{p_{tp}} w_{cloudy}(p) NO_2(p) dp}{\int_{p_{surf}}^{p_{tp}} LNO_x(p) dp}$$

Eq. (7). The overall differences of LNO₂Clean and NO₂Vis are smaller than those of LNO₂ and LNO₂Vis. Comparing the composition of numerator and denominator in the equations, it is clear why the impact of different simulating LNO amounts is smaller in Fig. 12(e) and (d) c and d. For LNO₂Clean and NO₂Vis, both the SCD and VCD will increase (decrease) when more (less) LNO₂ or NO₂ presents. The difference between Fig. 12(a) a and Fig. 12(b) b is the denominator: the total tropospheric

405 LNO₂ vertical column and visible LNO₂ vertical column respectively. As a result, the negative values in Fig. 12(a-a) is caused by the part of LNO₂ below the cloud. The comparison between [Figure 4 and Figure Fig. 4 and Fig. 9](#) shows that LNO₂Clean and LNO₂ values are more similar while LNO₂ and NO₂Vis values are same. The uncertainty of retrieved LNO₂ and LNO_x productions is driven by this error, and we conservatively estimate this to be $\pm 1315\%$ and $\pm 2629\%$ respectively.

4 Uncertainties Analysis

410 The uncertainties of the LNO₂ and LNO_x production are estimated following Pickering et al. (2016), [Allen et al. \(2019\)](#), [Bucsele et al. \(2019\)](#), Lapierre et al. (2019) and Laughner et al. (2019). We determine the uncertainty due to BEHR tropopause pressure, cloud radiance fraction, [cloud pressure](#), surface pressure, surface reflectivity, profile shape, profile location, V_{strat}, the detection efficiency of lightning, t_{window} and LNO₂ lifetime numerically by perturbing each parameter in turn and re-retrieval of the LNO₂ and LNO_x with the perturbed values (Table 5).

415 The GEOS-5 monthly tropopause pressure, which is consistent with the NASA Standard Product, is applied instead of the variable WRF tropopause height to evaluate the uncertainty (6% for LNO₂ and 4% for LNO_x) caused by the BEHR tropopause pressure. [Beirle et al. \(2009\) obtained a mean total sensitivity of 0.46 \(\$\sigma = 0.09\$ \) for LNO_x in the sensitivity study, implying an uncertainty of 23% due to cloud pressure in our study.](#) The resolution of GLOBE terrain height data is much higher than the OMI pixel and a fixed scale height is assumed in the BEHR algorithm. As a result, Laughner et al. (2019) compared the
420 average WRF surface pressures to the GLOBE surface pressures and arrived at the largest bias of 1.5%. Based on the largest bias, we vary the surface pressure (limited to less than 1020 hPa) and the uncertainty can be neglected.

The error in cloud radiance fraction is transformed from cloud fraction using:

$$\sigma = 0.05 \cdot \left. \frac{\partial f_r}{\partial f_g} \right|_{f_{g, pix}} \quad (10)$$

where f_r is the cloud radiance fraction, f_g is the cloud fraction and $f_{g, pix}$ is the cloud fraction of a specific pixel. We calculate
425 $\partial f_r / \partial f_g$ under $f_{g, pix}$ by the relationship between all binned f_r and f_g with the increment of 0.05 for the each specific OMI orbit. Considering the relationship, the error in cloud fraction is converted to an error in cloud radiance fraction of 2% for both LNO₂ and LNO_x.

The accuracy of the 500 m MODIS albedo product is usually within 5% of albedo observations at the validation sites and those exceptions with low quality flags have been found to be primarily within 10% of the field data (Schaaf et al., 2011). Since
430 we use the bidirectional reflectance distribution function (BRDF) data directly, rather than including a radiative transfer model, 14% Lambertian equivalent reflectivity (LER) error and 10% uncertainty are combined to get a perturbation of 17% (Laughner et al., 2019). The uncertainty due to surface reflectivity can be neglected with the 17% perturbation.

As discussed at the end of Sect. 3.4, another setting of LNO₂ ($2 \times 500 \text{ mol NO flash}^{-1}$) is applied to determine the uncertainty of the lightning parameterization and the vertical distribution of LNO in WRF-Chem. Differences between the two profiles lead
435 to an uncertainty of ~~13%~~ ~~and 2615%~~ ~~and 29%~~ in the resulting LNO₂ and LNO_x production. Another sensitivity test allows each pixel to shift by - 0.2, 0, or + 0.2 degrees in the directions of longitude and latitude, taking advantage of the high-resolution

profile location in WRF-Chem. The resulting uncertainty of LNO_x production is 1% including the error of transport and chemistry by shifting pixels.

440 Compared to the NASA standard product v2, Krotkov et al. (2017) demonstrated that the noise in V_{strat} is $1 \times 10^{14} \text{ cm}^{-2}$. Errors in polluted regions can be slightly larger than this value, while errors in the cleanest areas are typically significantly smaller (Bucsela et al., 2013). We estimated the uncertainty of V_{strat} component and the slant column errors to be ~~15~~10% and 5%, respectively, following Allen et al. (2019).

445 Based on the standard deviation of the detection efficiency estimation over the CONUS relative to LIS, ENTLN detection efficiency uncertainties are $\pm 16\%$ for total and IC flashes/strokes. Due to the high detection efficiency of CG over the CONUS, the uncertainty is estimated to be $\pm 5\%$ (Lapierre et al., 2019). It is found that the resulting uncertainty of detection efficiency is 15% in the production analysis. We have used the t_{window} of 2.4 h for counting ENTLN flashes and strokes to analyze LNO₂ and LNO_x production. Because t_{window} derived from the ERA5 reanalysis can not represent the variable wind speeds, a sensitivity test is performed which yields an uncertainty of 10% for production per flash and 8% for production per stroke using t_{window} of 2 h and 4 h. Meanwhile, the lifetime of UT NO_x ranges from 2 hours to 12 hours depending on the convective location, 450 the methyl peroxy nitrate and alkyl and multifunctional nitrates (Nault et al., 2017). The lifetime (τ) of NO₂ in Eq. (6) is replaced by 2 and 12 hours to determine the uncertainty as 24% due to lifetime. The lifetime is the most likely uncertainty in the production analysis of LNO₂ while the uncertainty caused by lightning parameterization is comparable with that for the LNO_x type.

455 Recent works revealed that the modeled NO/NO₂ ratio departs from the data in the SEAC⁴RS aircraft campaign (Travis et al., 2016; Silvern et al. (2018) attributed this to the positive interference on the NO₂ measurements or errors in the cold-temperature NO-NO₂-O₃ photochemical reaction rate. We assign an uncertainty of 20% to this error considering the possible positive NO₂ measurements interferences (Allen et al., 2019; Bucsela et al., 2019).

460 In addition, the estimation of LNO_x PE is also dependent on the tropospheric background NO₂. In our method, main factors affecting this factor are the emissions inventory and the amount of transported NO₂. For the emissions inventory, the sources of uncertainty are assumptions, methods, input data and calculation errors. As a result, the uncertainties for different species or pollutants related to NO₂ are different and EPA also doesn't publish the quantified uncertainty measures because the parties that submit emissions estimates to EPA are not asked to include quantitative uncertainty measurements or estimates (EPA, 2015). For the simulated convective transport, Li et al. (2018) compared the cloud-resolving simulations with these based on convective parameterization and pointed out that the convective transport was weaker in the parameterization. But, 465 we believe that the ratio condition (LNO₂Vis/NO₂Vis $\geq 50\%$) should reduce these two kinds of uncertainty and assume an uncertainty of 10%, which is less than 20% assigned in Allen et al. (2019) and Bucsela et al. (2019).

The overall uncertainty is estimated as the square root of the sum of the squares of all individual uncertainties in Table 5. The net uncertainty is ~~37% and 4348% and 54%~~ for LNO₂ type and LNO_x type respectively. The mean LNO₂/flash, LNO_x/flash, LNO₂/stroke, LNO_x/stroke based on the linear regression and summation method are ~~44-32~~ mol/flash, ~~120-90~~ mol/flash, ~~8-6~~ 470 mol/stroke and ~~22-17~~ mol/stroke. Applying the corresponding uncertainty to these mean values, we arrive at ~~44-32~~ \pm ~~16-15~~ mol LNO₂/flash, ~~120-90~~ \pm ~~52-49~~ mol LNO_x/flash, ~~8-6~~ \pm 3 mol LNO₂/stroke and ~~22-17~~ \pm 9 mol LNO_x/stroke. This is in the

range of current literature estimate ranging from 33 to 500 mol LNO_x/flash (Schumann and Huntrieser, 2007; Beirle et al., 2010; Bucselo et al., 2010). Bucselo et al. (2010) estimated LNO_x production of 100 – 250 mol/flash which is similar to our flash-based results. Pickering et al. (2016) estimated LNO_x production to be 80 ± 45 mol per flash for the Gulf of Mexico, which is 50% smaller than our flash-based results over the CONUS. Note that the criteria defined in Sect. 3.1 lead to many missing data over the Gulf of Mexico, thus it is actually a comparison between different regions. For the stroke-based results, Lapierre et al. (2019) yields lower LNO₂ production of 1.6 ± 0.1 mol per stroke, the difference is caused by the different version of BEHR algorithm and several settings as mentioned in Sect. 3.2. Bucselo et al. (2019) inferred an average value of 200 ± 110 moles (67% larger than our results) LNO_x produced per flash over the North America, this is related to the different algorithm and lightning data.

5 Conclusions

In this study, a new algorithm for retrieving LNO₂ (LNO_x) from OMI, including LNO₂ (LNO_x) below cloud, has been developed for application over active convection, ~~whether in clean or polluted regions~~. It works in both clean and polluted regions because of the consideration of tropospheric background pollution in the definition of AMFs. It uses specific criteria combining with several other conditions (sufficient CRF, coincident ENTLN data, TL ≥ 1000 and ratio ≥ 50%) to ensure that the electrically active regions are detected by OMI and simulated by WRF-Chem successfully. We conducted an analysis on 1° × 1° daily boxes in MJJA 2014 and obtained the seasonal mean LNO₂ and LNO_x PEs production efficiencies over the CONUS. Considering all the uncertainties (Table 5) and applying the summation and regression method, the final mean PEs production efficiencies are estimated to be 44-32 ± 16-15 mol LNO₂/flash, 120-90 ± 52-49 mol LNO_x/flash, 8-6 ± 3 mol LNO₂/stroke and 22-17 ± 9 mol LNO_x/stroke.

Compared with former methods, ~~we find that NO₂ Vis and LNO₂ Clean are more~~ our method has reduced the sensitive to background NO₂, while ~~NO₂ Vis underestimates PE~~ the method in Lapierre et al. (2019) underestimates LNO_x production efficiency because of the neglected below-cloud LNO₂ and LNO₂ ~~Clean overestimates LNO₂ production~~ production is overestimated using the method in Pickering et al. (2016) due to the over-cloud background NO₂ in polluted regions. Finally, implementing profiles generated with different model settings of lightning (1×200 mol NO flash⁻¹ and 2×500 mol NO flash⁻¹), we find that the ~~regionally dependent effect~~ larger LNO production model setting leads to larger retrieval of LNO_x despite some regionally dependent effects caused by nonlinear calculation of AMF. Both the ~~relative distribution of ratio of the tropospheric LNO₂ above the cloud to the total tropospheric LNO₂~~ and the ratio of LNO₂ to NO₂ ~~would take the comprehensive effect for differences by~~ cause different comprehensive effects due to the nonlinear calculation of AMF_{LNO₂} and AMF_{LNO_x}.

Since other regions, like China and India, have much more NO₂ ~~pollutions~~ pollution than the CONUS, it is necessary to consider the background NO₂ in detail. These analyses will be complemented by the recently launched satellite instrument (TROPOspheric Monitoring Instrument [TROPOMI]) (Veefkind et al., 2012; Boersma et al., 2018; Griffin et al., 2019) and Lightning Mapping Imager (LMI) on the new generation Chinese geostationary meteorological satellites Fengyun-4 (Min et al., 2017; Yang et al., 2017; Zhang et al., 2019). Future work investigating the flash channel length and more detailed

505 lightning parameterization in WRF-Chem would greatly benefit LNO_x estimation. Applying current method in future studies may enhance the accuracy of LNO_x production at both local and global [levelscales](#).

Code and data availability. The retrieval algorithm used in Sect. 2.4 is available at <https://github.com/zxdawn/BEHR-LNOx> (last access: February 7, 2020; Zhang and Laughner, 2019). The WRF-Chem model output and LNO_x product are available upon request to Xin Zhang (xinzhang1215@gmail.com).

510 Appendix A: AMF Definitions used in this Study

$$AMF_{LNO_2} = \frac{(1 - f_r) \int_{p_{surf}}^{p_{tp}} w_{clear}(p) NO_2(p) dp + f_r \int_{p_{cloud}}^{p_{tp}} w_{cloudy}(p) NO_2(p) dp}{\int_{p_{surf}}^{p_{tp}} LNO_2(p) dp} \quad (A1)$$

$$AMF_{LNO_x} = \frac{(1 - f_r) \int_{p_{surf}}^{p_{tp}} w_{clear}(p) NO_2(p) dp + f_r \int_{p_{cloud}}^{p_{tp}} w_{cloudy}(p) NO_2(p) dp}{\int_{p_{surf}}^{p_{tp}} LNO_x(p) dp} \quad (A2)$$

where f_r is the radiance cloud fraction, p_{surf} is the surface pressure, p_{tp} is the tropopause pressure, p_{cloud} is the cloud optical pressure (CP), w_{clear} and w_{cloudy} are respectively the pressure dependent scattering weights from the TOMRAD lookup table
 515 (Bucsela et al., 2013) for clear and cloudy parts, and $NO_2(p)$ is the modeled NO₂ vertical profile. $LNO_2(p)$ and $LNO_x(p)$ are respectively the LNO₂ and LNO_x vertical profile calculated by the difference of vertical profiles between WRF-Chem simulations with and without lightning.

$$AMF_{LNO_2Clean} = \frac{(1 - f_r) \int_{p_{surf}}^{p_{tp}} w_{clear}(p) LNO_2(p) dp + f_r \int_{p_{cloud}}^{p_{tp}} w_{cloudy}(p) LNO_2(p) dp}{\int_{p_{surf}}^{p_{tp}} LNO_2(p) dp} \quad (A3)$$

$$AMF_{NO_2Vis} = \frac{(1 - f_r) \int_{p_{surf}}^{p_{tp}} w_{clear}(p) NO_2(p) dp + f_r \int_{p_{cloud}}^{p_{tp}} w_{cloudy}(p) NO_2(p) dp}{(1 - f_g) \int_{p_{surf}}^{p_{tp}} NO_2(p) dp + f_g \int_{p_{cloud}}^{p_{tp}} NO_2(p) dp} \quad (A4)$$

$$520 \quad AMF_{NO_xVis} = \frac{(1 - f_r) \int_{p_{surf}}^{p_{tp}} w_{clear}(p) NO_2(p) dp + f_r \int_{p_{cloud}}^{p_{tp}} w_{cloudy}(p) NO_2(p) dp}{(1 - f_g) \int_{p_{surf}}^{p_{tp}} NO_x(p) dp + f_g \int_{p_{cloud}}^{p_{tp}} NO_x(p) dp} \quad (A5)$$

$$AMF_{LNO_2Vis} = \frac{(1 - f_r) \int_{p_{surf}}^{p_{tp}} w_{clear}(p) NO_2(p) dp + f_r \int_{p_{cloud}}^{p_{tp}} w_{cloudy}(p) NO_2(p) dp}{(1 - f_g) \int_{p_{surf}}^{p_{tp}} LNO_2(p) dp + f_g \int_{p_{cloud}}^{p_{tp}} LNO_2(p) dp} \quad (A6)$$

where f_g is the geometric cloud fraction and $NO_x(p)$ is the modeled NO_x vertical profile.

Author contributions. YY directed the research and RJvdA, XZ and YY designed the research with feedback from the other co-authors; RJvdA and XZ developed the algorithm; JLL provided guidance and supporting data on the ENTLN data; XZ performed simulations and analysis with the help of YY, RJvdA, QC, XK, SY, JC, CH and RS; YY, RJvdA, JLL and XZ interpreted the data and discussed the results. XZ drafted the manuscript with comments from the co-authors; JLL, RJvdA and YY edited the manuscript.

Competing interests. The authors declare that they have no conflict of interest.

Acknowledgements. This work was funded by the National Natural Science Foundation of China (91644224 and 41705118). We acknowledge use of the computational resource provided by the National Supercomputer Centre in Guangzhou (NSCC-GZ). We thank the University of California Berkeley Satellite Group for the basic BEHR algorithm. We also thank Earth Networks Company for providing the Earth Networks Total Lightning Network (ENTLN) datasets. We appreciate the discussions with Joshua L. Laughner for BEHR codes and Mary Barth for the WRF-Chem lightning NO_x module. MOZART-4 global model output is available at <https://www.acom.ucar.edu/wrf-chem/mozart.shtml> (last access: February 7, 2020). [Finally, we thank the three anonymous reviewers whose detailed comments helped us improve and clarify this manuscript.](#)

535 **References**

- Acarreta, J. R., de Haan, J. F., and Stammes, P.: Cloud pressure retrieval using the O₂ -O₂ absorption band at 477 nm, *Journal of Geophysical Research*, 109, 2165, <https://doi.org/10.1029/2003JD003915>, 2004.
- Allen, D. J., Pickering, K. E., Duncan, B. N., and Damon, M.: Impact of lightning NO emissions on North American photochemistry as determined using the Global Modeling Initiative (GMI) model, *Journal of Geophysical Research*, 115, 4711, <https://doi.org/10.1029/2010JD014062>, 2010.
- 540 Allen, D. J., Pickering, K. E., Pinder, R. W., Henderson, B. H., Appel, K. W., and Prados, A.: Impact of lightning-NO on eastern United States photochemistry during the summer of 2006 as determined using the CMAQ model, *Atmospheric Chemistry and Physics*, 12, 1737–1758, <https://doi.org/10.5194/acp-12-1737-2012>, 2012.
- Allen, D. J., Pickering, K. E., Bucselá, E. J., Krotkov, N., and Holzworth, R.: Lightning NO_x Production in the Tropics as Determined Using
545 OMI NO₂ Retrievals and WWLLN Stroke Data, *Journal of Geophysical Research: Atmospheres*, <https://doi.org/10.1029/2018JD029824>, 2019.
- Banerjee, A., Archibald, A. T., Maycock, A. C., Telford, P., Abraham, N. L., Yang, X., Braesicke, P., and Pyle, J. A.: Lightning NO_x, a key chemistry–climate interaction: impacts of future climate change and consequences for tropospheric oxidising capacity, *Atmospheric Chemistry and Physics*, 14, 9871–9881, <https://doi.org/10.5194/acp-14-9871-2014>, 2014.
- 550 Barth, M. C., Lee, J., Hodzic, A., Pfister, G., Skamarock, W. C., Worden, J., Wong, J., and Noone, D.: Thunderstorms and upper troposphere chemistry during the early stages of the 2006 North American Monsoon, *Atmospheric Chemistry and Physics*, 12, 11 003–11 026, <https://doi.org/10.5194/acp-12-11003-2012>, 2012.
- Beirle, S., Platt, U., Wenig, M., and Wagner, T.: NO_x production by lightning estimated with GOME, *Advances in Space Research*, 34, 793–797, <https://doi.org/10.1016/j.asr.2003.07.069>, 2004.
- 555 Beirle, S., Spichtinger, N., Stohl, A., Cummins, K. L., Turner, T., Boccippio, D., Cooper, O. R., Wenig, M., Grzegorski, M., Platt, U., and Wagner, T.: Estimating the NO_x produced by lightning from GOME and NLDN data: A case study in the Gulf of Mexico, *Atmospheric Chemistry and Physics*, 6, 1075–1089, <https://doi.org/10.5194/acp-6-1075-2006>, 2006.
- Beirle, S., Salzmann, M., Lawrence, M. G., and Wagner, T.: Sensitivity of satellite observations for freshly produced lightning NO_x, *Atmospheric Chemistry and Physics*, 9, 1077–1094, <https://doi.org/10.5194/acp-9-1077-2009>, 2009.
- 560 Beirle, S., Huntrieser, H., and Wagner, T.: Direct satellite observation of lightning-produced NO_x, *Atmospheric Chemistry and Physics*, 10, 10965–10986, <https://doi.org/10.5194/acp-10-10965-2010>, 2010.
- Bela, M. M., Barth, M. C., Toon, O. B., Fried, A., Homeyer, C. R., Morrison, H., Cummings, K. A., Li, Y., Pickering, K. E., Allen, D. J., Yang, Q., Wennberg, P. O., Crouse, J. D., St. Clair, J. M., Teng, A. P., O’Sullivan, D., Huey, L. G., Chen, D., Liu, X., Blake, D. R., Blake, N. J., Apel, E. C., Hornbrook, R. S., Flocke, F., Campos, T., and Diskin, G.: Wet scavenging of soluble gases in DC3 deep
565 convective storms using WRF-Chem simulations and aircraft observations, *Journal of Geophysical Research: Atmospheres*, 121, 4233–4257, <https://doi.org/10.1002/2015JD024623>, 2016.
- Boersma, K. F., Eskes, H. J., Meijer, E. W., and Kelder, H. M.: Estimates of lightning NO_x production from GOME satellite observations, *Atmospheric Chemistry and Physics*, 5, 2311–2331, <https://doi.org/10.5194/acp-5-2311-2005>, 2005.
- Boersma, K. F., Eskes, H. J., Richter, A., de Smedt, I., Lorente, A., Beirle, S., van Geffen, J. H. G. M., Zara, M., Peters, E., van Roozendaal,
570 M., Wagner, T., de Maasackers, J., van der A, R. J., Nightingale, J., de Rudder, A., Irie, H., Pinardi, G., Lambert, J.-C., and Compernelle, S. C.: Improving algorithms and uncertainty estimates for satellite NO₂ retrievals: results from the quality assurance for the essential

- climate variables (QA4ECV) project, *Atmospheric Measurement Techniques*, 11, 6651–6678, <https://doi.org/10.5194/amt-11-6651-2018>, 2018.
- 575 Bovensmann, H., Burrows, J. P., Buchwitz, M., Frerick, J., Noël, S., Rozanov, V. V., Chance, K. V., and Goede, A. P. H.: SCIAMACHY: Mission Objectives and Measurement Modes, *Journal of the Atmospheric Sciences*, 56, 127–150, [https://doi.org/10.1175/1520-0469\(1999\)056<0127:SMOAMM>2.0.CO;2](https://doi.org/10.1175/1520-0469(1999)056<0127:SMOAMM>2.0.CO;2), 1999.
- Browne, E. C., Wooldridge, P. J., Min, K.-E., and Cohen, R. C.: On the role of monoterpene chemistry in the remote continental boundary layer, *Atmospheric Chemistry and Physics*, 14, 1225–1238, <https://doi.org/10.5194/acp-14-1225-2014>, 2014.
- 580 Bucselá, E. J., Pickering, K. E., Huntemann, T. L., Cohen, R. C., Perring, A., Gleason, J. F., Blakeslee, R. J., Albrecht, R. I., Holzworth, R., Cipriani, J. P., Vargas-Navarro, D., Mora-Segura, I., Pacheco-Hernández, A., and Laporte-Molina, S.: Lightning-generated NO_x seen by the Ozone Monitoring Instrument during NASA's Tropical Composition, Cloud and Climate Coupling Experiment (TC⁴), *Journal of Geophysical Research*, 115, 793, <https://doi.org/10.1029/2009JD013118>, 2010.
- Bucselá, E. J., Krotkov, N. A., Celarier, E. A., Lamsal, L. N., Swartz, W. H., Bhartia, P. K., Boersma, K. F., Veefkind, J. P., Gleason, J. F., and Pickering, K. E.: A new stratospheric and tropospheric NO₂ retrieval algorithm for nadir-viewing satellite instruments: Applications
585 to OMI, *Atmospheric Measurement Techniques*, 6, 2607–2626, <https://doi.org/10.5194/amt-6-2607-2013>, 2013.
- Bucselá, E. J., Pickering, K. E., Allen, D. J., Holzworth, R., and Krotkov, N. A.: Midlatitude lightning NO_x production efficiency inferred from OMI and WLLN data, *Journal of Geophysical Research: Atmospheres*, <https://doi.org/10.1029/2019JD030561>, 2019.
- Burrows, J. P., Weber, M., Buchwitz, M., Rozanov, V., Ladstätter-Weißmayer, A., Richter, A., DeBeek, R., Hoogen, R., Bramstedt, K., Eichmann, K.-U., Eisinger, M., and Perner, D.: The Global Ozone Monitoring Experiment (GOME): Mission Concept and First Scientific Results, *Journal of the Atmospheric Sciences*, 56, 151–175, [https://doi.org/10.1175/1520-0469\(1999\)056<0151:TGOMEG>2.0.CO;2](https://doi.org/10.1175/1520-0469(1999)056<0151:TGOMEG>2.0.CO;2), 1999.
- 590 Callies, J., Corpaccioli, E., Eisinger, M., Hahne, A., and Lefebvre, A.: GOME-2-Metop's second-generation sensor for operational ozone monitoring, *ESA bulletin*, 102, 28–36, 2000.
- Carey, L. D., Koshak, W., Peterson, H., and Mecikalski, R. M.: The kinematic and microphysical control of lightning rate, extent, and NO_x production, *Journal of Geophysical Research: Atmospheres*, 121, 7975–7989, <https://doi.org/10.1002/2015JD024703>, 2016.
- 595 Choi, S., Joiner, J., Choi, Y., Duncan, B. N., Vasilkov, A., Krotkov, N., and Bucselá, E.: First estimates of global free-tropospheric NO₂ abundances derived using a cloud-slicing technique applied to satellite observations from the Aura Ozone Monitoring Instrument (OMI), *Atmospheric Chemistry and Physics*, 14, 10 565–10 588, <https://doi.org/10.5194/acp-14-10565-2014>, 2014.
- Clark, S. K., Ward, D. S., and Mahowald, N. M.: Parameterization-based uncertainty in future lightning flash density, *Geophysical Research Letters*, 44, 2893–2901, <https://doi.org/10.1002/2017GL073017>, 2017.
- 600 Davis, T. C., Rutledge, S. A., and Fuchs, B. R.: Lightning location, NO_x production, and transport by anomalous and normal polarity thunderstorms, *Journal of Geophysical Research: Atmospheres*, <https://doi.org/10.1029/2018JD029979>, 2019.
- DeCaria, A. J., Pickering, K. E., Stenichikov, G. L., Scala, J. R., Stith, J. L., Dye, J. E., Ridley, B. A., and Laroche, P.: A cloud-scale model study of lightning-generated NO_x in an individual thunderstorm during STERAO-A, *Journal of Geophysical Research*, 105, 11 601–11 616, <https://doi.org/10.1029/2000JD900033>, 2000.
- 605 DeCaria, A. J., Pickering, K. E., Stenichikov, G. L., and Ott, L. E.: Lightning-generated NO_x and its impact on tropospheric ozone production: A three-dimensional modeling study of a Stratosphere-Troposphere Experiment: Radiation, Aerosols and Ozone (STERAO-A) thunderstorm, *Journal of Geophysical Research*, 110, n/a–n/a, <https://doi.org/10.1029/2004JD005556>, 2005.

- Dobber, M., Kleipool, Q., Dirksen, R., Levelt, P., Jaross, G., Taylor, S., Kelly, T., Flynn, L., Leppelmeier, G., and Rozemeijer, N.: Validation of Ozone Monitoring Instrument level 1b data products, *Journal of Geophysical Research*, 113, 5224, <https://doi.org/10.1029/2007JD008665>, 2008.
- Emmons, L. K., Walters, S., Hess, P. G., Lamarque, J.-F., Pfister, G. G., Fillmore, D., Granier, C., Guenther, A., Kinnison, D., Laepple, T., Orlando, J., Tie, X., Tyndall, G., Wiedinmyer, C., Baughcum, S. L., and Kloster, S.: Description and evaluation of the Model for Ozone and Related chemical Tracers, version 4 (MOZART-4), *Geoscientific Model Development*, 3, 43–67, <https://doi.org/10.5194/gmd-3-43-2010>, 2010.
- EPA, U.: 2011 National Emissions Inventory, version 2—Technical support document, US Environmental Protection Agency, Office of Air Quality Planning and Standards. Accessed August 2017., 2015.
- EPA, U. S. and OAR: Air Pollutant Emissions Trends Data | US EPA, <https://www.epa.gov/air-emissions-inventories/air-pollutant-emissions-trends-data>, 2015.
- Finney, D. L., Doherty, R. M., Wild, O., Young, P. J., and Butler, A.: Response of lightning NO_x emissions and ozone production to climate change: Insights from the Atmospheric Chemistry and Climate Model Intercomparison Project, *Geophysical Research Letters*, 43, 5492–5500, <https://doi.org/10.1002/2016GL068825>, 2016.
- Finney, D. L., Doherty, R. M., Wild, O., Stevenson, D. S., MacKenzie, I. A., and Blyth, A. M.: A projected decrease in lightning under climate change, *Nature Climate Change*, 8, 210–213, <https://doi.org/10.1038/s41558-018-0072-6>, 2018.
- Fried, A., Barth, M. C., Bela, M., Weibring, P., Richter, D., Walega, J., Li, Y., Pickering, K., Apel, E., Hornbrook, R., Hills, A., Riemer, D. D., Blake, N., Blake, D. R., Schroeder, J. R., Luo, Z. J., Crawford, J. H., Olson, J., Rutledge, S., Betten, D., Biggerstaff, M. I., Diskin, G. S., Sachse, G., Campos, T., Flocke, F., Weinheimer, A., Cantrell, C., Pollack, I., Peischl, J., Froyd, K., Wisthaler, A., Mikoviny, T., and Woods, S.: Convective transport of formaldehyde to the upper troposphere and lower stratosphere and associated scavenging in thunderstorms over the central United States during the 2012 DC3 study, *Journal of Geophysical Research: Atmospheres*, 121, 7430–7460, <https://doi.org/10.1002/2015JD024477>, 2016.
- Fuchs, B. R. and Rutledge, S. A.: Investigation of Lightning Flash Locations in Isolated Convection Using LMA Observations, *Journal of Geophysical Research: Atmospheres*, 123, 6158–6174, <https://doi.org/10.1002/2017JD027569>, 2018.
- Goliff, W. S., Stockwell, W. R., and Lawson, C. V.: The regional atmospheric chemistry mechanism, version 2, *Atmospheric Environment*, 68, 174–185, <https://doi.org/10.1016/j.atmosenv.2012.11.038>, 2013.
- Grell, G. A., Peckham, S. E., Schmitz, R., McKeen, S. A., Frost, G., Skamarock, W. C., and Eder, B.: Fully coupled “online” chemistry within the WRF model, *Atmospheric Environment*, 39, 6957–6975, <https://doi.org/10.1016/j.atmosenv.2005.04.027>, 2005.
- Griffin, D., Zhao, X., McLinden, C. A., Boersma, F., Bourassa, A., Dammers, E., Degenstein, D., Eskes, H., Fehr, L., Fioletov, V., Hayden, K., Kharol, S. K., Li, S.-M., Makar, P., Martin, R. V., Mihele, C., Mittermeier, R. L., Krotkov, N., Snee, M., Lamsal, L. N., Linden, M. t., van Geffen, J., Veefkind, P., and Wolde, M.: High-Resolution Mapping of Nitrogen Dioxide With TROPOMI: First Results and Validation Over the Canadian Oil Sands, *Geophysical Research Letters*, 46, 1049–1060, <https://doi.org/10.1029/2018GL081095>, 2019.
- Guenther, A., Karl, T., Harley, P., Wiedinmyer, C., Palmer, P. I., and Geron, C.: Estimates of global terrestrial isoprene emissions using MEGAN (Model of Emissions of Gases and Aerosols from Nature), *Atmospheric Chemistry and Physics*, 6, 3181–3210, <https://hal.archives-ouvertes.fr/hal-00295995>, 2006.
- Hauglustaine, D., Emmons, L., Newchurch, M., Brasseur, G., Takao, T., Matsubara, K., Johnson, J., Ridley, B., Stith, J., and Dye, J.: On the Role of Lightning NO_x in the Formation of Tropospheric Ozone Plumes: A Global Model Perspective, *Journal of Atmospheric Chemistry*, 38, 277–294, <https://doi.org/10.1023/A:1006452309388>, 2001.

- Joiner, J., Vasilkov, A. P., Gupta, P., Bhartia, P. K., Veefkind, P., Sneep, M., de Haan, J., Polonsky, I., and Spurr, R.: Fast simulators for satellite cloud optical centroid pressure retrievals; evaluation of OMI cloud retrievals, *Atmospheric Measurement Techniques*, 5, 529–545, <https://doi.org/10.5194/amt-5-529-2012>, 2012.
- KNMI: Background information about the Row Anomaly in OMI, <http://projects.knmi.nl/omi/research/product/rowanomaly-background.php>, last access: February 7, 2020, 2012.
- 650 Krause, A., Kloster, S., Wilkenskjeld, S., and Paeth, H.: The sensitivity of global wildfires to simulated past, present, and future lightning frequency, *Journal of Geophysical Research: Biogeosciences*, 119, 312–322, <https://doi.org/10.1002/2013JG002502>, 2014.
- Krotkov, N. A., Lamsal, L. N., Celarier, E. A., Swartz, W. H., Marchenko, S. V., Bucsela, E. J., Chan, K. L., Wenig, M., and Zara, M.: The version 3 OMI NO₂ standard product, *Atmospheric Measurement Techniques*, 10, 3133–3149, <https://doi.org/10.5194/amt-10-3133-2017>,
655 2017.
- Kuhlmann, G., Hartl, A., Cheung, H. M., Lam, Y. F., and Wenig, M. O.: A novel gridding algorithm to create regional trace gas maps from satellite observations, *Atmospheric Measurement Techniques*, 7, 451–467, <https://doi.org/10.5194/amt-7-451-2014>, 2014.
- Lapierre, J. L., Laughner, J. L., Geddes, J. A., Koshack, W., Cohen, R. C., and Pusede, S. E.: Observing regional variability in lightning NO_x production rates, *Journal of Geophysical Research*, in review, 2019.
- 660 Laughner, J. L. and Cohen, R. C.: Quantification of the effect of modeled lightning NO₂ on UV–visible air mass factors, *Atmospheric Measurement Techniques*, 10, 4403–4419, <https://doi.org/10.5194/amt-10-4403-2017>, 2017.
- Laughner, J. L., Zhu, Q., and Cohen, R. C.: The Berkeley High Resolution Tropospheric NO₂ Product, *Earth System Science Data Discussions*, pp. 1–33, <https://doi.org/10.5194/essd-2018-66>, 2018a.
- Laughner, J. L., Zhu, Q., and Cohen, R. C.: Evaluation of version 3.0B of the BEHR OMI NO₂ product, *Atmospheric Measurement Techniques Discussions*, pp. 1–25, <https://doi.org/10.5194/amt-2018-248>, 2018b.
- 665 Laughner, J. L., Zhu, Q., and Cohen, R. C.: Evaluation of version 3.0B of the BEHR OMI NO₂ product, *Atmospheric Measurement Techniques*, 12, 129–146, <https://doi.org/10.5194/amt-12-129-2019>, 2019.
- Levelt, P. F., van den Oord, G., Dobber, M. R., Malkki, A., Visser, H., Vries, J. d., Stammes, P., Lundell, J., and Saari, H.: The ozone monitoring instrument, *IEEE Transactions on Geoscience and Remote Sensing*, 44, 1093–1101, <https://doi.org/10.1109/TGRS.2006.872333>,
670 2006.
- Levelt, P. F., Joiner, J., Tamminen, J., Veefkind, J. P., Bhartia, P. K., Stein Zweers, D. C., Duncan, B. N., Streets, D. G., Eskes, H., van der A, R., McLinden, C., Fioletov, V., Carn, S., de Laat, J., DeLand, M., Marchenko, S., McPeters, R., Ziemke, J., Fu, D., Liu, X., Pickering, K., Apituley, A., González Abad, G., Arola, A., Boersma, F., Chan Miller, C., Chance, K., de Graaf, M., Hakkarainen, J., Hassinen, S., Ialongo, I., Kleipool, Q., Krotkov, N., Li, C., Lamsal, L., Newman, P., Nowlan, C., Suleiman, R., Tilstra, L. G., Torres, O., Wang, H.,
675 and Wargan, K.: The Ozone Monitoring Instrument: overview of 14 years in space, *Atmospheric Chemistry and Physics*, 18, 5699–5745, <https://doi.org/10.5194/acp-18-5699-2018>, 2018.
- Li, Y., Pickering, K. E., Allen, D. J., Barth, M. C., Bela, M. M., Cummings, K. A., Carey, L. D., Mecikalski, R. M., Fierro, A. O., Campos, T. L., Weinheimer, A. J., Diskin, G. S., and Biggerstaff, M. I.: Evaluation of deep convective transport in storms from different convective regimes during the DC3 field campaign using WRF-Chem with lightning data assimilation, *Journal of Geophysical Research: Atmospheres*, 122, 7140–7163, <https://doi.org/10.1002/2017JD026461>, 2017.
- 680 Li, Y., Pickering, K. E., Barth, M. C., Bela, M. M., Cummings, K. A., and Allen, D. J.: Evaluation of Parameterized Convective Transport of Trace Gases in Simulation of Storms Observed During the DC3 Field Campaign, *Journal of Geophysical Research: Atmospheres*, 123, 11,238–11,261, <https://doi.org/10.1029/2018JD028779>, 2018.

- Luo, C., Wang, Y., and Koshak, W. J.: Development of a self-consistent lightning NO_x simulation in large-scale 3-D models, *Journal of Geophysical Research: Atmospheres*, 122, 3141–3154, <https://doi.org/10.1002/2016JD026225>, 2017.
- 685 Marais, E. A., Jacob, D. J., Choi, S., Joiner, J., Belmonte-Rivas, M., Cohen, R. C., Beirle, S., Murray, L. T., Schiferl, L., Shah, V., and Jaeglé, L.: Nitrogen oxides in the global upper troposphere: interpreting cloud-sliced NO₂ observations from the OMI satellite instrument, *Atmospheric Chemistry and Physics Discussions*, pp. 1–14, <https://doi.org/10.5194/acp-2018-556>, 2018.
- Martin, R. V., Sauvage, B., Folkins, I., Sioris, C. E., Boone, C., Bernath, P., and Ziemke, J.: Space-based constraints on the production of nitric oxide by lightning, *Journal of Geophysical Research*, 112, 1479, <https://doi.org/10.1029/2006JD007831>, 2007.
- 690 Mecikalski, R. M. and Carey, L. D.: Lightning characteristics relative to radar, altitude and temperature for a multicell, MCS and supercell over northern Alabama, *Atmospheric Research*, 191, 128–140, <https://doi.org/10.1016/j.atmosres.2017.03.001>, <http://www.sciencedirect.com/science/article/pii/S0169809516302812>, 2017.
- Min, M., Wu, C., Li, C., Liu, H., Xu, N., Wu, X., Chen, L., Wang, F., Sun, F., Qin, D., Wang, X., Li, B., Zheng, Z., Cao, G., and Dong, L.: Developing the science product algorithm testbed for Chinese next-generation geostationary meteorological satellites: Fengyun-4 series, *JOURNAL OF METEOROLOGICAL RESEARCH*, 31, 708–719, <https://doi.org/10.1007/s13351-017-6161-z>, 2017.
- 695 Myhre, G., Shindell, D., Bréon, F. M., Collins, W., Fuglestedt, J., Huang, J., Koch, D., Lamarque, J. F., Lee, D., and Mendoza, B.: Climate change 2013: the physical science basis. Contribution of Working Group I to the Fifth Assessment Report of the Intergovernmental Panel on Climate Change, K., Tignor, M., Allen, SK, Boschung, J., Nauels, A., Xia, Y., Bex, V., and Midgley, PM, Cambridge University Press
- 700 Cambridge, United Kingdom and New York, NY, USA, 2013.
- Nault, B. A., Garland, C., Wooldridge, P. J., Brune, W. H., Campuzano-Jost, P., Crouse, J. D., Day, D. A., Dibb, J., Hall, S. R., Huey, L. G., Jimenez, J. L., Liu, X., Mao, J., Mikoviny, T., Peischl, J., Pollack, I. B., Ren, X., Ryerson, T. B., Scheuer, E., Ullmann, K., Wennberg, P. O., Wisthaler, A., Zhang, L., and Cohen, R. C.: Observational Constraints on the Oxidation of NO_x in the Upper Troposphere, *The Journal of Physical Chemistry A*, 120, 1468–1478, <https://doi.org/10.1021/acs.jpca.5b07824>, 2016.
- 705 Nault, B. A., Laughner, J. L., Wooldridge, P. J., Crouse, J. D., Dibb, J., Diskin, G., Peischl, J., Podolske, J. R., Pollack, I. B., Ryerson, T. B., Scheuer, E., Wennberg, P. O., and Cohen, R. C.: Lightning NO_x Emissions: Reconciling Measured and Modeled Estimates With Updated NO_x Chemistry, *Geophysical Research Letters*, 44, 9479–9488, <https://doi.org/10.1002/2017GL074436>, 2017.
- Ott, L. E., Pickering, K. E., Stenchikov, G. L., Huntrieser, H., and Schumann, U.: Effects of lightning NO_x production during the 21 July European Lightning Nitrogen Oxides Project storm studied with a three-dimensional cloud-scale chemical transport model, *Journal of Geophysical Research*, 112, 61, <https://doi.org/10.1029/2006JD007365>, 2007.
- 710 Ott, L. E., Pickering, K. E., Stenchikov, G. L., Allen, D. J., DeCaria, A. J., Ridley, B., Lin, R.-F., Lang, S., and Tao, W.-K.: Production of lightning NO_x and its vertical distribution calculated from three-dimensional cloud-scale chemical transport model simulations, *Journal of Geophysical Research*, 115, 4711, <https://doi.org/10.1029/2009JD011880>, 2010.
- Pickering, K. E., Thompson, A. M., Wang, Y., Tao, W.-K., McNamara, D. P., Kirchhoff, V. W. J. H., Heikes, B. G., Sachse, G. W., Bradshaw, J. D., Gregory, G. L., and Blake, D. R.: Convective transport of biomass burning emissions over Brazil during TRACE A, *Journal of Geophysical Research*, 101, 23 993–24 012, <https://doi.org/10.1029/96JD00346>, 1996.
- 715 Pickering, K. E., Bucsela, E., Allen, D., Ring, A., Holzworth, R., and Krotkov, N.: Estimates of lightning NO_x production based on OMI NO₂ observations over the Gulf of Mexico, *Journal of Geophysical Research: Atmospheres*, 121, 8668–8691, <https://doi.org/10.1002/2015JD024179>, 2016.

- 720 Platt, U. and Perner, D.: Measurements of Atmospheric Trace Gases by Long Path Differential UV/Visible Absorption Spectroscopy, in: Optical and Laser Remote Sensing, edited by Schawlow, A. L., Killinger, D. K., and Mooradian, A., vol. 39 of *Springer Series in Optical Sciences*, pp. 97–105, Springer Berlin Heidelberg, Berlin, Heidelberg, https://doi.org/10.1007/978-3-540-39552-2_13, 1983.
- Price, C. and Rind, D.: A simple lightning parameterization for calculating global lightning distributions, *Journal of Geophysical Research*, 97, 9919–9933, <https://doi.org/10.1029/92JD00719>, 1992.
- 725 Richter, A., Burrows, J. P., Nüß, H., Granier, C., and Niemeier, U.: Increase in tropospheric nitrogen dioxide over China observed from space, *Nature*, 437, 129–132, <https://doi.org/10.1038/nature04092>, 2005.
- Romps, D. M.: Evaluating the future of lightning in cloud-resolving models, *Geophysical Research Letters*, <https://doi.org/10.1029/2019GL085748>, 2019.
- Romps, D. M., Seeley, J. T., Vollaro, and Molinari, J.: Projected increase in lightning strikes in the United States due to global warming, *Atmospheric Chemistry and Physics*, 346, 851–854, <https://doi.org/10.1126/science.1259100>, 2014.
- 730 Rudlosky, S.: Evaluating ENTLN performance relative to TRMM/LIS, *Journal of Operational Meteorology*, 3, 11–20, <https://doi.org/10.15191/nwajom.2015.0302>, 2015.
- Schaaf, C. B., Liu, J., Gao, F., and Strahler, A. H.: Aqua and Terra MODIS Albedo and Reflectance Anisotropy Products, in: *Land Remote Sensing and Global Environmental Change*, edited by Ramachandran, B., Justice, C. O., and Abrams, M. J., vol. 11 of *Remote Sensing and Digital Image Processing*, pp. 549–561, Springer New York, New York, NY, https://doi.org/10.1007/978-1-4419-6749-7_24, 2011.
- 735 Schumann, U. and Huntrieser, H.: The global lightning-induced nitrogen oxides source, *Atmospheric Chemistry and Physics*, 7, 3823–3907, <https://doi.org/10.5194/acp-7-3823-2007>, 2007.
- Schwantes, R. H., Teng, A. P., Nguyen, T. B., Coggon, M. M., Crouse, J. D., St Clair, J. M., Zhang, X., Schilling, K. A., Seinfeld, J. H., and Wennberg, P. O.: Isoprene NO₃ Oxidation Products from the RO₂ + HO₂ Pathway, *The Journal of Physical Chemistry A*, 119, 10 158–10 171, <https://doi.org/10.1021/acs.jpca.5b06355>, 2015.
- 740 Silvern, R. F., Jacob, D. J., Travis, K. R., Sherwen, T., Evans, M. J., Cohen, R. C., Laughner, J. L., Hall, S. R., Ullmann, K., Crouse, J. D., Wennberg, P. O., Peischl, J., and Pollack, I. B.: Observed NO/NO₂ ratios in the upper troposphere imply errors in NO-NO₂-O₃ cycling kinetics or an unaccounted NO_x reservoir, *Geophysical Research Letters*, <https://doi.org/10.1029/2018GL077728>, 2018.
- Sneep, M., de Haan, J. F., Stammes, P., Wang, P., Vanbauce, C., Joiner, J., Vasilkov, A. P., and Levelt, P. F.: Three-way comparison between OMI and PARASOL cloud pressure products, *Journal of Geophysical Research*, 113, D05 204, <https://doi.org/10.1029/2007JD008694>, 2008.
- 745 Stammes, P., Sneep, M., de Haan, J. F., Veefkind, J. P., Wang, P., and Levelt, P. F.: Effective cloud fractions from the Ozone Monitoring Instrument: Theoretical framework and validation, *Journal of Geophysical Research*, 113, D05 204, <https://doi.org/10.1029/2007JD008820>, 2008.
- 750 Strobe, S. A., Douglass, A. R., Ziemke, J. R., Manyin, M., Nielsen, J. E., and Oman, L. D.: A Model and Satellite-Based Analysis of the Tropospheric Ozone Distribution in Clear Versus Convectively Cloudy Conditions, *Journal of Geophysical Research: Atmospheres*, 122, 11,948–11,960, <https://doi.org/10.1002/2017JD027015>, 2017.
- Travis, K. R., Jacob, D. J., Fisher, J. A., Kim, P. S., Marais, E. A., Zhu, L., Yu, K., Miller, C. C., Yantosca, R. M., Sulprizio, M. P., Thompson, A. M., Wennberg, P. O., Crouse, J. D., St Clair, J. M., Cohen, R. C., Laughner, J. L., Dibb, J. E., Hall, S. R., Ullmann, K., Wolfe, G. M., 755 Pollack, I. B., Peischl, J., Neuman, J. A., and Zhou, X.: Why do Models Overestimate Surface Ozone in the Southeastern United States?, *Atmospheric Chemistry and Physics*, 16, 13 561–13 577, <https://doi.org/10.5194/acp-16-13561-2016>, 2016.

- Vasilkov, A., Joiner, J., Spurr, R., Bhartia, P. K., Levelt, P., and Stephens, G.: Evaluation of the OMI cloud pressures derived from rotational Raman scattering by comparisons with other satellite data and radiative transfer simulations, *Journal of Geophysical Research*, 113, D05 204, <https://doi.org/10.1029/2007JD008689>, 2008.
- 760 Veefkind, J. P., Aben, I., McMullan, K., Förster, H., de Vries, J., Otter, G., Claas, J., Eskes, H. J., de Haan, J. F., Kleipool, Q., van Weele, M., Hasekamp, O., Hoogeveen, R., Landgraf, J., Snel, R., Tol, P., Ingmann, P., Voors, R., Kruizinga, B., Vink, R., Visser, H., and Levelt, P. F.: TROPOMI on the ESA Sentinel-5 Precursor: A GMES mission for global observations of the atmospheric composition for climate, air quality and ozone layer applications, *Remote Sensing of Environment*, 120, 70–83, <https://doi.org/10.1016/j.rse.2011.09.027>, 2012.
- 765 Wang, L., Follette-Cook, M. B., Newchurch, M. J., Pickering, K. E., Pour-Biazar, A., Kuang, S., Koshak, W., and Peterson, H.: Evaluation of lightning-induced tropospheric ozone enhancements observed by ozone lidar and simulated by WRF/Chem, *Atmospheric Environment*, 115, 185–191, <https://doi.org/10.1016/j.atmosenv.2015.05.054>, 2015.
- Williams, E. R.: The tripole structure of thunderstorms, *Journal of Geophysical Research*, 94, 13 151, <https://doi.org/10.1029/JD094iD11p13151>, 1989.
- Wong, J., Barth, M. C., and Noone, D.: Evaluating a lightning parameterization based on cloud-top height for mesoscale numerical model simulations, *Geoscientific Model Development*, 6, 429–443, <https://doi.org/10.5194/gmd-6-429-2013>, 2013.
- 770 Xu, K.-M. and Randall, D. A.: A Semiempirical Cloudiness Parameterization for Use in Climate Models, *Journal of the Atmospheric Sciences*, 53, 3084–3102, [https://doi.org/10.1175/1520-0469\(1996\)053<3084:ASCPFU>2.0.CO;2](https://doi.org/10.1175/1520-0469(1996)053<3084:ASCPFU>2.0.CO;2), 1996.
- Yang, J., Zhang, Z., Wei, C., Lu, F., and Guo, Q.: Introducing the New Generation of Chinese Geostationary Weather Satellites, Fengyun-4, *Bulletin of the American Meteorological Society*, 98, 1637–1658, <https://doi.org/10.1175/BAMS-D-16-0065.1>, 2017.
- 775 Zel'dovich, Y. and Raizer, Y.: VIII - Physical and chemical kinetics in hydrodynamic processes, in: *Physics of Shock Waves and High-Temperature Hydrodynamic Phenomena*, edited by Hayes, W. D., Probstein, R. F., Zel'dovich, Y., and Raizer, Y., pp. 566–571, Academic Press, <https://doi.org/10.1016/B978-0-12-395672-9.50009-6>, 1967.
- Zhang, P., Lu, Q., Hu, X., Gu, S., Yang, L., Min, M., Chen, L., Xu, N., Sun, L., Bai, W., Ma, G., and Di Xian: Latest Progress of the Chinese Meteorological Satellite Program and Core Data Processing Technologies, *Advances in Atmospheric Sciences*, 36, 1027–1045, <https://doi.org/10.1007/s00376-019-8215-x>, 2019.
- 780 Zhang, X. and Laughner, J.: zxdawn/BEHR-LNOx: v1.0, Zenodo, <https://doi.org/10.5281/zenodo.3553426>, 2019.
- Zhao, C., Wang, Y., Choi, Y., and Zeng, T.: Summertime impact of convective transport and lightning NO_x production over North America: modeling dependence on meteorological simulations, *Atmospheric Chemistry and Physics*, 9, 4315–4327, <https://doi.org/10.5194/acp-9-4315-2009>, 2009.
- 785 Zhou, Y., Brunner, D., Boersma, K. F., Dirksen, R., and Wang, P.: An improved tropospheric NO₂ retrieval for OMI observations in the vicinity of mountainous terrain, *Atmospheric Measurement Techniques*, 2, 401–416, <https://doi.org/10.5194/amt-2-401-2009>, 2009.
- Zhu, Q., Laughner, J. L., and Cohen, R. C.: Lightning NO₂ simulation over the contiguous US and its effects on satellite NO₂ retrievals, *Atmospheric Chemistry and Physics*, 19, 13 067–13 078, <https://doi.org/10.5194/acp-19-13067-2019>, 2019.
- 790 Zhu, Y., Rakov, V. A., Tran, M. D., and Nag, A.: A study of National Lightning Detection Network responses to natural lightning based on ground truth data acquired at LOG with emphasis on cloud discharge activity, *Journal of Geophysical Research: Atmospheres*, 121, 14,651–14,660, <https://doi.org/10.1002/2016JD025574>, 2016.
- Zhu, Y., Rakov, V. A., Tran, M. D., Stock, M. G., Heckman, S., Liu, C., Sloop, C. D., Jordan, D. M., Uman, M. A., Caicedo, J. A., Kotovsky, D. A., Wilkes, R. A., Carvalho, F. L., Ngin, T., Gamerota, W. R., Pilkey, J. T., and Hare, B. M.: Evaluation of ENTLN Performance

- 795 Characteristics Based on the Ground Truth Natural and Rocket-Triggered Lightning Data Acquired in Florida, *Journal of Geophysical Research: Atmospheres*, 122, 9858–9866, <https://doi.org/10.1002/2017JD027270>, 2017.
- Ziemke, J. R., Joiner, J., Chandra, S., Bhartia, P. K., Vasilkov, A., Haffner, D. P., Yang, K., Schoeberl, M. R., Froidevaux, L., and Levelt, P. F.: Ozone mixing ratios inside tropical deep convective clouds from OMI satellite measurements, *Atmospheric Chemistry and Physics*, 9, 573–583, <https://doi.org/10.5194/acp-9-573-2009>, 2009.
- 800 Ziemke, J. R., Strode, S. A., Douglass, A. R., Joiner, J., Vasilkov, A., Oman, L. D., Liu, J., Strahan, S. E., Bhartia, P. K., and Haffner, D. P.: A cloud-ozone data product from Aura OMI and MLS satellite measurements, *Atmospheric Measurement Techniques*, 10, 4067–4078, <https://doi.org/10.5194/amt-10-4067-2017>, 2017.

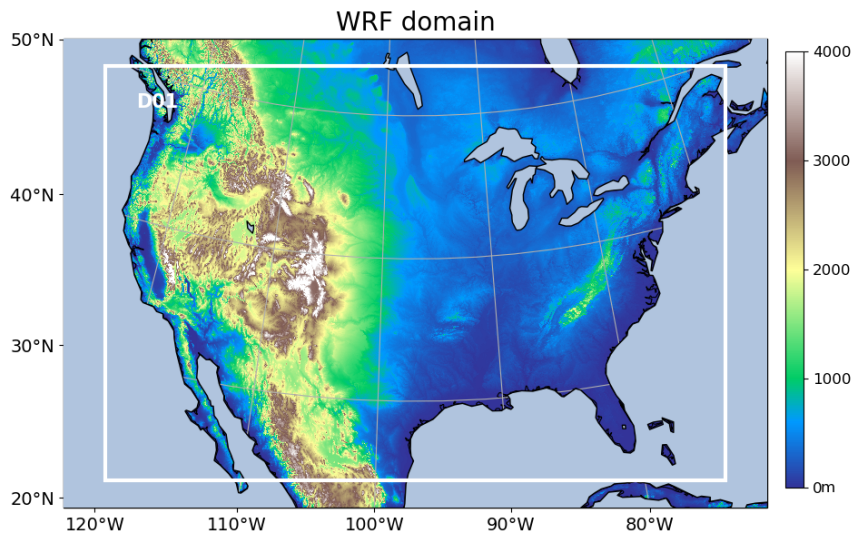


Figure 1. The 12-km-resolution domain for Domain and terrain height (m) of the WRF-Chem simulation with 350 x 290 grid cells and a horizontal resolution of 12 km.

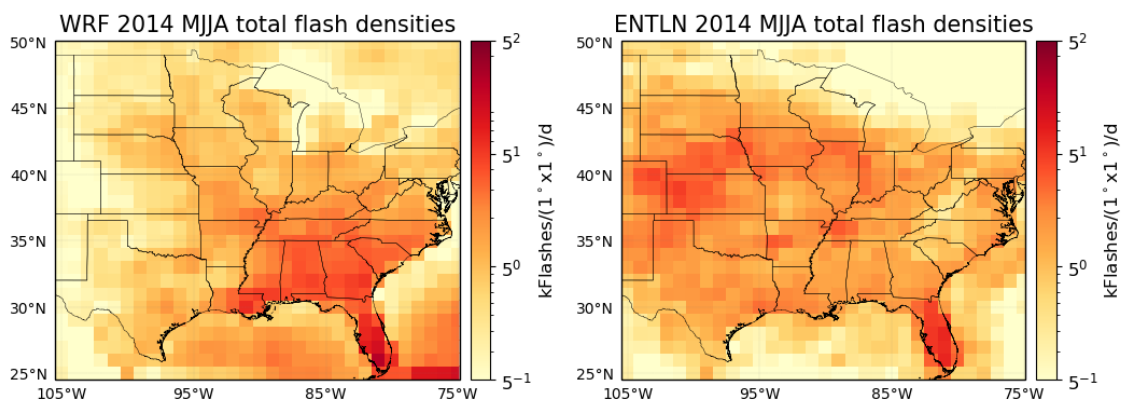


Figure 2. Comparison between total flash densities from ENTNLN and WRF-Chem during MJJA 2014.

Table 1. Definitions of the abbreviations for the criteria used in this study.

Abbreviations	Full form [source]
CRF	Cloud radiance fraction [OMI]
CP	Cloud optical pressure [OMI]
CF	Cloud fraction [WRF-Chem]
TL	Total lightning flashes [WRF-Chem]
ratio	modeled LNO ₂ Vis / modeled NO ₂ Vis [WRF-Chem]
$\text{erf}(\text{CRF}_{\alpha} - \text{entln} - \text{ENTLN})$	$\text{CRF} \geq \alpha + \text{entln} - \text{ENTLN}$ flashes(strokes) $\geq 2400(8160)$ [ENTLN]
$\text{erf}(\text{CRF}_{\alpha} - \text{ef40} - \text{entln} - \text{CF40} - \text{ENTLN})$	$\text{CRF} \geq \alpha + \text{entln} - \text{ENTLN}$ flashes(strokes) $\geq 2400(8160) + \text{CF} \geq 40\%$
$\text{erf}(\text{CRF}_{\alpha} - \text{entln} - \text{tl1000} - \text{ENTLN} - \text{TL1000})$	$\text{CRF} \geq \alpha + \text{entln} - \text{ENTLN}$ flashes(strokes) $\geq 2400(8160) + \text{TL} \geq 1000$
$\text{erf}(\text{CRF}_{\alpha} - \text{ef40} - \text{entln} - \text{tl1000} - \text{CF40} - \text{ENTLN} - \text{TL1000})$	$\text{CRF} \geq \alpha + \text{entln} - \text{ENTLN}$ flashes(strokes) $\geq 2400(8160) + \text{CF} \geq 40\% + \text{TL} \geq 1000$
$\text{erf}(\text{CRF}_{\alpha} - \text{entln} - \text{tl1000} - \text{ENTLN} - \text{TL1000} - \text{ratio50})$	$\text{CRF} \geq \alpha + \text{entln} - \text{ENTLN}$ flashes(strokes) $\geq 2400(8160) + \text{TL} \geq 1000 + \text{ratio} \geq 50\%$
$\text{erf}(\text{CRF}_{\alpha} - \text{ef40} - \text{entln} - \text{tl1000} - \text{CF40} - \text{ENTLN} - \text{TL1000} - \text{ratio50})$	$\text{CRF} \geq \alpha + \text{entln} - \text{ENTLN}$ flashes(strokes) $\geq 2400(8160) + \text{CF} \geq 40\% + \text{TL} \geq 1000 +$

α has three options: 70%, 90% and 100%

Table 2. LNO_x production for different combinations of criteria defined in Table 1.

Condition ¹	ENTLN data type ²	LNO _x /flash or LNO _x /stroke	R value	Intercept (10 ⁶ mol)	Days ³
<u>CRF90_ENTLN</u>	<u>Flash</u>	<u>52.1 ± 51.1</u>	<u>0.20</u>	<u>0.21</u>	<u>99</u>
<u>CRF90_CF40_ENTLN</u>	<u>Flash</u>	<u>84.2 ± 31.5</u>	<u>0.54</u>	<u>-0.04</u>	<u>70</u>
<u>CRF90_ENTLN_TL1000</u>	<u>Flash</u>	<u>61.9 ± 49.1</u>	<u>0.27</u>	<u>0.33</u>	<u>83</u>
<u>CRF90_CF40_ENTLN_TL1000</u>	<u>Flash</u>	<u>63.4 ± 52.9</u>	<u>0.38</u>	<u>0.26</u>	<u>38</u>
<u>CRF90_ENTLN_TL1000_ratio50</u>	<u>Flash</u>	<u>54.5 ± 48.1</u>	<u>0.25</u>	<u>0.39</u>	<u>81</u>
<u>CRF90_CF40_ENTLN_TL1000_ratio50</u>	<u>Flash</u>	<u>90.0 ± 65.0</u>	<u>0.46</u>	<u>0.15</u>	<u>32</u>
<u>CRF90_ENTLN</u>	<u>Stroke</u>	<u>6.7 ± 4.1</u>	<u>0.31</u>	<u>0.23</u>	<u>102</u>
<u>CRF90_CF40_ENTLN</u>	<u>Stroke</u>	<u>10.3 ± 3.6</u>	<u>0.55</u>	<u>0.08</u>	<u>79</u>
<u>CRF90_ENTLN_TL1000</u>	<u>Stroke</u>	<u>7.5 ± 5.1</u>	<u>0.29</u>	<u>0.38</u>	<u>94</u>
<u>CRF90_CF40_ENTLN_TL1000</u>	<u>Stroke</u>	<u>8.6 ± 6.2</u>	<u>0.39</u>	<u>0.27</u>	<u>46</u>
<u>CRF90_ENTLN_TL1000_ratio50</u>	<u>Stroke</u>	<u>7.0 ± 4.8</u>	<u>0.29</u>	<u>0.42</u>	<u>93</u>
<u>CRF90_CF40_ENTLN_TL1000_ratio50</u>	<u>Stroke</u>	<u>8.9 ± 7.0</u>	<u>0.39</u>	<u>0.31</u>	<u>40</u>

¹These conditions are defined in Table 1. ²The threshold of ENTLN data is 2400 flashes box⁻¹ and 8160 strokes box⁻¹ during the period of 2.4 h before OMI overpass time. ³The number of valid days with specific criteria in MJJA 2014.

Table 3. LNO_x production under for different conditions thresholds of CRF with coincident ENTNLN data, TL ≥ 1000 and ratio ≥ 50%.

CRF (%)	ENTLN data type ¹	LNO _x /flash or LNO _x /stroke	R value	Intercept (10 ^{6.5} mol)	Days ²
70	Flash	109.0-35.7 ± 15.3-36.8	0.84-0.21	0.23-4.91	85
90	Flash	114.8-54.5 ± 18.2-48.1	0.82-0.25	0.15-3.90	81
100	Flash	99.4-20.8 ± 15.3-37.4	0.84-0.13	0.10-5.67	71
70	Stroke	16.7-4.1 ± 2.6-3.9	0.79-0.21	0.58-5.16	96
90	Stroke	17.8-7.0 ± 2.9-4.8	0.78-0.29	4.16	93
100	Stroke	15.6-2.6 ± 3.1-4.0	0.75-0.14	0.16-5.41	82

¹The threshold of ENTNLN data is 2400 flashes box⁻¹ and 8160 strokes box⁻¹ during the period of 2.4 h before OMI overpass time. ²The number of valid days with specific criteria in MJJA 2014.

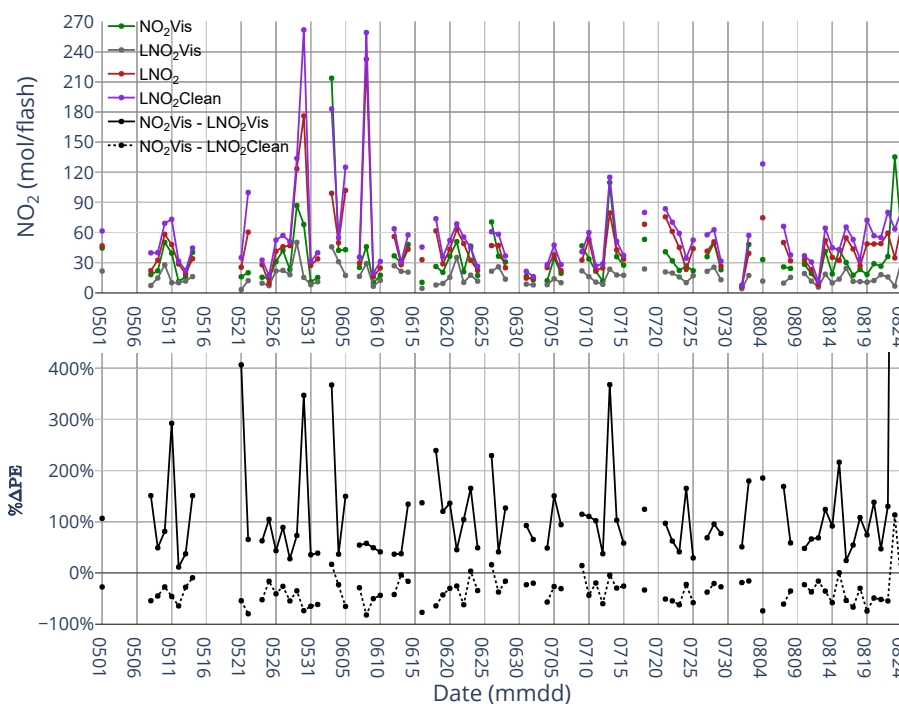


Figure 3. (top) Time series of NO₂ Vis, LNO₂ Vis, LNO₂ and LNO₂ Clean production per day over the CONUS for MJJA 2014 with CRF ≥ 90% and a flash threshold of 2400 flashes per 2.4 h. (bottom) Time series of the percent differences between NO₂ Vis and LNO₂ Vis and the percent differences between NO₂ Vis and LNO₂ Clean with CRF ≥ 90%. The value of black dot on August 23 (not shown) is 1958%.

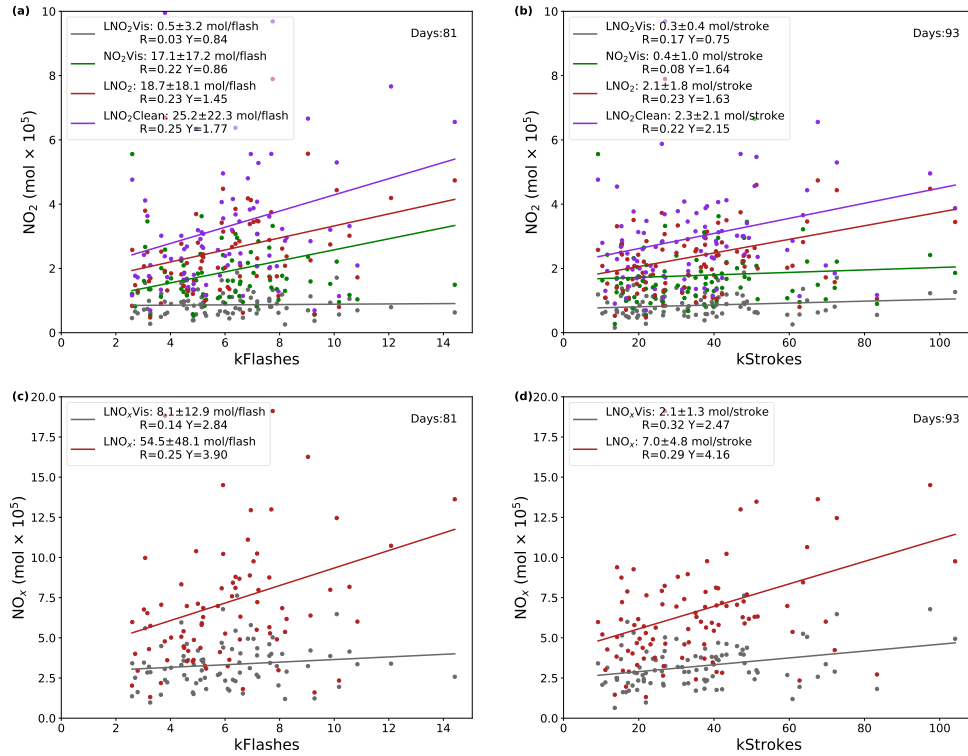


Figure 4. (a) Daily NO₂ Vis, LNO₂ Vis, LNO₂ and LNO₂Clean versus ENTTLN total flashes data. (b) Same as (a) but for strokes. (c) Daily LNO_x Vis and LNO_x versus total flashes. (d) Same as (c) but for strokes.

Table 4. The percent change in the estimated production when using different methods based on the same a priori profiles.

	City ¹	$(\text{LNO}_2\text{Clean} - \text{LNO}_2)/\text{LNO}_2$	$(\text{LNO}_2 - \text{TropVis})/\text{TropVis}$	$(\text{LNO}_2\text{Clean} - \text{TropVis})/\text{TropVis}$
Polluted	Lansing	24.2%	49.5%	85.6%
	New Orleans	13.3%	121.2%	153.8%
	Orlando	46.3%	37.5%	101.3%
Clean	Huron	12.0%	56.4%	75.2%
	Charles Town	12.0%	82.2%	104.1%
	Tarboro	5.0%	86.0%	95.3%

¹Locations are denoted in Fig. 6a.

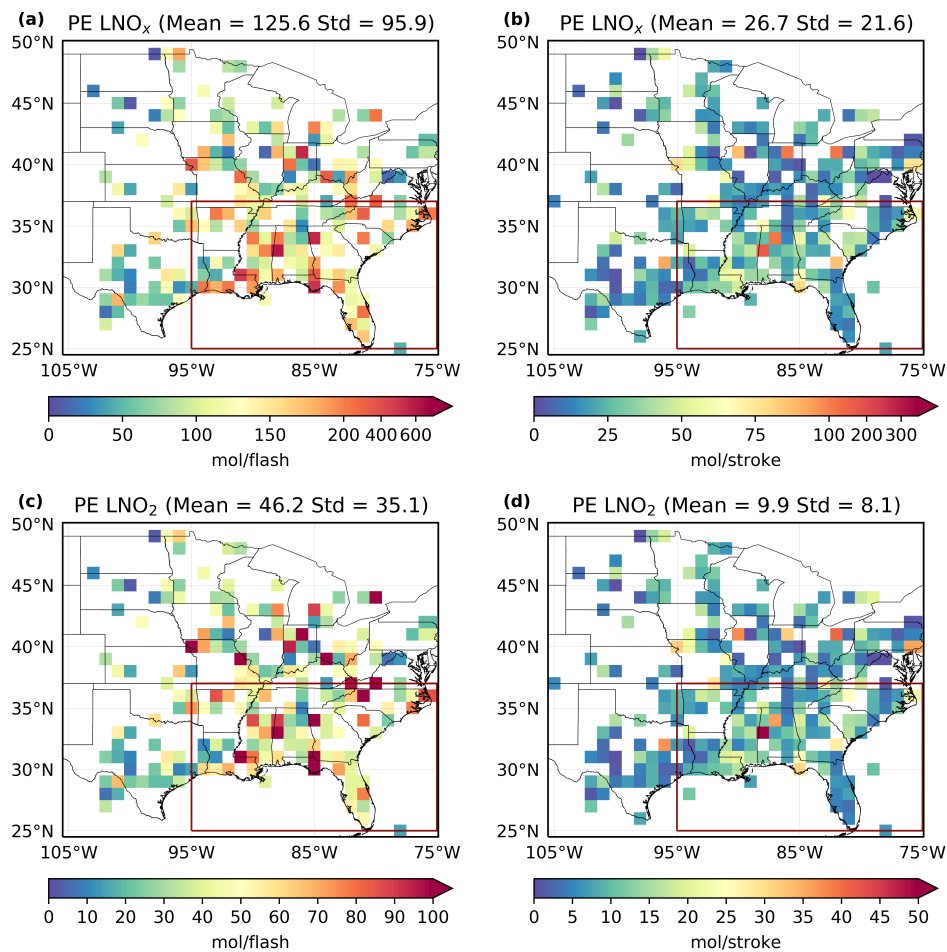


Figure 5. (a) and (c) Maps of $1^\circ \times 1^\circ$ gridded values of mean LNO_x and LNO₂ production per flash with CRF $\geq 90\%$ for MJJA 2014. (b) and (d) Same as (a) and (c) except for strokes. The southeastern US is denoted by the red box in panels a – d.

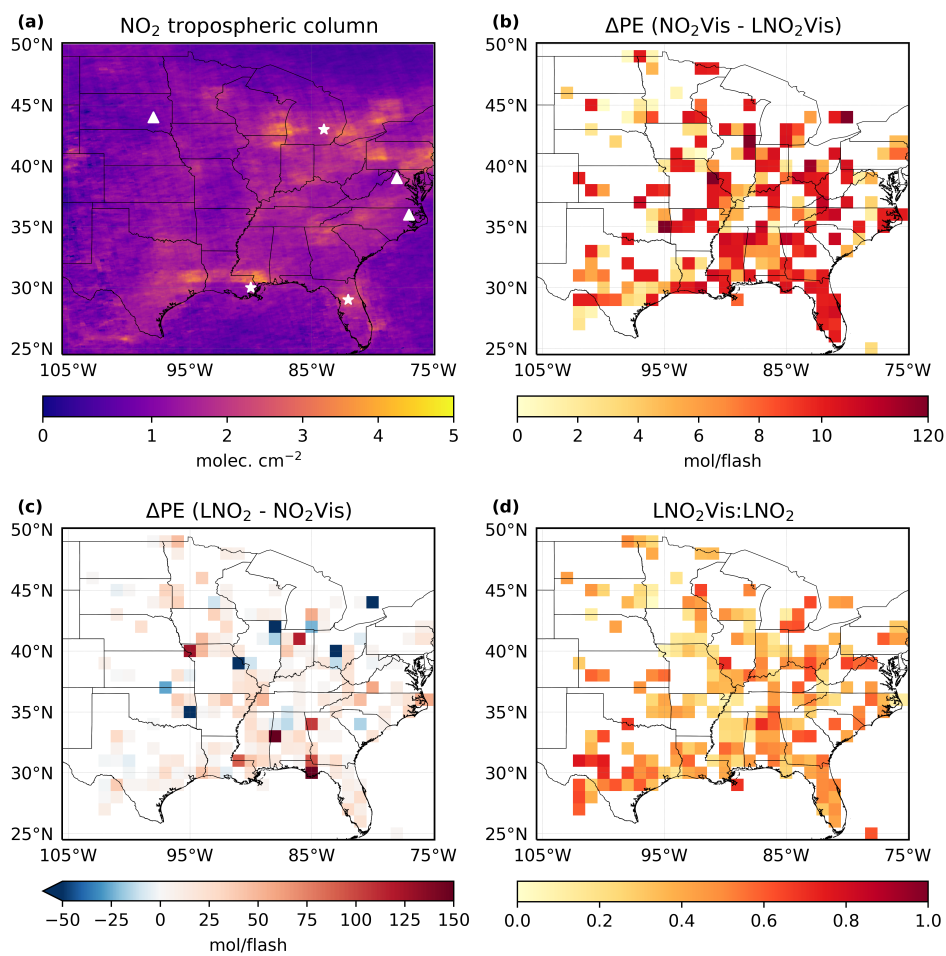


Figure 6. (a) Mean (MJJA 2014) NO₂ tropospheric column. Polluted cities are denoted by stars: Lansing, New Orleans and Orlando while clean cities are denoted by triangles: Huron, Charles Town and Tarboro. (b) The differences of the estimated mean production efficiency between NO₂ Vis and LNO₂ Vis with CRF \geq 90%. (c) The same differences as (b) but between LNO₂ and NO₂ Vis. (d) The ratio of LNO₂ Vis to LNO₂.

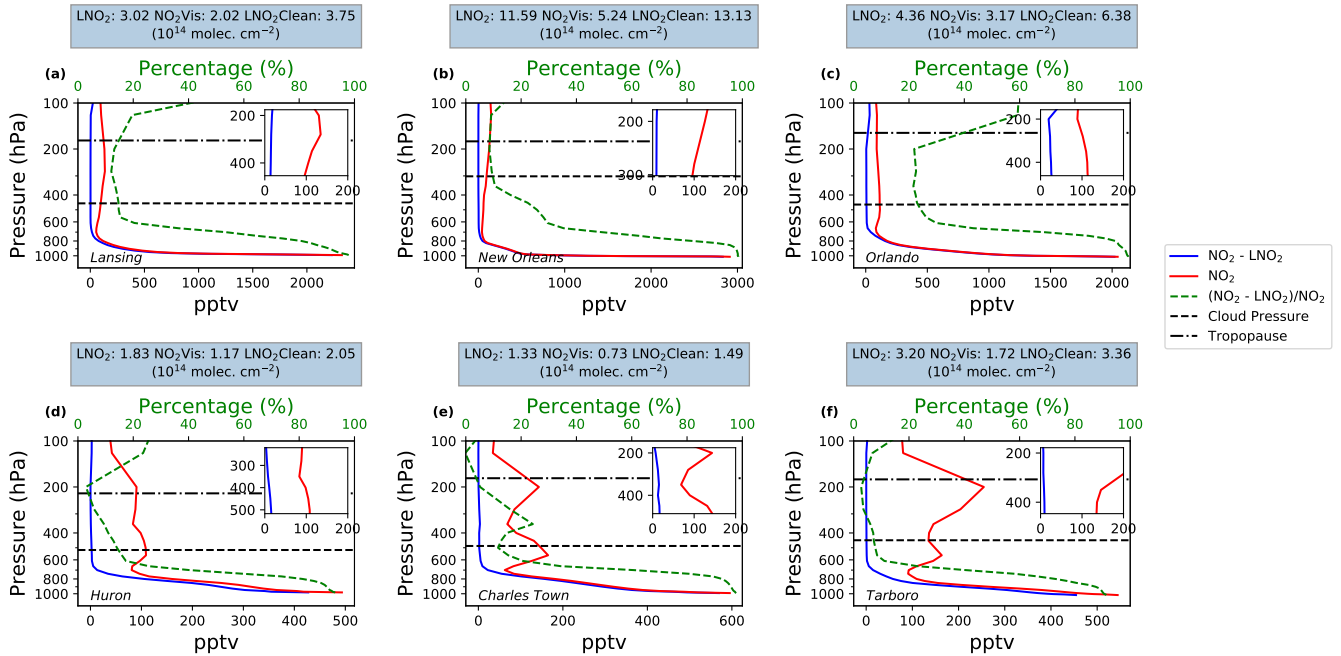


Figure 7. Comparison of mean WRF-Chem NO_2 and background NO_2 profiles in six grids with $\text{CRF} > 100\%$ on specific days during MJJA 2014. The top row data are selected from polluted regions (stars in Fig. 6a) while the bottom row data are from clean regions (triangles in Fig. 6a). The green dashed lines are the mean ratio profiles of background NO_2 to NO_2 . The zoomed figures show the profiles from the cloud pressure to the tropopause. The titles present the mean productions based on three different methods mentioned in Sect. 2.4.

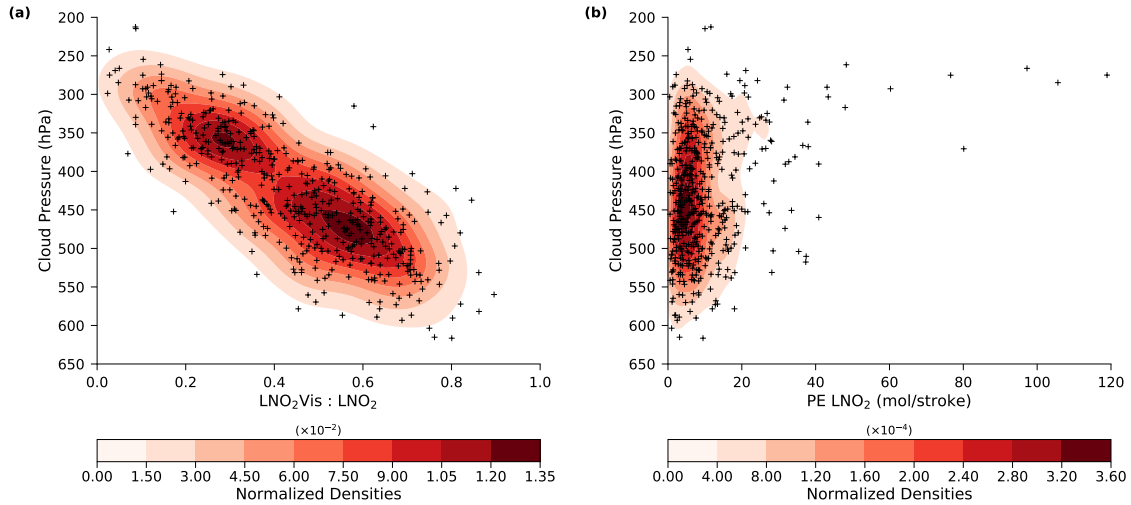


Figure 8. Scatter-plots Kernel density estimation of the (a) daily ratio of LNO_2Vis to LNO_2 and (b) daily LNO_2 production efficiency versus the daily cloud pressure measured by OMI with $\text{CRF} \geq 90\%$ for MJJA 2014.

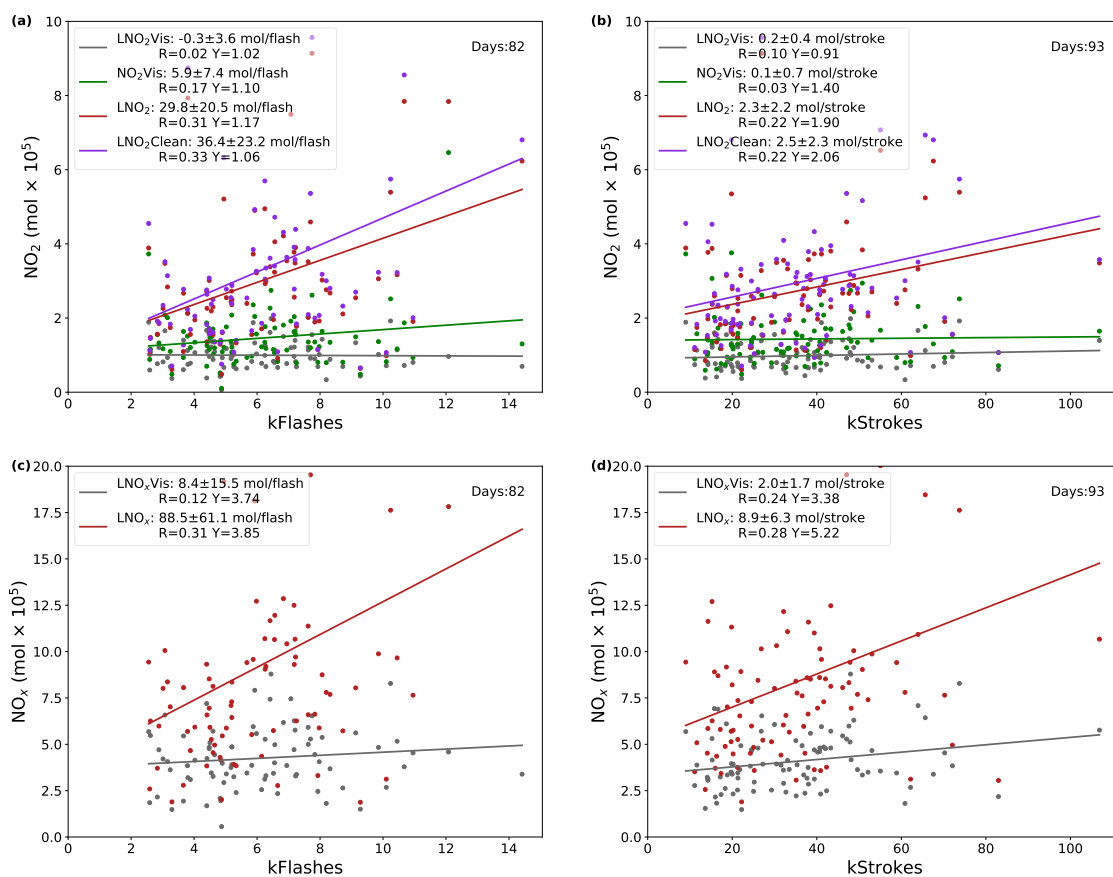


Figure 9. Same as Figure Fig. 4 except for 2×500 mol NO flash⁻¹ configuration.

(top) Time-series of LNO_2 production per day over the CONUS for MJJA 2014 with $CRF \geq 90\%$ and a flash threshold of 2400 flashes per 2.4 h. Blue lines mark the basic LNO configuration (200 mol NO flash⁻¹ and 1×base flashrate) while red lines mark 500 mol NO flash⁻¹ and 2×base flashrate. (bottom) Daily LNO_2 and LNO_x versus ENTFLN total flashes data. Dashed lines are based on basic LNO configuration while solid lines stand for the larger LNO configuration.

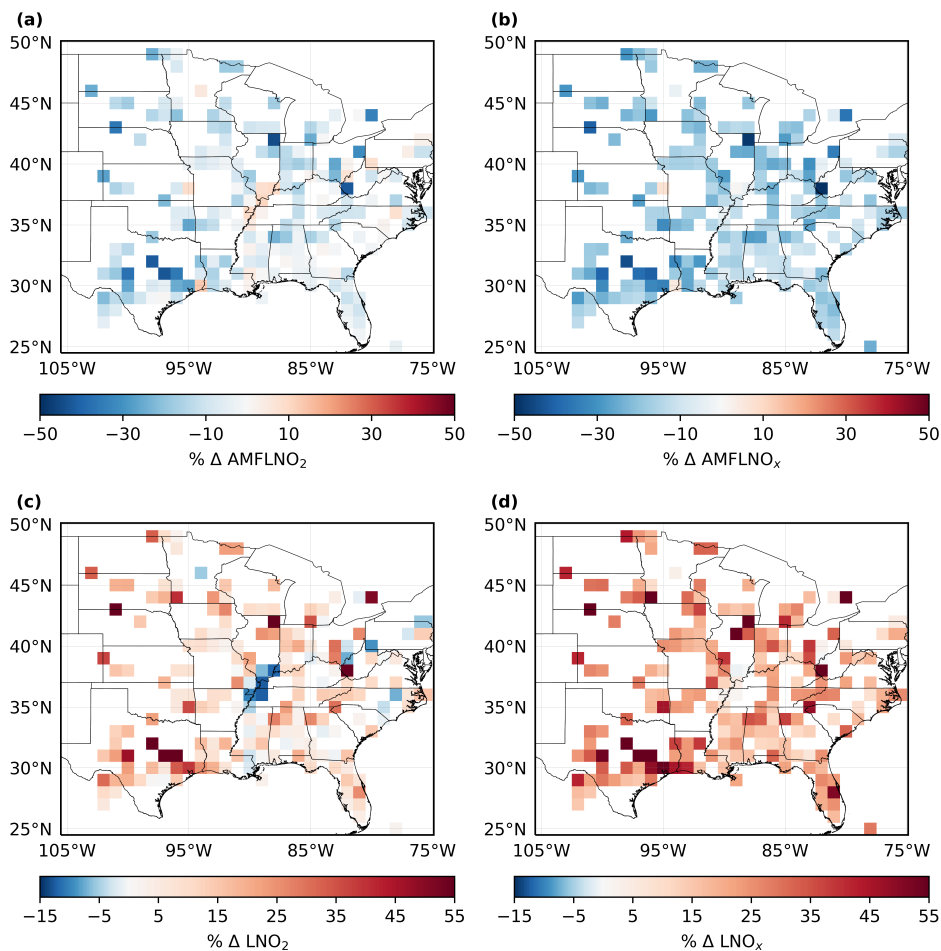


Figure 10. Average percent difference in (a) AMF_{LNO_2} , (b) AMF_{LNO_x} , (c) LNO_2 and (d) LNO_x with $CRF \geq 90\%$ over MJJA 2014. Difference between profiles are generated by 2×500 mol NO flash⁻¹ and 1×200 mol NO flash⁻¹.

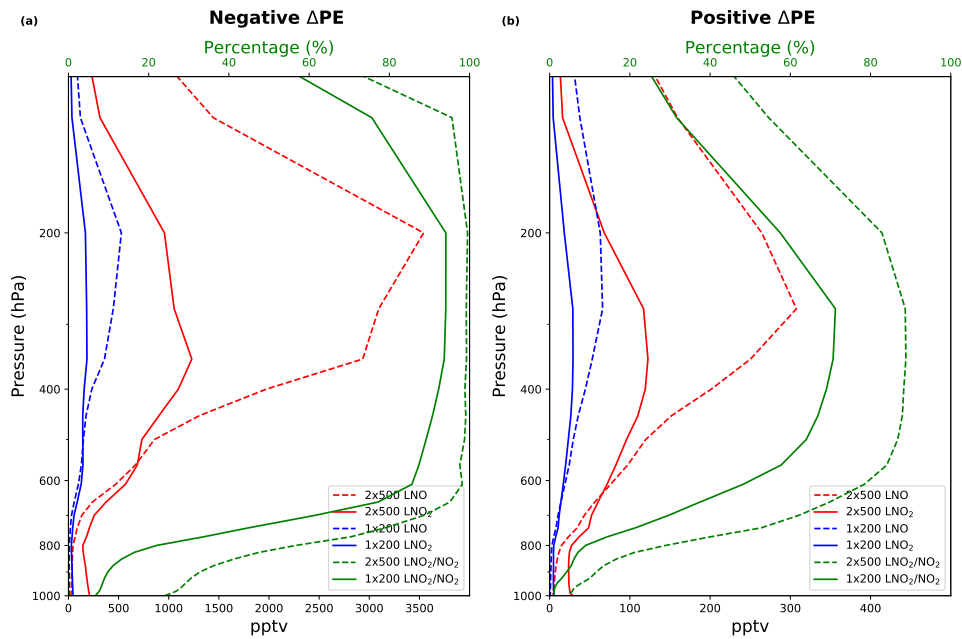


Figure 11. LNO and LNO₂ profiles with different LNO settings at (a) the region containing the minimal negative percent change in LNO₂ and (b) the region containing the largest positive percent change in LNO₂ when the LNO setting is changed from 1×200 mol NO flash⁻¹ to 2×500 mol NO flash⁻¹, averaged over MJJA 2014. The profiles using 1×200 (2×500) mol NO flash⁻¹ are shown in blue (red) lines. Solid (dashed) green lines are the mean ratio of LNO₂ to NO₂ with 1×200 (2×500) mol NO flash⁻¹.

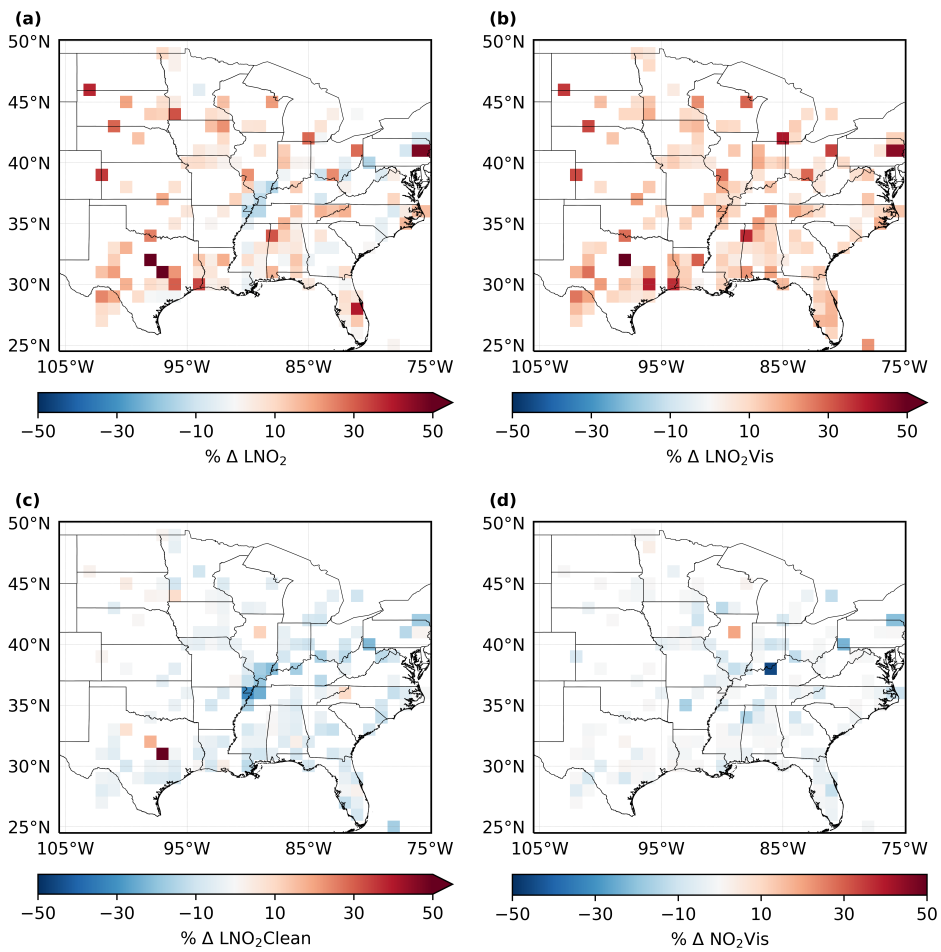


Figure 12. Average percent difference in (a) LNO_2 , (b) LNO_2Vis , (c) LNO_2Clean and (d) NO_2Vis with CRF = 100% over MJJA 2014.

Table 5. Uncertainties for the estimation of LNO₂/flash, LNO_x/flash, LNO₂/stroke and LNO_x/stroke.

Type	Perturbation	LNO ₂ /flash ^{4,5}	LNO _x /flash ^{4,5}	LNO ₂ /stroke ^{4,5}	LNO _x /stroke ^{4,5}
BEHR tropopause pressure ¹	NASA product tropopause	6	4	6	4
Cloud radiance fraction ¹	± 5%	2	2	2	2
<u>Cloud pressure²</u>	<u>Constant AMF: 0.46</u>	<u>23</u>	<u>23</u>	<u>23</u>	<u>23</u>
Surface pressure ¹	± 1.5%	0	0	0	0
Surface reflectivity ¹	± 17%	0	0	0	0
LNO ₂ Profile <u>profile</u> ¹	2×500 mol NO flash ⁻¹	13-15	26-29	13-14	26-29
Profile location ¹	Quasi-Monte Carlo	0	1	0	1
Lightning detection efficiency ^{2,3}	IC: ± 16%, CG: ± 5%	15	15	15	15
t _{window} ^{2,3}	2 – 4 hours	10	10	8	8
LNO _x lifetime ^{2,3}	2 – 12 hours	24	24	24	24
V _{strat} ^{3,4}	-	15-10	15-10	15-10	15-10
Systematic errors in slant column ^{3,4}	-	5	5	5	5
<u>Tropospheric background⁴</u>	-	<u>10</u>	<u>10</u>	<u>10</u>	<u>10</u>
<u>NO/NO₂⁴</u>	-	<u>20</u>	<u>20</u>	<u>20</u>	<u>20</u>
Net	-	37-48	43-54	36-47	43-54

PE_{uncertainty} = (Error_{rising perturbed value} - Error_{lowering perturbed value})/2 where Error perturbed value = (PE perturbed value - PE_{original value})/PE_{original value}.

¹Laughner et al. (2019) ²Beirle et al. (2009) ³Lapierre et al. (2019) ⁴Allen et al. (2019) and Bucselá et al. (2019) ⁵Uncertainty (%)

Table A1. Simple forms of abbreviations for AMFs.

Abbreviations	Numerator ¹	Denominator ²
AMF _{LNO₂}	S _{NO₂}	V _{LNO₂}
AMF _{LNO₂ Vis}	S _{NO₂}	V _{LNO₂ Vis}
AMF _{LNO₂ Clean}	S _{LNO₂}	V _{LNO₂}
AMF _{NO₂ Vis}	S _{NO₂}	V _{NO₂ Vis}
AMF _{LNO_x}	S _{NO₂}	V _{LNO_x}
AMF _{NO_x Vis}	S _{NO₂}	V _{NO_x Vis}

¹The part of simulated VCD seen by OMI ²The simulated VCD